DEVELOPMENT OF TARGETED LIPOSOMAL FORMULATION APPROACHES FOR ENHANCED COLORECTAL CANCER THERAPY

By

KALYANI PRASHANT EKTATE

Bachelors in Veterinary Science and Animal Husbandry

Nagpur Veterinary College

Nagpur, Maharashtra

India

2012

Submitted to the Faculty of the

Graduate College of the

Oklahoma State University

in partial fulfillment of

the Degree of

DOCTOR OF PHILOSOPHY

May, 2019

DEVELOPMENT OF TARGETED LIPOSOMAL FORMULATION APPROACHES FOR ENHANCED COLORECTAL CANCER THERAPY

Dissertation Approved:

Dr. Ashish Ranjan

Dissertation Adviser

Dr. Jerry Malayer

Dr. Keith Bailey

Dr. Daqing Piao

Name: KALYANI P. EKTATE

Date of Degree: MAY, 2019

Title of Study: DEVELOPMENT OF TARGETED LIPOSOMAL FORMULATION APPROACHES FOR ENHANCED COLORECTAL CANCER THERAPY

Major Field: VETERINARY BIOMEDICAL SCIENCE

Abstract: Colorectal cancer (CRC) is the 4th most commonly detected cancer in the USA. Despite promising advances, the 5-year survival rate for the metastatic disease remains dismal (<15%) due to the presence of chemo-resistant and immune-suppressive tumor microenvironment. In addition, CRC outcomes can suffer from a lack of real-time treatment monitoring, preventing rapid treatment interventions. To overcome these barriers, we hypothesized that, modifying low temperature sensitive liposomes (LTSLs) that release the encapsulated doxorubicin at >40^{0}C with ultrasound contrast agents and bacterial attachments can improve the real-time chemo-immunotherapy of CRC. Towards these goals, we investigated the following specific aims in murine models of colon cancer: 1) Develop echogenic-LTSL (E-LTSL) for real-time ultrasound-enhanced reporting of tumor temperature and doxorubicin delivery, 2) Utilize tumor homing *Salmonella typhimurium* for LTSL delivery and enhanced chemo-immunotherapy with High Intensity Focused Ultrasound (HIFU) tumor heating (~42°C), and 3) Investigate the ability of magnetic bacteria *Magnetospirillim magneticum* (AMB-1) to aid LTSL tumor drug delivery under magnetic guidance. Our data showed that intratumoral vascular contrast of E-LTSL as a function of temperature and doxorubicin delivery was strongly correlated, enabling robust estimation of temporal variation in colon tumor temperature and drug delivery. LTSL attachment didn't impact Salmonella viability and improved chemo-immunotherapy outcomes in murine colon cancers by promoting the population of M1 macrophages with HIFU heating. Finally, the use of magnetic guidance for AMB-LTSL significantly reduced the colon cancer viability by enhancing cellular and tumor localizations of doxorubicin. In conclusion, we found that multifunctional LTSL formulations significantly improved the CRC treatment outcomes in murine models by aiding the real-time monitoring and removing the resistive and suppressive tumor microenvironment features.

TABLE OF CONTENTS

Chapter **Page**

LIST OF TABLES

Table **Page**

LIST OF FIGURES

Figure **Page**

Figure **Page**

CHAPTER I

REVIEW OF LITERATURE

Cancer statistics and gaps in current treatment protocols

According to the American Cancer Society, a total of 1.7 million new cancer cases and 609,640 cancer deaths is estimated to occur in the United States in 2018[1]. Despite promising advances, cancer remains a challenging disease to treat, thereby putting significant burdens on the healthcare system. Currently, surgery, radiation, and chemotherapy are regarded as the gold standard approaches for cancer treatment[2]. Depending on the type and stage of cancer, each of these modalities, or a combination, are administered to the patient, however, achieving a robust response in malignant diseases has been dismal. To overcome these barriers, newer treatment options such as gene therapy, bone marrow transplantation and targeted treatments are increasingly being translated in patients to improve outcomes and enhance survival [3-5]. This is promising but cancer cells notoriously evolve, adapt and switch their survival pathways to develop resistance against therapeutic approaches. Most cancer treatment modalities are also often accompanied by severe side effects, reducing patient's quality of life. *All of these challenges underscore the need to enhance targeted therapy approaches such that they provide robust and non-toxic outcomes in cancer patients*.

In particular, colon cancer is the 4th most commonly detected cancer in USA[6]. The outcomes in colon cancer are highly dependent on the stage of disease, and tumor microenvironments[78]. For example, early stage colorectal cancer is efficiently managed by surgical resection; however advanced staged disease (III and IV) typically requires chemotherapy with oxaliplatin, fluoropyrimidine 5-fluorocil, leucovorin, doxorubicin, or combinations of these drugs [9-11]. Chemotherapy with such agents typically has low specificity, demonstrate gastrointestinal toxicities and drug resistance[12-14]. The objective of this dissertation is to address such treatment barriers by developing novel device-directed approaches with nanoparticles. To do so, we focused on the aspects of localized chemotherapy delivery and immunotherapy with heat, magnetic field and bacteria in murine colon cancer model to ease clinical translation.

Role of nanotechnology in improving chemotherapy outcomes in colon cancer patients

Conventional chemotherapy of colon cancer can be limited by the low specificity, rapid drug clearance, and biodegradation of anticancer drugs[15]. According to Hong et al, <2% of the total administered drug typically reaches the tumor site[16]. One approach to enhance drug accumulation can be by targeting specific therapeutic cargo into the tumor cells. This is done using antibody directed enzyme pro-drug therapy, immune- and protein conjugates and nano-sized drug carriers[17-19]. Amongst these agents, nano-sized drug carriers of various composition that encapsulate anti-cancer drugs has gained significant interest and testing in clinical trials[20]. Nanomedicines have high surface-to-volume ratios and favorable drug release profile which provides enhanced specificity[21]. Nanomedicines exploit the enhanced permeability and retention effect (EPR), characteristic of tumor tissues to boost the passive accumulation of chemotherapy in the tumors[22,23]. Further, the incorporation of targeting ligands for the active targeting of over-expressed targets in the cancer cell can significantly improve the localized bioavailability by ~2-10 fold compared to conventional medicine[24,25]. Thus, the versatility of nanomedicines has made it possible to bridge translational gaps in tumor imaging, targeting, drug delivery, and treatment monitoring[26,27].

In this project, we primarily focus on liposomes. Liposomes have demonstrated the greatest success in clinical trials[28]. Liposomes are biocompatible, moderately immunogenic[29], andtunable for controlled drug release in tumors[30]. Liposomes also protect the drugs from

premature degradation in blood vessels[30,31], accumulate in tumors by the EPR effect[32], and are capable of delivering a wide-spectrum of cargo agents[33,34]. A detailed description of the current liposomal approach and translational barriers are described below.

Liposomes

Liposomes are vesicular structure composed of a lipid bilayer enclosing a hydrophilic inner phase. They were first described by Alec Bangham in 1961 and since then have been extensively investigated for drug and gene delivery[35]. Liposomes enter a cell by endocytosis, adsorption, and lipid transfer. Most liposomes are composed of phospholipid or synthetic amphiphiles incorporated with sterols such as cholesterol. The phospholipids spontaneously form vesicular structures upon hydration in aqueous solutions, and thus are ideal for ferrying hydrophobic and hydrophilic drugs[36,37]. Several methods such as thin film hydration, reverse phase evaporation, ethanol injections, sonication, and freeze-drying have been employed for the synthesis of liposomes[38]. Properties of the liposomes particles can differ considerably with the lipid composition, surface charge, size and the method of preparation, resulting in unique therapeutics tailored to physical properties of a tumor.

Characteristics of liposomes

Liposomes can be unilamellar or multilamellar, and their sizes can range from 0.025μm to 2.5 μm[39]. The essential physical parameter that determines the pharmacokinetics and pharmacodynamics of liposomes are the number of membrane layers (Table 1) and size. These features can influence the drug encapsulation efficiencies and release rates upon parenteral injections[39]. Liposomes with single phospholipid bilayer are divided into two categories: (1) Small unilamellar vesicles with <0.1μm diameter that have low entrapped volume to lipid ratio and long circulation half-life , and (2) Large unilamellar vesicles (>0.1μm) with high encapsulation efficiency, presumably due to their larger volumes, but shorter half-lives (Table 1). In contrast, large multilayered vesicles have an onion-like structure formed by the concentric phospholipid layers separated by an aqueous layer. They are mechanically stable, but have moderate encapsulatin efficiencies and are cleared rapidly by the RES [40].

Table 1: Size range of liposomes

Liposome	Subcategory	Size range (nm)
Multilamellar vesicles		>100nm
Unilamellar vesicles	Small Unilamellar vesicles	20-40
	Large Unilamellar Vesicles	100-1000

History of liposomes

1st generation liposomes

The first generation of liposomes, the "classical liposomes", were considered to be naked formulations as they lacked a surface grafted with the protective molecule such as polyethylene glycol, texposing them to the external environment. Classical liposomes demonstrated short half-lives upon intravenous injection and were susceptible to opsonins and protein adsorption on the surface, marking the liposomes clearance by the reticuloendothelial system (RES)[41,42]. Some studies also found that the short half-life of classical liposome was in part due to the self-aggregation in the systemic circulation. To overcome these barriers, in later years, the liposomes were modified by altering the lipid composition with neutral rather than anionic/charged lipids, long-chain high phase transition lipids, and cholesterol in the bilayer [43]. In particular, the incorporation of the cholesterol was critical for the tight packing of lipid acyl chains to create a less fluid membrane, resisting opsonization and consequently increasing their plasma half-life[44,45]. Additionally, the inclusion of sphingolipids in cholesterol-based liposomes further enhanced the liposomes stability by forming hydrogen bonds with cholesterol, increasing membrane rigidity and decreasing opsonization. Furthermore, the addition of a small amount of negative charge from lipid-like phosphatidylglycerol prevented aggregation and clearance rates[41]. Although these innovations were promising advances, the half-livers were still sub-optimal, eventually paving the way for the second generation long-circulating liposomes as described below [46-49].

Second Generation liposomes

The second generation of liposomes as Stealth® or PEGylated liposomes showed superior retention and delayed detection by the RES. These liposomes incorporated ganglioside (GM1) and biocompatible polymers, particularly poly (ethylene glycol) (PEG)[50-53]. Typically, PEGylated/Stealth® liposomes were formulated with ~5-10 mol% (total phospholipid) of polyethylene glycol (PEG) with molecular weights in the range of 2,000-5,000 Daltons[46,54]. PEG's are non-toxic, and moderately- immunogenic. The long chains on the PEG molecules that were hydrophilic could form an aqueous shell around the surface of the liposome, reducing self-aggregation[42,55,56]. The surface grafting of PEG also weakened the Van-der-Waals forces that attracted opsonins to the lipid membrane, reducing uptake of liposomes by RES[52,57,42]. Other theories proposed for de-opsonization included binding to certain proteins to shield the lipid charges resulting in delayed detection by RES[58,59]. Examples of 2nd generation liposomes included Doxil/Caelyx that passively accumulate in the tumor microenvironment by exploiting EPR, however, recent studies have found that the poor intratumoral accumulation (~10%) and release rates are the rate-limiting process, impacting the overall clinical efficacy[4760].

Third generation of liposomes

With the advancements in liposomal research, the need for targeting and triggered release of encapsulated content in the tumor milieu gained prominence, leading to the development of the third generation of liposomes. Examples of 3rd generation liposomes include antibody decorated, pH-sensitive, thermosensitive, fusogenic and cationic liposomes. Each of these approaches has merit and can be used for a variety of indications as shown in Table 2[61].

Table 2: Liposomal drug combinations in clinics list

	Particle	Trade name	Approved year	Drug	Indication	Ref
1	Lipid complex	Abelcet	1995	Amphotericin B	Invasive severe fungal infection	[62]
2	Lipid	Amphotec	1996	Amphotericin B	Severe fungal	[63-65]

	complex				infection	
3	Liposome	Ambisome	1997	Amphotericin B	Presumed fungal infection	[63]
4	Liposome	DaunoXome	1996	Daunorubicine	AIDS related Kaposi's sarcoma	[66,67]
5	Liposome	DepoCyt	1999	Cytarabine	Neoplastic and lymphomatous meningitis	[68,69]
6	Liposome	DepoDur	2004	Morphine Sulphate	Pain management	[70,71]
7	Liposome	Exparel	2011	Bupivacaine	Pain management	[72]
8	Liposome	Epaxal	1993	Inactivated Hepatitis A virus(strain RGSB)	Hepatitis A	[73,74]
9	Liposome	Inflexal	1997	Inactivated hemagglutinin of Influenza virus strain A and B	Influenza	[75,76]
10	Liposome	Myocet	2000	Doxorubicin	Metastatic breast cancer	[77,78]
11	Liposome	Marqibo	2012	Vincristine	Acute lymphoblastic leukemia	[79,80]
12	Liposome Photo-dynamic	Visudyne	2000	Verteporphin	Macular degeneration, choroidal	[81]

	therapy				neovascularization	
13	PEGylated Liposome	Doxil	1995	Doxorubicin	Kaposi's sarcoma, Ovarian and breast cancer	[82,83]
14	PEGylated Liposome	Lipodox	2013	Doxorubicin	Kaposi's sarcoma, Ovarian and breast cancer	[83-85]
15	PEGylated Liposome	Onivyde	2015	Irinotecan	Combination therapy with fluorouracil and leucovorin in metastatic adenocarcinoma of the pancreas	[86,87]
16	Liposome	Mepact	2004	Mifamurtide	High grade resectable, non-metastatic osteosarcoma	[88-90]
17	Lipid complex	Estrasorb	2003	Estradiol topical emulsion	Menopausal therapy	[91,92]

We specifically focus on the thermosensitive liposomes in this dissertation[93].

Low temperature sensitive liposomes (LTSLs)

LTSLs were developed for targeted active delivery of encapsulated cargo at elevated temperature[61]. LTSLs were first introduced by Yatvin et al in 1978 [94]. LTSLs can be made by

lipids such as DPPC, Myristoylstearoyl phosphatidylcholine (MSPC) and PEG conjugated lipid, and have phase transition temperature ~40°-45°C. At these temperatures, LTSLs attain sharp thermal transition, causing rapid gel-to-liquid phase transitions, and enhanced membrane permeability[95] releasing the encapsulated drug. LTSLs primarily release contents in the blood vessels within tumors, thereby increasing the accumulation of drug-cargo in the tumors. An example of LTSL in clinical trials is Thermodox® that was developed by Celsion Corporation. Thermodox is in phase III clinical trials for doxorubicin chemotherapy of primary liver cancer (hepatocellular carcinoma) and recurring chest-wall breast cancer [95]. Thermodox was shown to result in a 5-fold higher doxorubicin concentration in blood compared to non-thermal sensitive Dox liposomes and 25-fold greater accumulation of the drug in the treatment area than intravenous administration of doxorubicin alone[96]. ThemoDox® is composed of DPPC, MSPC and 1, 2-distearoyl-sn-glycero-3-phosphoethanolamine-N- [amino (polyethylene glycol)-2000] (DSPE-PEG-2000) with a phase transition temperature of ~ 41.5°C. The addition of MSPC is crucial for the slight reduction in the transition temperature of DPPC, while DSPE-PEG-2000 enhances the circulation time of liposomes. The presence of PEG-lipid helps in attaining lysolipid-induced permeability at a faster rate[97]. ThemoDox® was primarily introduced in the market for systemic treatment in combination with Radio-Frequency Ablation (RFA), but recent studies have expanded their use with other hyperthermia modalities such as microwave hyperthermia and/or High Intensity Focused Ultrasound (HIFU) [98]. Overall, LTSL can control drug release[99], and reduce non-specific toxicities by spatially and temporally controlling local release in tumors.

Role of High intensity focused ultrasound (HIFU) in localized tumor heating

HIFU is a non-invasive, non-ionizing modality for inducing thermal and non-thermal effects in biological tissue[100]. HIFU was first used to ablate inoperable brain tissue to manage Parkinson's disease. Unfortunately this therapy was not completely developed at that time due to lack of necessary imaging devices[101]. HIFU precisely deliver focused ultrasound energy locally in the body, sparing the healthy tissues. At the focal point of the ultrasound field, contraction and rarefaction of sound waves cause mechanical stress and strain. By varying the parameters such as the pressure amplitude, pulse repetition frequency,

propagation length, and power, the resultant sound waves achieved thermal or non-thermal outcomes[102], coagulative necrosis, ablation, mild-heating, and tissue vaporization or a combination of multiple effects[103].

In this dissertation, we utilized HIFU for mild hyperthermia (~40-45°C) generations for active drug release from LTSL's and immune modulation.

Factors governing mild hyperthermia based treatment responses in tumors

Hyperthermia is an innovative approach for enhancement of therapeutic efficacy in combination with chemotherapy and radiotherapy[104]. Hyperthermia also is leveraged for inducing drug delivery from nanoparticles[105]. In 1984, Sapareto and Dewey reported an effective reduction in tumor growth by uniformly heating tumors at 42°C for an hour[106]. Hyperthermia was thought to affect tumor sensitivity to other treatments by direct effect on immune cells, change in pH, alterations of tumor vasculature, and release of Heat Shock Proteins (HSP's) and exosomes, and are shown in Figure 1[107,108].

Physiological effects of hyperthermia on tumor blood vessel

Unlike healthy tissues, the tumor vasculature is abnormal and devoid of smooth muscle. Thus, when tumors are heated with hyperthermia, the result is vasodilation, enhanced membrane fluidity and vascular permeability resulting in hemorrhage and occlusion. Previously, it was believed that tumor vasculature was more susceptible to occlusion and hemorrhage compared to normal tissue. However, recent studies have established that tumors vasculatures demonstrate similar behaviors to normal tissue when subjected to mild hyperthermia (41-42°C) and increase the blood flow by 1.5 to 2 times in the treated regions compared to untreated regions[109]. Further, Horseman et al and Dewhirst et al. showed that hyperthermia increased tumor oxygenation, that in turn impacted chemotherapeutic outcomes[110]. Additionally, the increased blood flow to the target region was found to augment the liposome circulation in the tumors [93] and mediate drug release from TSLs. Furthermore, hyperthermia enhanced perfusion altered the immune environment and trafficking of immune cells such as dendritic cells and T cells between tumors and lymph nodes[111].

Role of hyperthermia in modulating tumor cell profiles

Exposure of cancer cells to temperatures from 39 to 45°C can change the cell membrane fluidity to affect active and passive diffusion, intracellular Na^+ and Ca^{2+} levels, and the overall membrane potential, without directly impacting the cell viability[112,113]. Hyperthermia also induces cytotoxic effects via denaturation and aggregation of enzymes such as synthetases and polymerases[114,115]. These enzymes are important for DNA polymerization and de novo synthesis, and thus their denaturation by hyperthermia impact the DNA repair causing cell cycle arrest and death[116]. Hyperthermic exposures has also shown to increase the surface expression of MHC class I polypeptide-related sequence A (MICA), an NKG2D ligand on tumor cells, enhancing the sensitivity of cells to lysis by Natural Killer (NK) cells [117]. Ito et al showed that exposing cells in-vitro to 43°C for 30 minutes enhances recognitions by the CD8+ T cells via surface expressed Major histocompatibility complex (MHC) class I molecules[118]. Therefore, hyperthermia generates a multitude of changes in the membrane dynamics of tumor cells, altering the permeability and the inflammatory profiles of the tumor cells.

Relationship of hyperthermia exposures of immune cells with cellular processes

Hyperthermia stimulates the lymphocytes to improve survival from infections and tumor growth[119]. Local and systemic hyperthermia mimics fever to enhance the body's natural response to inflammation[120,121]. For example, phagocytosis activity in murine macrophages briefly treated with hyperthermia (40°C) was found to be enhanced by approximately 40% compared to cells cultured at 37°C [122]. Likewise, the migration of the epidermal dendritic cells (DC's), also known as Langerhans cells, to lymph nodes and interactions with T-cells was found to be significantly increased with heat[123]. DC's derived from murine bone marrow (BALB/c ($H\text{-}2^d$))mice treated with mild hyperthermia (39-40°C) for 3hours decreased the secretion of IL-10 and Tumor Necrosis Factor (TNF-α) by maturing DC's. While the produced IL12, a cytokine responsible for stimulation of the innate immune system (like Natural killer (NK) cells, which are a type of lymphocyte that plays an important role in rejection of tumors) and cells of the adaptive immune system (T and B cells) was enhanced [124]. This is not always consistent, and studies conducted in BALB/c mice lacking heat shock factors (*Hsf*) kept in a cage at 42°C for 20 minutes reported no changes in the expression of

IL-12[125]. Overall, the cellular stress from hyperthermia treatment has the potential to elevate the activity of antigen presenting cells (APC's) like DC's and macrophages, which can affect the downstream activation of T cells to reduce immune-tolerance to tumors.

Heat shock proteins (HSP's) expression is highly correlated with tumor hyperthermia

Hyperthermia has been found to induce heat shock protein (HSP) expression in cancer cells. HSP's are a heterogeneous group of molecular chaperones and are upregulated in tumor cells upon thermal stress[126]. In contrast to short duration (<1min) ablative range temperatures, long-duration hyperthermia (>15min) is relatively more stimulatory for surface expression of HSP on cancer cells, presumably due to slow activation of expression profiles over time[111]. HSP's are subdivided into groups based on their molecular size such as Hsp40, Hsp60, Hsp70, Hsp90 and Hsp100-110, among which Hsp 70 is proven to be immunostimulatory[127]. Hsp70 binds to the Toll-like Receptors (TLR) 2 and 4 on DC's and stimulate NK cell proliferation and cytolytic activities are considered to have a high immunostimulatory activity[127,128]. It has been shown that Hsp70 released/ attached to proteins on dying tumor cells is directly taken into DC's and may therefore chaperone antigens directly into DC's [129]. Shrivastava et al have shown that those DC's are able to cross present the tumor antigens from Hsp tp CD8+ T cells inciting a CD8+ T cells response against tumors MHC-I presentation[130-132]. While HSPs are considered immunostimulatory, negative role of HSP's in suppressing tumor growth are also reported for example Hsp90 represses tumor suppressor protein p53 and block apoptosis of cancer cells[133]. The amount and type of HSP expression is discretely controlled by temperature. For instance, B16F10 melanoma cells heated for 30min start to release the HSP70 at 41°C, reaching the peak expression at 43°C and stopping at 45°C [134]. Thus, a careful choice of temperatures can potentially tune the HSP release and functional outcomes.

Hyperthermia is a critical mediator of exosome release from tumor cells

Exosomes are small 30-100nm membrane vesicles that are released from cells for intercellular signalling[135]. Exosomes released from tumor cells thermal stress can serve as immunostimulatory factors enriched with tumor antigens[136]. Exosomes released in response to thermal stress activate the DC and cross-priming of tumor-specific CD8+ T cells. Cao et al

demonstrated that exosomes from hyperthermia treated cells activated DC's and T cells due to the expression of chemokines such as CCL2, CCL3, CCL4, CCL5, and CCL20[137]. Consequently, exosomes from heated tumor cells acted as in-built vaccines, enhancing the antitumor immune response.

Cancer and the immune system

In 2013, Science magazine declared cancer immunotherapy as the "2013 Breakthrough of the year" due to exceptional treatment outcomes in cancer patients[138]. Cancer immunotherapy utilizes the body's immune system to reverse the immune suppressive pathways to produce long-lasting anti-tumor immunological memory.

The immune system is broadly divided into the innate and adaptive immune system. The innate immune system is nonspecific and relies on the action of phagocytes (e.g. macrophages; reference). In contrast, the adaptive system uses T cells and B cells to provide protection against foreign pathogens. The adaptive immune system is made up of two arms: humoral immunity and cell-mediated immunity. Humoral immunity is B cell dependent, and eradicates foreign toxins and microbes via antibodies circulating through the body. Cellular immunity is coordinated by the T cells, and such cells eradicate foreign agents upon antigen presentation by the APC's.

The crosstalk between the innate and adaptive immune systems is the key to responses against cancer cells. The humoral immunity activates effector T-cells, other endogenous immune cells and antibodies against the tumors. Additionally, the DCs serve as the major histocompatibility complex (MHC) class–II APCs presenting antigens to a cluster of differentiation 8+ (CD8+) T cells to mount cytolytic responses against cancer cells[138]. The interplay of cellular signaling is critical for the priming and activation in the lymph nodes and trafficking to the tumor beds for the recognition of the cancer cells by the effector and memory T cells[139]. Although well-orchestrated, antitumor immunity is influenced by the tumor microenvironment immune cells, and are described below.

(a) Neutrophils: Neutrophils are the most abundant type of innate cells and are known as the first line of defense for the detection for the elimination of a foreign pathogen. Neutrophils release granules containing antimicrobial peptides and proteases, and

extracellular neutrophil traps (NETosis) to aid cellular phagocytosis[140]. The role of neutrophils in cancer is controversial as it is associated with poor outcomes and aggressive cancer phenotypes in some cases[141]. Such neutrophils are typically of the myeloid origin and inhibit the T-cell response and accumulation via multiple pathways such as lowering the FcγR(immunoglobulin (Ig) G immune complex receptor)-mediated neutrophil and activation macrophage-1 antigen (MAC-1)[142,143]. Neutrophils also releases Neutrophil Elastase (NE), Neutrophil collagenase (MMP8) and Gelatinase (MMP9) factors that promote remodeling of the extracellular matrix in tumors, drug resistance and cancer progression [144].

(b) Myeloid-derived suppressor cells (MDSC): MDSCs are a heterogeneous subset of cells of myeloid origin that expand during cancer, inflammation, and infections. Myeloid cells in a healthy person differentiate into mature granulocytes, macrophages or dendritic cells (DC's). In cancer patients, myeloid cell differentiation is partially blocked, so the MDSC's are somewhat immature and suppresses T-cell response, promoting tumor angiogenesis and modulating cytokine production from the macrophages [145-147].

(c) Macrophages: Macrophages are the most important arm of the innate immunity, and are present in a high population in the tumor microenvironment. The resident macrophage population in tumors can be differentiate into a pro-inflammatory, anti-microbial (M1) and anti-inflammatory (M2) subset. The M1 phenotype is stimulated in the presence of lipopolysaccharide (LPS), interferon-γ (IFN-γ), and granulocyte-macrophage colony stimulating factor (GM-CSF). Anti-inflammatory (M2) phenotype is dominant in the presence of macrophage colony stimulating factor (M-CSF), IL-4, IL13, IL-10, immunosuppressive agents such as corticosteroids, vitamin D3 and prostaglandins[148]. M1 macrophages produce copious amounts of pro-inflammatory cytokines upon activation by bacterial products and thus are capable of effective tumor suppression. In contrast, the M2 macrophages induce tumor progression by undertaking scavenging, matrix remodeling, tissue repair and angiogenesis [149].

(d) Cytotoxic T-Lymphocyte-associated protein 4 (CTLA-4):CTLA-4 on T-cells binds to the B7 molecule on dendritic cells and other APC's inhibiting auto-immune inflammation[150]. CTL4s are an endogenous regulator of T-cell function and increase the activation threshold of T cells, increasing immunological tolerance and weakening immune responses against

tumor antigens. CTL4 also promote immune suppression on bystander cells via Tregs, indirectly diminishing signaling through co-stimulatory receptor CD-28 [151]. CTLA-4 and CD28 are expressed on the surface of T cells and have higher affinity for CD80 and CD86 present on APC's, reducing their availability[152]. This blocks stimulatory activity of CD28 increasing the activation of threshold of T-cells and reducing the immune response to weak tumor self antigens[153].

(e) Programmed death-1 (PD-1): PD1 is a transmembrane protein expressed on T cells, B cells and natural killer (NK) cells. It is primarily involved in regulating adaptive immune cell response and inhibiting immune signaling and is homologous to CD28 [154]. It binds to the programmed death ligand 1 and 2 (PDL-1&PDL-2). Both of these ligands are found on the surface of APC's such as dendritic cells, macrophages and monocytes and non-lymphoid tissues (example)[155]. Binding of PD-1 to PDL receptors causes peripheral T-effector exhaustion, promotes conversions of T-effector cells to Tregs, and directly inhibit tumor cell apoptosis[138156].

(f) Regulatory T cells (Treg): Tregs are a unique subset of FOX-P3$^+$CD25$^+$CD4$^+$ expressing T cells that suppress the effective antitumor immune response. The normal physiological function of Treg is to sub-due autoimmune response in the body by suppressing self-antigens[157]. The abundance of Tregs in tumors correlates with poor clinical prognosis[158]. Tregs suppress conventional T cells, and influence the function of DC's, macrophages, B cells, and NK cells[159]. IL-2, IL-2 receptor subunits and CTLA-4 (cytotoxic T-lymphocyte-associated protein 4) are the most significant molecules impacted with the Treg suppression. Treg is also identified by the MHC/self- peptide ligand that has a greater affinity for the TCR (T-cell receptors), influencing the activity of IL-2 and CTLA-4[160]. CTLA-4 on the Treg can also downregulate the expression of CD80 and CD86 molecules on DC's, hindering activation of conventional T cell and suppressing anti-tumor immune response [152].

Bacteria can be a critical link to tumor immune modulation and chemotherapy responses

Nanomedicine and immunotherapy have undoubtedly improved targeted therapy. However, outcomes against advanced stage colon cancer remain challenging due to emergence of drug resistance and immune tolerance. Therefore, agents that can help overcome immune escape mechanisms is critically needed for robust clinical responses[161].

History of tumoricidal therapies with microbial agents

Attenuated bacterial agents have shown to improve outcomes in inflammatory bowel disease, cancer, autoimmune disorder, and obesity [162,163]. Bacterial genetics can be easily manipulated to induce production of the 'perfect' anticancer effects in the tumor microenvironment. Intracellular bacteria such as *Salmonellatyphimurium* and *Listeria monocytogenes* penetrate non-phagocytic mammalian cells. The earliest reported use of bacteria as an anticancer agent was reported in the writings of Ebers Papyrus by Imhotep in 2600 BC, an Egyptian physician. Imhotep recommended a poultice for tumors (swellings) followed by an incision, which would inevitably lead to an infection at the tumor site. In early 1813, when bacteria had not yet been identified as an infectious agent, it was found that cancer patients who developed *Clostridium* infections with gas gangrene exhibited tumor regression[164]. Subsequently, in 1868 German physician W. Busch cauterized a female patient's neck tumor and placed the woman in bedding previously occupied by a patient suffering from "erysipelas," a *Streptococcus pyogenes* infection, thus performing the first intentional bacterial cancer treatment[165]. The infected patient's primary tumor shrunk to half and was also observed to be accompanied by the reduced size of lymph nodes in the neck. Unfortunately, the patient died 9 days later due to complications of uncontrolled infection[166]. In 1893, William Coley, a young physician in New York reported a significant tumor reduction by injecting patients with erysipelas after being inspired by accidental tumor regression in an immigrant patient with frequent fever due to an infected tumor [167]. Dr. Coley's experimental studies found that injecting live bacteria had strong side effects, and thus proposed using a combination of heat-killed *Streptococcus pyogenes* and *Serratia marcescens*. Such combinationsreduced the strong inflammatory and immune activation of bacteria, improving outcomes, and this was later referred to as Coley's vaccine or Coley's toxin[168]. Coley treated hundreds of patients with sarcomas, carcinomas, lymphomas, melanomas, and myelomas in early to advanced stages, becoming a pioneer in the field of

bacterial cancer immunotherapy. Despite the cure and remarkable improvements, Coley's studies were considered anecdotal, inconsistent and unsafe according to current standards of clinical trials[169]. Sixteen different preparations of Coley's toxin have been used since 1892. In 1963, Coley's vaccine was assigned a new drug status by FDA and strict guidelines were set for clinical trials. Eventually, the FDA refused to acknowledge "Coley's toxin as an approved drug, paving the way for radiotherapy and chemotherapy to gain greater acceptance as the gold standards for cancer treatment. Interestingly, a retrospective study conducted by Hoption et al compared data from the Surveillance Epidemiology End Result cancer registry to evaluate 10-year survival rates of patients treated by either Coley 's toxin or conventional treatments with surgery and chemotherapy, and found that patients receiving modern conventional therapies did not fare better than patients receiving the treatment initiated by Coley over 100 years ago [166].

Tumor microenvironment provides the optimal niche for bacteria homing

Bacteria display a number of properties that seem relevant for effective cancer treatment. Studies conducted with attenuated strains of *Clostridium, Listeria, Salmonella, Shigella, and E-coli* have shown preferential accumulation and multiplication in the solid tumors [170-175]. That said, the type of antitumor response with bacterial agents depends on the motility, tumor chemotaxis, cytotoxic potential, and pathogen-associated molecular patterns (PAMP). It may be noted that the mechanisms of bacterial entry in tumor is yet to be determined, but it is speculated that the differences between tumor and normal vasculature and blood flow patterns favors the entry and entrapment of bacteria within tumors. Some studies also suggest that the macrophages or monocyte entrap and release bacteria in the tumor [176]. These processes can be aided by the anaerobic hypoxic microenvironment, enhancing the chemotaxis and proliferation within the heterogeneous tumor tissue [177,178]. Thus, even a small number of bacteria can home and proliferate within the necrotic and hypoxic solid tumors[179180] . This coupled with slower clearance from tumors relative to healthy tissues could imparts cancer specific targeting[179]. In nude or SCID relative, a 5-50-fold decrease in tolerance to bacteria compared to immunocompetent mice is generally observed, suggesting that the T-cell may be playing role in its clearance. The clearance and suppression of virulence of bacteria in tumor can also be mediated by the host defenses including

macrophage-phagocytosis, antibacterial peptides, antibodies, and elements of the complement system, and physical barriers to the entry of of the infecting pathogens[181 182].

Bacterial agents for tumor therapy

Currently, Bacillus Calmette-Guerin (BCG) is the only bacterial agent approved by the FDA for the treatment of superficial, non-muscle invasive bladder cancer (NMIBC). BCG is highly effective in high-risk NMIBC especially when the live attenuated bacteria is administered repeatedly into the bladder[183]. Unlike Coley's toxin, BCG does not induce fever, and the local administration appears to outperform chemotherapy likely via the stimulation of regional immune response [184]. A key challenge of BCG is that its effectiveness is limited to superficial bladder cancer. Thus, developing novel bactericidal approaches that allow targeting of small and large tumor lesions irrespective of tumor locations are needed, and is the focus of the Ph.D. dissertation.

Salmonella typhimurium is a motile, non-spore forming, gram-negative, facultative anaerobic bacteria belonging to the family *Enterobacteriaceae*[185]. *Salmonella* species are known to cause localized gastrointestinal infections in humans and animals. In 1997, Pawelek et al demonstrated that *Salmonella* preferentially accumulates within tumors and achieves tumor to normal tissue ratios of approximately 1000:1 (Table 3). It was observed that the high accumulation of *Salmonella* improved survival rates compared to untreated controls[186,187]. The tumor homing and bactericidal properties of attenuated *Salmonella* spp. in the quiescent and necrotic environment is likely due to the chemotaxis towards the serine, ribose, and aspartate that are produced by the quiescent cells within the tumor[177]. Additionally, the irregular vasculature and positive pressure prevent the delivery of antibiotics and serum complement in the hypoxic areas of tumor, preventing the *Salmonella* lysis and resulting in increased overall numbers in tumor[181]. Luo et al showed that *Salmonella* can accumulate and homogeneously distribute in murine tumors as small as 0.05 g to 0.3 g[188]. Low et al genetically engineered *Salmonella* to produce VNP 20009/YS1646 strain to overcome virulence to render it safe to be used an anticancer agent[187]. VNP 20009 has *msb* and *pur 1* gene deletions. *pur1* deletions lead to purine auxotrophy, attracting the bacteria to the tumor leading to enrichment of the bacteria at that site, whereas *msb* deletion reduces LPS-induced shock by interfering with addition of terminal myristyl group to Lipid A VNP20009 strain

also has a significantly reduced capacity to induce TNF-αstimulation and production in the host[182,187].

The exact mechanism behind the direct cancer cell killing of *Salmonella* is still unclear, but is attributed to the competition for extracellular nutrients and growth factors within the tumor microenvironment, localized production of cytotoxins, and stimulation of the immune system[189190,191,178,192]. *Salmonella* has been shown to enhance tumor cell gap junction activity in melanoma cells (B16F10) by increasing the expression of CX43 proteins. Gap junctions are responsible for intercellular communication and are often absent on the tumor cells [193]. Thus, increased expression of CX43 proteins upon *Salmonella* injection facilitates the passage of antitumor drugs and trigger death signal between adjacent tumor cells [193]. This is especially evident in the first 24-48h, suggesting a role of CX43 proteins upregulation and apoptosis induction. The enhanced colonization of *Salmonella* in the hypoxic regions disables the bactericidal activity of the macrophages and neutrophils[194]. This is evidenced by an absence of effector granulocytes in tumor biopsies, and lack of growth factor β that is produced by tumor cells for the activation of the innate immune system [195]. LPS present in the cell wall of gram-negative *Salmonella* can activate TLRs to initiate a pro-inflammatory cytokine production that recruits immune cells at the tumor site [196,197]. CD8+ T cell infiltration in tumors increases, because of inflammation against Salmonella present within the tumors. The recruited T cells inhibit tumor growth and development via the cross-presentation of tumor antigen by the bacteria. Thus, Salmonella-induced T-cell response in the tumor is proposed to be against both Salmonella and tumor antigen [193]. Additional contributing factors to antitumor efficacy include the type III secretion mechanism, that causes the delivery of toxic peptides from the bacterial cytoplasm directly into the cytoplasm of mammalian cells, selective intra-tumoral intravascular coagulation of tumors, and production or secretion of toxins into the extracellular environment [198]. Thus, *Salmonella* typhimurium(YS1646) is a tumor homing microbe with excellent potential to increase tumor immunotherapy.

Use of Salmonella in clinical trials

Salmonella entered Phase 1 human trials in 2000 for the treatment of metastatic melanoma, however, the outcomes weren't successful [199]. *Salmonella* accumulated focally in two

patients out of 25 receiving dose and one patient was reportedly disease free in a follow-up study [200]. Majority of the patients showed insignificant tumor regression, a consequence of the over-attenuation of *Salmonella*[201]. Thus, the failure of bacteriolytic therapies to elicit significant clinical effect by themselves in humans (despite promising results in murine models) highlights the need to develop modified approaches.

Table 3: Ratio of Colony forming unit of *Salmonella* accumulating in tumors compared to the liver. [179,202]

Tumor type	Tumor:Liver (CFU ratios)
B16 melanoma	9,000:1
C-8186 melanoma	1500:1
LOX melanoma	3,000:1
M27 lung carcinoma	10,000:1
A549 lung carcinoma	300:1
HTB177 lung carcinoma	4,000:1
Murine spontaneous breast tumor	700:1
MDA-MB-231 breast carcinoma	34,000:1
SW-620 colon carcinoma	275:1
HCT 116 colon carcinoma	17,000:1
DLD1 colon carcinoma	15,000:1
CAKI renal carcinoma	250:1

Other bacterial Agents

***Magnetospirillum magneticum* (AMB-1)**

Magnetospirillum magneticum (AMB-1) is a gram-negative motile magnetotactic bacteria [203]. AMB is non-pathogenic and naturally orient along the geomagnetic lines to migrate toward low oxygen tension area[204]. The alignment and movement of AMB-1 towards the magnet (magnetotaxis) is caused by the presence of magnetosomes within the bacteria[205]. Magnetosomes are crystals of iron oxide particles and organize as chains via a dedicated cytoskeleton[206]. Each AMB-1 contains approximately 10 elongated cuboctahedral magnetosomes in a single chain. The magnetosomes provide a positive or negative contrast

on MRI and generate a T1 weighted contrast on MRI[207]. The magnetosomes can also be leveraged to provide thermotherapy with alternative magnetic field[208], especially against colon cancer[209]. Complete disappearance of tumor 30 days following treatment was reported in MDA-MB-231 mice breast cancer model treated with magnetosomes and Alternating Magnetic Field (AMF) induced hyperthermia for 20 minutes[210]. Magnetosomes can be tailored for the delivery of nucleic acids and drugs. For example, cross-linking nanoliposomes on the surface of magnetic bacteria *Magnetococcus Marinus* has been shown to improve the targeting of nanocarriers in HCT116 colorectal xenograft[211]. A key challenge of AMB-1 approach is the required peritumoral injections, which may not be suitable clinically for deep-seated tumors (Table 4). Interestingly, Benoit et al in 2009 using MRI showed that AMB-1 can naturally home to tumors when administered intravenously. They found that AMB-1 colonies from other organs such as spleen and liver depleted after 4 hours, but were present in tumors by day 6[207]. Thus, modifying AMB-1 to attach nanoparticles (e.g. LTSL) for specifically delivering therapeutic agents in the tumors can be an innovative idea[212]. Additionally, AMB-1 can aid the cytokine-induced NK cell tracking, thermotherapy, MRI imaging, and disease diagnosis[213,214].

Table 4: Summary of magnetic bacteria/ magnetosomes application in drug delivery and hyperthermia treatments

Application		**Key results**	**Disadvantage**	**Ref**
Magnetic bacteria				
Drug Delivery	Mc Marinus bound to nanoliposomes for targeted tumor treatment	Cells were magnetically guided for delivery to the hypoxic tumor area	Relied on peritumoral injection	211
MRI contrast agent	AMB-1 injected IV was tested for contrast development	AMB-1 colonized in tumors and generated the T1 weighted positive contrast	Time-dependent accumulation with no magnetic guidance	207

Magnetosomes				
Drug/gene delivery	Delivery of doxorubicin, cytarabine, daunorubicin, CercopinB, apoptin (VP3)	Reduction in drug toxicity and enhanced anti-tumor effect against hepatic and osteosarcoma was noted	Unclear biological fate with delayed drug release was noted [215]	[215-219]
Hyperthermia	Hyperthermia(~42°-43°C) treatment in combination with AMF	Reduced toxicity with improved treatment outcomes for glioblastoma, colon cancer was observed	Long term evaluation of biological fate required	[209,220-222]
MRI contrast agent	Diagnostic detection of tumors; Targeting with specific peptides	Enhanced specificity and sensitivity than conventional imaging for EGFR/HER2+ cells, brain, and pancreatic tumors were observed[223]	Long term evaluation of biological fate required	[224-226]

CENTRAL HYPOTHESIS AND SPECIFIC AIMS of the PhD Dissertation

CENTRAL HYPOTHESIS

Multifunctional LTSLs would enhance chemo-immunotherapy efficacy and real-time monitoring against colorectal cancer

AIM 1: Develop imageable thermosensitive liposomes for real-time estimation of drug delivery and tumor temperature

Hypothesis: Predictable change in tumor ultrasound contrast with imageable LTSL and hyperthermia treatment can act as surrogate marker for real time tumor temperature and drug release.

a. Develop imageable and echogenic LTSLs (E-LTSL) co-loaded with doxorubicin and ultrasound contrast agent (perfluoropentane; PFP) for image-guided doxorubicin delivery.

b. Compare doxorubicin delivery of E-LTSL with echogenic non-temperature sensitive liposomes (E-NTSL) in mouse colon cancer.

c. Correlate ultrasound contrast of E-LTSL and E-NTSL with tumor temperatures

AIM 2: Utilize Salmonella as the LTSL carrier for targeting of tumor hypoxic cores, and modulation of tumor immune environments

Hypothesis: LTSL-laden *Salmonella* (Thermobots) in combination with hyperthermia (40-42ºC) will generate a pro-inflammatory immune environment to improve doxorubicin efficacy against colorectal cancer therapy.

a. Attach LTSL to *Salmonella* via Biotin Streptavidin chemistry to synthesize "thermobots". Evaluate cytotoxicity and cellular uptake of thermobots in vitro.

b. Assess efficacy of thermobots to deliver doxorubicin in combination with High Intensity focused ultrasound (HIFU) mediated hyperthermia.

c. Evaluate the immune cell response and doxorubicin efficacy of thermobot treatment in combination with (HIFU) hyperthermia in murine colon cancer

AIM 3: Augment LTSL delivery with AMB-1 under magnetic guidance to murine colon cancer

Hypothesis: LTSLs attached to AMB-1 and targeting with hyperthermia (40-42ºC) and

halbach array will improve localized chemotherapy of colon cancer.

a. Optimize LTSL attachment to AMB-1 membrane via Biotin Streptavidin chemistry (AMB-LTSL).

b. Evaluate magnetotaxis, imageability and viability of AMB-LTSLs.

c. Determine the cytotoxicity of AMB-LTSL, Dox-LTSL, and AMB-1 with mild hyperthermia C26 colon cancer in vitro.

d. Assess efficiency of Halbach array to magnetically guide AMB-LTSL to tumor core for doxorubicin delivery.

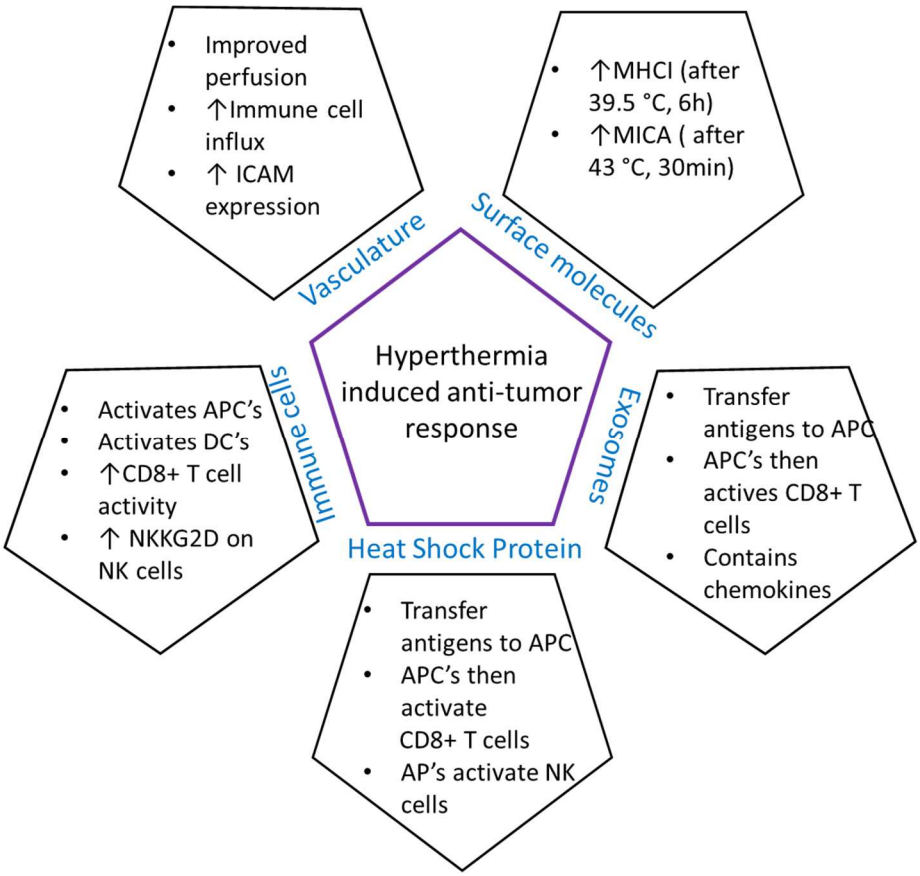

Figure 1: Mechanisms of immune activation with tumor hyperthermia

Tumor hyperthermia enhances the surface expression of MICA, a NKG2D ligand, and MHC class I to improve lysis by natural killer (NK) cells and CD8+ T cells. Heat shock proteins (HSPs) and exosomes released from heated tumor cells can be presented by the antigen presenting cells (APCs) to CD8+ T cells for tumor cell lysis by the NK cells. Hyperthermia can also facilitate trafficking of immune cells in the tumor and draining lymph node.

References

1. Cancer Facts and Figures 2017. *Atlanta: American cancer society;2017* (2017).
2. Cancer Facts & Figures 2018. *Atlanta: American cancer society; 2019* (2019).
3. Meisel, J.L., Venur, V.A., Gnant, M. & Carey, L. Evolution of Targeted Therapy in Breast Cancer: Where Precision Medicine Began. *American Society of Clinical Oncology Educational Book*, 78-86 (2018).
4. Amer, M.H. Gene therapy for cancer: present status and future perspective. *Molecular and cellular therapies***2**, 27-27 (2014).
5. Klingemann, H.G.*, et al.* Bone marrow transplantation in patients aged 45 years and older. *Blood***67**, 770-776 (1986).
6. Miller, K.D.*, et al.* Cancer treatment and survivorship statistics, 2016. *CA Cancer J Clin***66**, 271-289 (2016).
7. Hermann Brenner, M.K., Christian Peter Pox. Colorectal cancer. *Lancet (London, England)***383: 1490–502**(2014).
8. Ciombor, K.K., Wu, C. & Goldberg, R.M. Recent therapeutic advances in the treatment of colorectal cancer. *Annual review of medicine***66**, 83-95 (2015).
9. Zaniboni, A. & Labianca, R. Adjuvant therapy for stage II colon cancer: an elephant in the living room? *Annals of oncology : official journal of the European Society for Medical Oncology***15**, 1310-1318 (2004).
10. Field, K.M.*, et al.* Chemotherapy treatments for metastatic colorectal cancer: is evidence-based medicine in practice? *Journal of oncology practice***4**, 271-276 (2008).
11. Andre, T.*, et al.* Oxaliplatin, fluorouracil, and leucovorin as adjuvant treatment for colon cancer. *The New England journal of medicine***350**, 2343-2351 (2004).
12. Chabner, B.A. & Roberts, T.G., Jr. Timeline: Chemotherapy and the war on cancer. *Nat Rev Cancer***5**, 65-72 (2005).
13. Hill, B.T.*, et al.* Low-dose twice-daily fractionated X-irradiation of ovarian tumor cells in vitro generates drug-resistant cells overexpressing two multidrug resistance-associated proteins, P-glycoprotein and MRP1. *Anti-cancer drugs***11**, 193-200 (2000).
14. Fraile, R.J., Baker, L.H., Buroker, T.R., Horwitz, J. & Vaitkevicius, V.K. Pharmacokinetics of 5-fluorouracil administered orally, by rapid intravenous and by slow infusion. *Cancer research***40**, 2223-2228 (1980).
15. Sinha, R., Kim, G.J., Nie, S. & Shin, D.M. Nanotechnology in cancer therapeutics: bioconjugated nanoparticles for drug delivery. *Molecular cancer therapeutics***5**, 1909-1917 (2006).
16. Hong, M., Zhu, S., Jiang, Y., Tang, G. & Pei, Y. Efficient tumor targeting of hydroxycamptothecin loaded PEGylated niosomes modified with transferrin. *Journal of controlled release : official journal of the Controlled Release Society***133**, 96-102 (2009).
17. Bagshawe, K.D., Sharma, S.K. & Begent, R.H. Antibody-directed enzyme prodrug therapy (ADEPT) for cancer. *Expert opinion on biological therapy***4**, 1777-1789 (2004).
18. Smaglo, B.G., Aldeghaither, D. & Weiner, L.M. The development of immunoconjugates for targeted cancer therapy. *Nature reviews. Clinical oncology***11**, 637-648 (2014).

19. Brigger, I., Dubernet, C. & Couvreur, P. Nanoparticles in cancer therapy and diagnosis. *Advanced drug delivery reviews***64**, 24-36 (2012).
20. Tran, S., DeGiovanni, P.-J., Piel, B. & Rai, P. Cancer nanomedicine: a review of recent success in drug delivery. *Clinical and translational medicine***6**, 44-44 (2017).
21. Wicki, A., Witzigmann, D., Balasubramanian, V. & Huwyler, J. Nanomedicine in cancer therapy: challenges, opportunities, and clinical applications. *Journal of controlled release : official journal of the Controlled Release Society***200**, 138-157 (2015).
22. Bregoli, L.*, et al.* Nanomedicine applied to translational oncology: A future perspective on cancer treatment. *Nanomedicine : nanotechnology, biology, and medicine***12**, 81-103 (2016).
23. Albanese, A., Tang, P.S. & Chan, W.C. The effect of nanoparticle size, shape, and surface chemistry on biological systems. *Annual review of biomedical engineering***14**, 1-16 (2012).
24. Cho, K., Wang, X., Nie, S., Chen, Z.G. & Shin, D.M. Therapeutic nanoparticles for drug delivery in cancer. *Clinical cancer research : an official journal of the American Association for Cancer Research***14**, 1310-1316 (2008).
25. Eckert, F.*, et al.* Potential Role of CXCR4 Targeting in the Context of Radiotherapy and Immunotherapy of Cancer. *Frontiers in immunology***9**, 3018-3018 (2018).
26. Ektate, K.*, et al.* Motion Compensated Ultrasound Imaging Allows Thermometry and Image Guided Drug Delivery Monitoring from Echogenic Liposomes. *Theranostics***6**, 1963 (2016).
27. VanOsdol, J.*, et al.* Sequential HIFU heating and nanobubble encapsulation provide efficient drug penetration from stealth and temperature sensitive liposomes in colon cancer. *Journal of Controlled Release***247**, 55-63 (2017).
28. Northfelt, D.W.*, et al.* Pegylated-liposomal doxorubicin versus doxorubicin, bleomycin, and vincristine in the treatment of AIDS-related Kaposi's sarcoma: results of a randomized phase III clinical trial. *Journal of Clinical Oncology***16**, 2445-2451 (1998).
29. Audouy, S.L., de Leij, L.M.H., Hoekstra, D. & Molema, G. In Vivo Characteristics of Cationic Liposomes as Delivery Vectors for Gene Therapy. *Pharm Res***19**, 1599-1605 (2002).
30. Ruoslahti, E., Bhatia, S.N. & Sailor, M.J. Targeting of drugs and nanoparticles to tumors. *The Journal of Cell Biology***188**, 759-768 (2010).
31. Bandak, S., Goren, D., Horowitz, A., Tzemach, D. & Gabizon, A. Pharmacological studies of cisplatin encapsulated in long-circulating liposomes in mouse tumor models. *Anti-Cancer Drugs***10**, 911-920 (1999).
32. Krishnamurthy, S., Ke, X. & Yang, Y.Y. Delivery of therapeutics using nanocarriers for targeting cancer cells and cancer stem cells. *Nanomedicine (London, England)***10**, 143-160 (2015).
33. Mitchell, N.*, et al.* Incorporation of paramagnetic, fluorescent and PET/SPECT contrast agents into liposomes for multimodal imaging. *Biomaterials***34**, 1179-1192 (2013).
34. Maples, D.*, et al.* Synthesis and characterisation of ultrasound imageable heat-sensitive liposomes for HIFU therapy. *International Journal of Hyperthermia*, 1-12 (2015);31(6):674–685.

35. Bangham, A.D., Standish, M.M. & Watkins, J.C. Diffusion of univalent ions across the lamellae of swollen phospholipids. *Journal of molecular biology***13**, 238-252 (1965).
36. Chrai SS, M.R., Imran A. . Liposomes: a review. . *Bio Pharm.*, 10–14 (2001).
37. Sun, T.*, et al.* Engineered nanoparticles for drug delivery in cancer therapy. *Angewandte Chemie (International ed. in English)***53**, 12320-12364 (2014).
38. Torchilin, V.W., V. & 77–101., p. *Liposomes: A Practical Approach*, (Oxford University Press, Kettering, UK, 2003).
39. Sharma, A. & Sharma, U.S. Liposomes in drug delivery: Progress and limitations. *International journal of pharmaceutics***154**, 123-140 (1997).
40. Sharif Mohammad Shaheen, F.R.S.A., Md. Nazir Hossen , Maruf Ahmed , Md. Shah Amran and Md. Anwar-UL-Islam Liposome as a Carrier for Advanced Drug Delivery. *Pakistan Journal of Biological Sciences***9**, 1181-1191 (2006).
41. Ahl, P.L.*, et al.* Enhancement of the in vivo circulation lifetime of L-alpha-distearoylphosphatidylcholine liposomes: importance of liposomal aggregation versus complement opsonization. *Biochimica et biophysica acta***1329**, 370-382 (1997).
42. Allen, C.*, et al.* Controlling the physical behavior and biological performance of liposome formulations through use of surface grafted poly(ethylene glycol). *Bioscience reports***22**, 225-250 (2002).
43. Drummond, D.C., Meyer, O., Hong, K., Kirpotin, D.B. & Papahadjopoulos, D. Optimizing liposomes for delivery of chemotherapeutic agents to solid tumors. *Pharmacological reviews***51**, 691-743 (1999).
44. Allen, T.M. A study of phospholipid interactions between high-density lipoproteins and small unilamellar vesicles. *Biochimica et Biophysica Acta (BBA) - Biomembranes***640**, 385-397 (1981).
45. Scherphof, G., Roerdink, F., Waite, M. & Parks, J. Disintegration of phosphatidylcholine liposomes in plasma as a result of interaction with high-density lipoproteins. *Biochimica et biophysica acta***542**, 296-307 (1978).
46. Papahadjopoulos, D.*, et al.* Sterically stabilized liposomes: improvements in pharmacokinetics and antitumor therapeutic efficacy. *Proceedings of the National Academy of Sciences of the United States of America***88**, 11460-11464 (1991).
47. Gabizon, A.*, et al.* Prolonged circulation time and enhanced accumulation in malignant exudates of doxorubicin encapsulated in polyethylene-glycol coated liposomes. *Cancer research***54**, 987-992 (1994).
48. Gabizon, A.A. Selective tumor localization and improved therapeutic index of anthracyclines encapsulated in long-circulating liposomes. *Cancer research***52**, 891-896 (1992).
49. Gabizon, A. & Papahadjopoulos, D. Liposome formulations with prolonged circulation time in blood and enhanced uptake by tumors. *Proceedings of the National Academy of Sciences of the United States of America***85**, 6949-6953 (1988).
50. Klibanov, A.L., Maruyama, K., Torchilin, V.P. & Huang, L. Amphipathic polyethyleneglycols effectively prolong the circulation time of liposomes. *FEBS letters***268**, 235-237 (1990).
51. Blume, G. & Cevc, G. Liposomes for the sustained drug release in vivo. *Biochimica et biophysica acta***1029**, 91-97 (1990).

52. Allen, T.M., Hansen, C., Martin, F., Redemann, C. & Yau-Young, A. Liposomes containing synthetic lipid derivatives of poly(ethylene glycol) show prolonged circulation half-lives in vivo. *Biochimica et biophysica acta***1066**, 29-36 (1991).
53. Allen, T.M. & Chonn, A. Large unilamellar liposomes with low uptake into the reticuloendothelial system. *FEBS letters***223**, 42-46 (1987).
54. Senior, J., Delgado, C., Fisher, D., Tilcock, C. & Gregoriadis, G. Influence of surface hydrophilicity of liposomes on their interaction with plasma protein and clearance from the circulation: studies with poly(ethylene glycol)-coated vesicles. *Biochimica et biophysica acta***1062**, 77-82 (1991).
55. Allen, T.M. & Hansen, C. Pharmacokinetics of stealth versus conventional liposomes: effect of dose. *Biochimica et biophysica acta***1068**, 133-141 (1991).
56. Needham D, K.K., Mcintosh TJ, Dewhirst M, Wu N, Lasic DD. Polymer-grafted liposomes, Physical basis for the "Stealth" property. *J. Liposome Res.* , 411-430 (1992).
57. Woodle, M.C. & Lasic, D.D. Sterically stabilized liposomes. *Biochimica et biophysica acta***1113**, 171-199 (1992).
58. Moghimi, S.M., Muir, I.S., Illum, L., Davis, S.S. & Kolb-Bachofen, V. Coating particles with a block co-polymer (poloxamine-908) suppresses opsonization but permits the activity of dysopsonins in the serum. *Biochimica et biophysica acta***1179**, 157-165 (1993).
59. Johnstone, S.A., Masin, D., Mayer, L. & Bally, M.B. Surface-associated serum proteins inhibit the uptake of phosphatidylserine and poly(ethylene glycol) liposomes by mouse macrophages. *Biochimica et biophysica acta***1513**, 25-37 (2001).
60. Maeda, H. The enhanced permeability and retention (EPR) effect in tumor vasculature: the key role of tumor-selective macromolecular drug targeting. *Advances in enzyme regulation***41**, 189-207 (2001).
61. Dass, C.R., Walker, T.L., Burton, M.A. & Decruz, E.E. Enhanced Anticancer Therapy Mediated by Specialized Liposomes. *Journal of Pharmacy and Pharmacology***49**, 972-975 (1997).
62. Adedoyin, A*., et al.* Pharmacokinetic profile of ABELCET (amphotericin B lipid complex injection): combined experience from phase I and phase II studies. *Antimicrobial agents and chemotherapy***41**, 2201-2208 (1997).
63. Boswell, G.W., Buell, D. & Bekersky, I. AmBisome (liposomal amphotericin B): a comparative review. *Journal of clinical pharmacology***38**, 583-592 (1998).
64. White, M.H*., et al.* Amphotericin B colloidal dispersion vs. amphotericin B as therapy for invasive aspergillosis. *Clinical infectious diseases : an official publication of the Infectious Diseases Society of America***24**, 635-642 (1997).
65. Sanders, S.W., Buchi, K.N., Goddard, M.S., Lang, J.K. & Tolman, K.G. Single-dose pharmacokinetics and tolerance of a cholesteryl sulfate complex of amphotericin B administered to healthy volunteers. *Antimicrobial agents and chemotherapy***35**, 1029-1034 (1991).
66. Petre, C.E. & Dittmer, D.P. Liposomal daunorubicin as treatment for Kaposi's sarcoma. *Int J Nanomedicine***2**, 277-288 (2007).
67. Fumagalli, L*., et al.* The pharmacokinetics of liposomal encapsulated daunorubicin are not modified by HAART in patients with HIV-associated Kaposi's sarcoma. *Cancer chemotherapy and pharmacology***45**, 495-501 (2000).

68. Murry, D.J. & Blaney, S.M. Clinical pharmacology of encapsulated sustained-release cytarabine. *The Annals of pharmacotherapy***34**, 1173-1178 (2000).
69. Chamberlain, M.C., Kormanik, P., Howell, S.B. & Kim, S. Pharmacokinetics of intralumbar DTC-101 for the treatment of leptomeningeal metastases. *Archives of neurology***52**, 912-917 (1995).
70. Viscusi, E.R., Kopacz, D., Hartrick, C., Martin, G. & Manvelian, G. Single-dose extended-release epidural morphine for pain following hip arthroplasty. *American journal of therapeutics***13**, 423-431 (2006).
71. Hartrick, C.T. & Hartrick, K.A. Extended-release epidural morphine (DepoDur): review and safety analysis. *Expert review of neurotherapeutics***8**, 1641-1648 (2008).
72. Angst, M.S. & Drover, D.R. Pharmacology of drugs formulated with DepoFoam: a sustained release drug delivery system for parenteral administration using multivesicular liposome technology. *Clinical pharmacokinetics***45**, 1153-1176 (2006).
73. Clarke, P.D., Adams, P., Ibanez, R. & Herzog, C. Rate, intensity, and duration of local reactions to a virosome-adjuvanted vs. an aluminium-adsorbed hepatitis A vaccine in UK travellers. *Travel medicine and infectious disease***4**, 313-318 (2006).
74. Bovier, P.A*., et al.* Long-term immunogenicity of an inactivated virosome hepatitis A vaccine. *Journal of medical virology***68**, 489-493 (2002).
75. Conne, P*., et al.* Immunogenicity of trivalent subunit versus virosome-formulated influenza vaccines in geriatric patients. *Vaccine***15**, 1675-1679 (1997).
76. Gluck, R*., et al.* Immunogenicity of new virosome influenza vaccine in elderly people. *Lancet (London, England)***344**, 160-163 (1994).
77. Balazsovits, J.A*., et al.* Analysis of the effect of liposome encapsulation on the vesicant properties, acute and cardiac toxicities, and antitumor efficacy of doxorubicin. *Cancer chemotherapy and pharmacology***23**, 81-86 (1989).
78. Cowens, J.W*., et al.* Initial clinical (phase I) trial of TLC D-99 (doxorubicin encapsulated in liposomes). *Cancer research***53**, 2796-2802 (1993).
79. Webb, M.S., Harasym, T.O., Masin, D., Bally, M.B. & Mayer, L.D. Sphingomyelin-cholesterol liposomes significantly enhance the pharmacokinetic and therapeutic properties of vincristine in murine and human tumour models. *British journal of cancer***72**, 896-904 (1995).
80. Rodriguez, M.A*., et al.* Vincristine sulfate liposomes injection (Marqibo) in heavily pretreated patients with refractory aggressive non-Hodgkin lymphoma: report of the pivotal phase 2 study. *Cancer***115**, 3475-3482 (2009).
81. Photodynamic therapy of subfoveal choroidal neovascularization in age-related macular degeneration with verteporfin: one-year results of 2 randomized clinical trials--TAP report. Treatment of age-related macular degeneration with photodynamic therapy (TAP) Study Group. *Archives of ophthalmology (Chicago, Ill. : 1960)***117**, 1329-1345 (1999).
82. Working, P.K. & Dayan, A.D. Pharmacological-toxicological expert report. CAELYX. (Stealth liposomal doxorubicin HCl). *Human & experimental toxicology***15**, 751-785 (1996).
83. Smith, J.A*., et al.* Is it equivalent? Evaluation of the clinical activity of single agent Lipodox® compared to single agent Doxil® in ovarian cancer treatment. *Journal of Oncology Pharmacy Practice***22**, 599-604 (2015).

84. Burade, V.*, et al.* Lipodox® (generic doxorubicin hydrochloride liposome injection): in vivo efficacy and bioequivalence versus Caelyx® (doxorubicin hydrochloride liposome injection) in human mammary carcinoma (MX-1) xenograft and syngeneic fibrosarcoma (WEHI 164) mouse models. *BMC cancer***17**, 405-405 (2017).
85. Tagami, T. & Ozeki, T. Recent Trends in Clinical Trials Related to Carrier-Based Drugs. *Journal of Pharmaceutical Sciences***106**, 2219-2226 (2017).
86. Drummond, D.C.*, et al.* Development of a highly active nanoliposomal irinotecan using a novel intraliposomal stabilization strategy. *Cancer research***66**, 3271-3277 (2006).
87. Wang-Gillam, A.*, et al.* Nanoliposomal irinotecan with fluorouracil and folinic acid in metastatic pancreatic cancer after previous gemcitabine-based therapy (NAPOLI-1): a global, randomised, open-label, phase 3 trial. *Lancet (London, England)***387**, 545-557 (2016).
88. Alphandery, E., Grand-Dewyse, P., Lefevre, R., Mandawala, C. & Durand-Dubief, M. Cancer therapy using nanoformulated substances: scientific, regulatory and financial aspects. *Expert review of anticancer therapy***15**, 1233-1255 (2015).
89. Anderson, P.M.*, et al.* Mifamurtide in metastatic and recurrent osteosarcoma: a patient access study with pharmacokinetic, pharmacodynamic, and safety assessments. *Pediatric blood & cancer***61**, 238-244 (2014).
90. Meyers, P.A.*, et al.* Osteosarcoma: the addition of muramyl tripeptide to chemotherapy improves overall survival--a report from the Children's Oncology Group. *J Clin Oncol***26**, 633-638 (2008).
91. Kopper, N.W., Gudeman, J. & Thompson, D.J. Transdermal hormone therapy in postmenopausal women: a review of metabolic effects and drug delivery technologies. *Drug design, development and therapy***2**, 193-202 (2009).
92. Hua, S. Lipid-based nano-delivery systems for skin delivery of drugs and bioactives. *Frontiers in pharmacology***6**, 219-219 (2015).
93. Review Hyperthermia and liposomes AU - G. KONG, M. W. DEWHIRST. *International Journal of Hyperthermia***15**, 345-370 (1999).
94. Yatvin, M.B., Weinstein, J.N., Dennis, W.H. & Blumenthal, R. Design of liposomes for enhanced local release of drugs by hyperthermia. *Science (New York, N.Y.)***202**, 1290-1293 (1978).
95. Chen, J.*, et al.* Thermosensitive liposomes with higher phase transition temperature for targeted drug delivery to tumor. *International journal of pharmaceutics***475**, 408-415 (2014).
96. Slingerland, M., Guchelaar, H.J. & Gelderblom, H. Liposomal drug formulations in cancer therapy: 15 years along the road. *Drug discovery today***17**, 160-166 (2012).
97. Puri, A. Phototriggerable liposomes: current research and future perspectives. *Pharmaceutics***6**, 1-25 (2013).
98. Dromi, S.*, et al.* Pulsed-high intensity focused ultrasound and low temperature-sensitive liposomes for enhanced targeted drug delivery and antitumor effect. *Clinical cancer research : an official journal of the American Association for Cancer Research***13**, 2722-2727 (2007).
99. Kneidl, B., Peller, M., Winter, G., Lindner, L.H. & Hossann, M. Thermosensitive liposomal drug delivery systems: state of the art review. *International journal of nanomedicine***9**, 4387-4398 (2014).

100. Wen, D. Nanoparticle-Related Heat Transfer Phenomenon and Its Application in Biomedical Fields AU - Wen, Dongsheng. *Heat Transfer Engineering***34**, 1171-1179 (2013).
101. Kennedy, J.E., Ter Haar, G.R. & Cranston, D. High intensity focused ultrasound: surgery of the future? *Br J Radiol***76**, 590-599 (2003).
102. Haar, G.T. & Coussios, C. High intensity focused ultrasound: physical principles and devices. *International journal of hyperthermia : the official journal of European Society for Hyperthermic Oncology, North American Hyperthermia Group***23**, 89-104 (2007).
103. Miller, D.L.*, et al.* Overview of therapeutic ultrasound applications and safety considerations. *Journal of ultrasound in medicine : official journal of the American Institute of Ultrasound in Medicine***31**, 623-634 (2012).
104. Moroz, P., Jones, S.K. & Gray, B.N. Magnetically mediated hyperthermia: current status and future directions. *International journal of hyperthermia : the official journal of European Society for Hyperthermic Oncology, North American Hyperthermia Group***18**, 267-284 (2002).
105. Kong, G.*, et al.* Efficacy of liposomes and hyperthermia in a human tumor xenograft model: importance of triggered drug release. *Cancer research***60**, 6950-6957 (2000).
106. Sapareto, S.A. & Dewey, W.C. Thermal dose determination in cancer therapy. *International journal of radiation oncology, biology, physics***10**, 787-800 (1984).
107. Horowitz, M. & Robinson, S.D. Heat shock proteins and the heat shock response during hyperthermia and its modulation by altered physiological conditions. *Progress in brain research***162**, 433-446 (2007).
108. Song, C.W. Effect of local hyperthermia on blood flow and microenvironment: a review. *Cancer research***44**, 4721s-4730s (1984).
109. Meyer, R.E., Braun, R.D., Rosner, G.L. & Dewhirst, M.W. Local 42°C Hyperthermia Improves Vascular Conductance of the R3230Ac Rat Mammary Adenocarcinoma during Sodium Nitroprusside Infusion. *Radiation research***154**, 196-201 (2000).
110. Kong, G., Braun, R.D. & Dewhirst, M.W. Characterization of the effect of hyperthermia on nanoparticle extravasation from tumor vasculature. *Cancer research***61**, 3027-3032 (2001).
111. Toraya-Brown, S. & Fiering, S. Local tumour hyperthermia as immunotherapy for metastatic cancer. *International journal of hyperthermia : the official journal of European Society for Hyperthermic Oncology, North American Hyperthermia Group***30**, 531-539 (2014).
112. Nishida, T., Akagi, K. & Tanaka, Y. Correlation between cell killing effect and cell membrane potential after heat treatment: analysis using fluorescent dye and flow cytometry. *International journal of hyperthermia : the official journal of European Society for Hyperthermic Oncology, North American Hyperthermia Group***13**, 227-234 (1997).
113. Malhotra, A., Heynen, M.L.P. & Lepock, J.R. Role of Extracellular Calcium in the Hyperthermic Killing of CHL V79 Cells. *Radiation research***112**, 478-489 (1987).
114. Jorritsma, J.B.M., Kampinga, H.H., Scaf, A.H.J. & Konings, A.W.T. Strand break repair, DNA polymerase activity and heat radiosensitization in thermotolerant cells. *International Journal of Hyperthermia***1**, 131-145 (1985).

115. Spiro, I.J., Denman, D.L. & Dewey, W.C. Effect of Hyperthermia on CHO DNA Polymerases α and β. *Radiation research***89**, 134-149 (1982).
116. Henle, K.J. & Leeper, D.B. Effects of hyperthermia (45 degrees) on macromolecular synthesis in Chinese hamster ovary cells. *Cancer research***39**, 2665-2674 (1979).
117. Ostberg, J.R., Dayanc, B.E., Yuan, M., Oflazoglu, E. & Repasky, E.A. Enhancement of natural killer (NK) cell cytotoxicity by fever-range thermal stress is dependent on NKG2D function and is associated with plasma membrane NKG2D clustering and increased expression of MICA on target cells. *Journal of leukocyte biology***82**, 1322-1331 (2007).
118. Ito, A.*, et al.* Tumor regression by combined immunotherapy and hyperthermia using magnetic nanoparticles in an experimental subcutaneous murine melanoma. *Cancer Sci***94**, 308-313 (2003).
119. Burd, R.*, et al.* Tumor cell apoptosis, lymphocyte recruitment and tumor vascular changes are induced by low temperature, long duration (fever-like) whole body hyperthermia. *Journal of cellular physiology***177**, 137-147 (1998).
120. Ostberg, J.R. & Repasky, E.A. Emerging evidence indicates that physiologically relevant thermal stress regulates dendritic cell function. *Cancer immunology, immunotherapy : CII***55**, 292-298 (2006).
121. Kluger, M.J., Ringler, D.H. & Anver, M.R. Fever and survival. *Science (New York, N.Y.)***188**, 166-168 (1975).
122. van Bruggen, I., Robertson, T.A. & Papadimitriou, J.M. The effect of mild hyperthermia on the morphology and function of murine resident peritoneal macrophages. *Experimental and molecular pathology***55**, 119-134 (1991).
123. Ostberg, J.R., Patel, R. & Repasky, E.A. Regulation of immune activity by mild (fever-range) whole body hyperthermia: effects on epidermal Langerhans cells. *Cell stress & chaperones***5**, 458-461 (2000).
124. Tournier, J.N.*, et al.* Fever-like thermal conditions regulate the activation of maturing dendritic cells. *Journal of leukocyte biology***73**, 493-501 (2003).
125. Zheng, H., Benjamin, I.J., Basu, S. & Li, Z. Heat shock factor 1-independent activation of dendritic cells by heat shock: implication for the uncoupling of heat-mediated immunoregulation from the heat shock response. *European journal of immunology***33**, 1754-1762 (2003).
126. Jaattela, M. Heat shock proteins as cellular lifeguards. *Annals of medicine***31**, 261-271 (1999).
127. Multhoff, G.*, et al.* Heat shock protein 72 on tumor cells: a recognition structure for natural killer cells. *Journal of immunology (Baltimore, Md. : 1950)***158**, 4341-4350 (1997).
128. Vabulas, R.M.*, et al.* HSP70 as endogenous stimulus of the Toll/interleukin-1 receptor signal pathway. *The Journal of biological chemistry***277**, 15107-15112 (2002).
129. Todryk, S.*, et al.* Heat shock protein 70 induced during tumor cell killing induces Th1 cytokines and targets immature dendritic cell precursors to enhance antigen uptake. *Journal of immunology (Baltimore, Md. : 1950)***163**, 1398-1408 (1999).
130. Noessner, E.*, et al.* Tumor-derived heat shock protein 70 peptide complexes are cross-presented by human dendritic cells. *Journal of immunology (Baltimore, Md. : 1950)***169**, 5424-5432 (2002).

131. Suzue, K., Zhou, X., Eisen, H.N. & Young, R.A. Heat shock fusion proteins as vehicles for antigen delivery into the major histocompatibility complex class I presentation pathway. *Proceedings of the National Academy of Sciences of the United States of America***94**, 13146-13151 (1997).
132. Binder, R.J. & Srivastava, P.K. Peptides chaperoned by heat-shock proteins are a necessary and sufficient source of antigen in the cross-priming of CD8+ T cells. *Nature immunology***6**, 593-599 (2005).
133. Lin, K., Rockliffe, N., Johnson, G.G., Sherrington, P.D. & Pettitt, A.R. Hsp90 inhibition has opposing effects on wild-type and mutant p53 and induces p21 expression and cytotoxicity irrespective of p53/ATM status in chronic lymphocytic leukaemia cells. *Oncogene***27**, 2445-2455 (2008).
134. Ito, A., Fujioka, M., Tanaka, K., Kobayashi, T. & Honda, H. Screening of cytokines to enhance vaccine effects of heat shock protein 70-rich tumor cell lysate. *Journal of bioscience and bioengineering***100**, 36-42 (2005).
135. Thery, C., Zitvogel, L. & Amigorena, S. Exosomes: composition, biogenesis and function. *Nature reviews. Immunology***2**, 569-579 (2002).
136. Wolfers, J.*, et al.* Tumor-derived exosomes are a source of shared tumor rejection antigens for CTL cross-priming. *Nat Med***7**, 297-303 (2001).
137. Chen, T., Guo, J., Yang, M., Zhu, X. & Cao, X. Chemokine-containing exosomes are released from heat-stressed tumor cells via lipid raft-dependent pathway and act as efficient tumor vaccine. *Journal of immunology (Baltimore, Md. : 1950)***186**, 2219-2228 (2011).
138. Sukari, A., Nagasaka, M., Al-Hadidi, A. & Lum, L.G. Cancer Immunology and Immunotherapy. *Anticancer research***36**, 5593-5606 (2016).
139. Chen, D.S. & Mellman, I. Oncology meets immunology: the cancer-immunity cycle. *Immunity***39**, 1-10 (2013).
140. Kolaczkowska, E. & Kubes, P. Neutrophil recruitment and function in health and inflammation. *Nature reviews. Immunology***13**, 159-175 (2013).
141. Powell, D.R. & Huttenlocher, A. Neutrophils in the Tumor Microenvironment. *Trends in Immunology***37**, 41-52 (2016).
142. Mayadas, T.N., Cullere, X. & Lowell, C.A. The multifaceted functions of neutrophils. *Annual review of pathology***9**, 181-218 (2014).
143. Pillay, J.*, et al.* A subset of neutrophils in human systemic inflammation inhibits T cell responses through Mac-1. *J Clin Invest***122**, 327-336 (2012).
144. Bekes, E.M.*, et al.* Tumor-recruited neutrophils and neutrophil TIMP-free MMP-9 regulate coordinately the levels of tumor angiogenesis and efficiency of malignant cell intravasation. *The American journal of pathology***179**, 1455-1470 (2011).
145. Gabrilovich, D.I. & Nagaraj, S. Myeloid-derived suppressor cells as regulators of the immune system. *Nature reviews. Immunology***9**, 162-174 (2009).
146. Sinha, P., Clements, V.K., Bunt, S.K., Albelda, S.M. & Ostrand-Rosenberg, S. Cross-talk between myeloid-derived suppressor cells and macrophages subverts tumor immunity toward a type 2 response. *Journal of immunology (Baltimore, Md. : 1950)***179**, 977-983 (2007).
147. Murdoch, C., Muthana, M., Coffelt, S.B. & Lewis, C.E. The role of myeloid cells in the promotion of tumour angiogenesis. *Nature Reviews Cancer***8**, 618 (2008).

148. Sica, A., Schioppa, T., Mantovani, A. & Allavena, P. Tumour-associated macrophages are a distinct M2 polarised population promoting tumour progression: Potential targets of anti-cancer therapy. *European Journal of Cancer***42**, 717-727 (2006).
149. Dey, A., Allen, J. & Hankey-Giblin, P.A. Ontogeny and Polarization of Macrophages in Inflammation: Blood Monocytes Versus Tissue Macrophages. *Frontiers in immunology***5**(2015).
150. Seidel, J.A., Otsuka, A. & Kabashima, K. Anti-PD-1 and Anti-CTLA-4 Therapies in Cancer: Mechanisms of Action, Efficacy, and Limitations. *Frontiers in oncology***8**, 86-86 (2018).
151. Wing, K.*, et al.* CTLA-4 control over Foxp3+ regulatory T cell function. *Science (New York, N.Y.)***322**, 271-275 (2008).
152. Qureshi, O.S.*, et al.* Trans-endocytosis of CD80 and CD86: a molecular basis for the cell-extrinsic function of CTLA-4. *Science (New York, N.Y.)***332**, 600-603 (2011).
153. Rudd, C.E., Taylor, A. & Schneider, H. CD28 and CTLA-4 coreceptor expression and signal transduction. *Immunological reviews***229**, 12-26 (2009).
154. Nishimura, H., Nose, M., Hiai, H., Minato, N. & Honjo, T. Development of lupus-like autoimmune diseases by disruption of the PD-1 gene encoding an ITIM motif-carrying immunoreceptor. *Immunity***11**, 141-151 (1999).
155. Latchman, Y.*, et al.* PD-L2 is a second ligand for PD-1 and inhibits T cell activation. *Nature immunology***2**, 261-268 (2001).
156. Francisco, L.M.*, et al.* PD-L1 regulates the development, maintenance, and function of induced regulatory T cells. *The Journal of experimental medicine***206**, 3015-3029 (2009).
157. Tanaka, A. & Sakaguchi, S. Regulatory T cells in cancer immunotherapy. *Cell Research***27**, 109 (2016).
158. Rosenberg, S.A., Yang, J.C. & Restifo, N.P. Cancer immunotherapy: moving beyond current vaccines. *Nat Med***10**, 909-915 (2004).
159. Sakaguchi, S., Yamaguchi, T., Nomura, T. & Ono, M. Regulatory T cells and immune tolerance. *Cell***133**, 775-787 (2008).
160. Morikawa, H. & Sakaguchi, S. Genetic and epigenetic basis of Treg cell development and function: from a FoxP3-centered view to an epigenome-defined view of natural Treg cells. *Immunological reviews***259**, 192-205 (2014).
161. Avogadri, F.*, et al.* Cancer Immunotherapy Based on Killing of Salmonella-Infected Tumor Cells. *Cancer research***65**, 3920-3927 (2005).
162. Sartor, R.B. Therapeutic manipulation of the enteric microflora in inflammatory bowel diseases: antibiotics, probiotics, and prebiotics. *Gastroenterology***126**, 1620-1633 (2004).
163. Ruckdeschel, J.C., Codish, S.D., Stranahan, A. & McKneally, M.F. Postoperative Empyema Improves Survival in Lung Cancer. *New England Journal of Medicine***287**, 1013-1017 (1972).
164. Felgner, S., Kocijancic, D., Frahm, M. & Weiss, S. Bacteria in Cancer Therapy: Renaissance of an Old Concept. *International journal of microbiology***2016**, 8451728-8451728 (2016).

165. Roussakow, S. The History of Hyperthermia Rise and Decline. *Conference Papers in Medicine***2013**, 40 (2013).
166. Hoption Cann, S.A., van Netten, J.P. & van Netten, C. Dr William Coley and tumour regression: a place in history or in the future. *Postgraduate Medical Journal***79**, 672-680 (2003).
167. Coley, W.B. The treatment of malignant tumors by repeated inoculations of *Erysipelas*: with a report of ten original cases. *The American Journal of the Medical Sciences* **105**, 487 ((1827-1924)).
168. Coley, W.B. II. Contribution to the Knowledge of Sarcoma. *Annals of surgery***14**, 199-220 (1891).
169. McCarthy, J., Sullivan, P. & Wright, P. Culture, personal experience and agency. *British Journal of Social Psychology***45**, 421-439 (2006).
170. Dang, L.H., Bettegowda, C., Huso, D.L., Kinzler, K.W. & Vogelstein, B. Combination bacteriolytic therapy for the treatment of experimental tumors. *Proc Natl Acad Sci U S A***98**, 15155-15160 (2001).
171. Fernando, R., Downs, J., Maples, D. & Ranjan, A. MRI-guided monitoring of thermal dose and targeted drug delivery for cancer therapy. *Pharmaceutical research***30**, 2709-2717 (2013).
172. Park, S.M.*, et al.* Novel temperature-triggered liposome with high stability: formulation, in vitro evaluation, and in vivo study combined with high-intensity focused ultrasound (HIFU). *Journal of controlled release : official journal of the Controlled Release Society***170**, 373-379 (2013).
173. Chen, H. & Hwang, J.H. Ultrasound-targeted microbubble destruction for chemotherapeutic drug delivery to solid tumors. *Journal of Therapeutic Ultrasound***1**, 10-10 (2013).
174. Solomon, R. & Gabizon, A.A. Clinical Pharmacology of Liposomal Anthracyclines: Focus on Pegylated Liposomal Doxorubicin. *Clinical Lymphoma and Myeloma***8**, 21-32 (2008).
175. Yu, Y.A.*, et al.* Visualization of tumors and metastases in live animals with bacteria and vaccinia virus encoding light-emitting proteins. *Nature biotechnology***22**, 313-320 (2004).
176. Sznol, M., Lin, S.L., Bermudes, D., Zheng, L.M. & King, I. Use of preferentially replicating bacteria for the treatment of cancer. *The Journal of clinical investigation***105**, 1027-1030 (2000).
177. Kasinskas, R.W. & Forbes, N.S. Salmonella typhimurium specifically chemotax and proliferate in heterogeneous tumor tissue in vitro. *Biotechnol Bioeng***94**, 710-721 (2006).
178. Kasinskas, R.W. & Forbes, N.S. Salmonella typhimurium lacking ribose chemoreceptors localize in tumor quiescence and induce apoptosis. *Cancer research***67**, 3201-3209 (2007).
179. Sznol, M., Lin, S.L., Bermudes, D., Zheng, L.-m. & King, I. Use of preferentially replicating bacteria for the treatment of cancer. *The Journal of Clinical Investigation***105**, 1027-1030 (2000).
180. Park, D.*, et al.* Motility analysis of bacteria-based microrobot (bacteriobot) using chemical gradient microchamber. *Biotechnology and bioengineering***111**, 134-143 (2014).

181. Jain, R.K. Haemodynamic and transport barriers to the treatment of solid tumors. *Interniational Journal of Radiation Biology***60,** 85-100 (1991).
182. Pawelek, J.M., Low, K.B. & Bermudes, D. Bacteria as tumour-targeting vectors. *The Lancet Oncology***4**, 548-556 (2003).
183. Herr, H.W. & Morales, A. History of bacillus Calmette-Guerin and bladder cancer: an immunotherapy success story. *The Journal of urology***179**, 53-56 (2008).
184. Bohle, A. & Brandau, S. Immune mechanisms in bacillus Calmette-Guerin immunotherapy for superficial bladder cancer. *The Journal of urology***170**, 964-969 (2003).
185. Guentzel, M.N. Escherichia, Klebsiella, Enterobacter, Serratia, Citrobacter, and Proteus. in *Medical Microbiology* (ed. Baron, S.) (1996).
186. Pawelek, J.M., Low, K.B. & Bermudes, D. Tumor-targeted Salmonella as a novel anticancer vector. *Cancer research***57**, 4537-4544 (1997).
187. Low, K.B.*, et al.* Lipid A mutant Salmonella with suppressed virulence and TNF[alpha] induction retain tumor-targeting in vivo. *Nat Biotech***17**, 37-41 (1999).
188. Moese, J.R. & Moese, G. Oncolysis by Clostridia I. activity *Clostridium Butyricum* (M-55) and other non pathogenic Clostridia against the ehrlich carcinoma. *Cancer research***24**, 212-216 (1964).
189. Kim, B.J. & Forbes, N.S. Single-cell analysis demonstrates how nutrient deprivation creates apoptotic and quiescent cell populations in tumor cylindroids. *Biotechnol Bioeng***101**, 797-810 (2008).
190. Lee, C.H., Wu, C.L. & Shiau, A.L. Salmonella choleraesuis as an anticancer agent in a syngeneic model of orthotopic hepatocellular carcinoma. *Int J Cancer***122**, 930-935 (2008).
191. Rosenberg, S.A., Spiess, P.J. & Kleiner, D.E. Antitumor Effects in Mice of the Intravenous Injection of Attenuated Salmonella Typhimurium. *Journal of immunotherapy (Hagerstown, Md. : 1997)***25**, 218-225 (2002).
192. Ganai, S., Arenas, R.B., Sauer, J.P., Bentley, B. & Forbes, N.S. In tumors Salmonella migrate away from vasculature toward the transition zone and induce apoptosis. *Cancer gene therapy***18**, 457-466 (2011).
193. Chang, W.W.*, et al.* Salmonella enhance chemosensitivity in tumor through connexin 43 upregulation. *Int J Cancer***133**, 1926-1935 (2013).
194. Kaimala, S.*, et al.* Salmonella-mediated tumor regression involves targeting of tumor myeloid suppressor cells causing a shift to M1-like phenotype and reduction in suppressive capacity. *Cancer Immunol Immunother***63**, 587-599 (2014).
195. Wang, C.-Z., Kazmierczak, R.A. & Eisenstark, A. Strains, Mechanism, and Perspective: Salmonella-Based Cancer Therapy. *International journal of microbiology***2016**, 5678702-5678702 (2016).
196. Lee, C.H., Wu, C.L. & Shiau, A.L. Toll-like receptor 4 mediates an antitumor host response induced by Salmonella choleraesuis. *Clinical cancer research : an official journal of the American Association for Cancer Research***14**, 1905-1912 (2008).
197. Henderson, B. Microbial/host interactions in health and disease: Who controls the cytokine network? *Immunopharmacology* **35(1), 1.**((1996).).
198. Galan, J.E. & Collmer, A. Type III secretion machines: bacterial devices for protein delivery into host cells. *Science (New York, N.Y.)***284**, 1322-1328 (1999).

199. Toso, J.F.*, et al.* Phase I Study of the Intravenous Administration of Attenuated Salmonella typhimurium to Patients With Metastatic Melanoma. *Journal of clinical oncology : official journal of the American Society of Clinical Oncology***20**, 142-152 (2002).
200. Heimann, D.M. & Rosenberg, S.A. Continuous intravenous administration of live genetically modified salmonella typhimurium in patients with metastatic melanoma. *Journal of immunotherapy (Hagerstown, Md. : 1997)***26**, 179-180 (2003).
201. Hoffman, R.M. The preclinical discovery of bacterial therapy for the treatment of metastatic cancer with unique advantages. *Expert opinion on drug discovery***7**, 73-83 (2012).
202. David Bermudes, K.B.L., John Pawelek, Ming Feng, Michael Belcourt, Li-Mou Zheng and Ivan King Tumour-Selective Salmonella-Based Cancer Therapy *Biotechnology and Genetic Engineering Reviews* **18**(2001).
203. Morillo, V.*, et al.* Isolation, cultivation and genomic analysis of magnetosome biomineralization genes of a new genus of South-seeking magnetotactic cocci within the Alphaproteobacteria. *Frontiers in microbiology***5**, 72-72 (2014).
204. Vargas, G.*, et al.* Applications of Magnetotactic Bacteria, Magnetosomes and Magnetosome Crystals in Biotechnology and Nanotechnology: Mini-Review. *Molecules (Basel, Switzerland)***23**(2018).
205. Lower, B.H. & Bazylinski, D.A. The bacterial magnetosome: a unique prokaryotic organelle. *Journal of molecular microbiology and biotechnology***23**, 63-80 (2013).
206. Yan, L.*, et al.* Magnetotactic bacteria, magnetosomes and their application. *Microbiological Research***167**, 507-519 (2012).
207. Benoit, M.R.*, et al.* Visualizing implanted tumors in mice with magnetic resonance imaging using magnetotactic bacteria. *Clinical cancer research : an official journal of the American Association for Cancer Research***15**, 5170-5177 (2009).
208. Hergt, R., Dutz, S. & Roder, M. Effects of size distribution on hysteresis losses of magnetic nanoparticles for hyperthermia. *Journal of physics. Condensed matter : an Institute of Physics journal***20**, 385214 (2008).
209. Mannucci, S.*, et al.* Magnetic Nanoparticles from Magnetospirillum gryphiswaldense Increase the Efficacy of Thermotherapy in a Model of Colon Carcinoma. *PLOS ONE***9**, e108959 (2014).
210. Alphandéry, E.*, et al.* Heat Production by Bacterial Magnetosomes Exposed to an Oscillating Magnetic Field. *The Journal of Physical Chemistry C***115**, 18-22 (2011).
211. Felfoul, O.*, et al.* Magneto-aerotactic bacteria deliver drug-containing nanoliposomes to tumour hypoxic regions. *Nat Nano***11**, 941-947 (2016).
212. Yoshino, T.*, et al.* Biosynthesis of Thermoresponsive Magnetic Nanoparticles by Magnetosome Display System. *Bioconjugate chemistry***29**, 1756-1762 (2018).
213. Alphandéry, E. Applications of magnetosomes synthesized by magnetotactic bacteria in medicine. *Frontiers in bioengineering and biotechnology***2**, 5-5 (2014).
214. Edinger, M.*, et al.* Revealing lymphoma growth and the efficacy of immune cell therapies using in vivo bioluminescence imaging. *Blood***101**, 640-648 (2003).
215. Long, R.*, et al.* A Natural Bacterium-Produced Membrane-Bound Nanocarrier for Drug Combination Therapy. *Materials (Basel, Switzerland)***9**, 889 (2016).

216. Wang, X.*, et al.* An enhanced anti-tumor effect of apoptin-cecropin B on human hepatoma cells by using bacterial magnetic particle gene delivery system. *Biochemical and biophysical research communications***496**, 719-725 (2018).
217. Guan, F., Li, X., Guo, J., Yang, G. & Li, X. Ganglioside-magnetosome complex formation enhances uptake of gangliosides by cells. *Int J Nanomedicine***10**, 6919-6930 (2015).
218. Cheng, L., Ke, Y., Yu, S. & Jing, J. Co-delivery of doxorubicin and recombinant plasmid pHSP70-Plk1-shRNA by bacterial magnetosomes for osteosarcoma therapy. *Int J Nanomedicine***11**, 5277-5286 (2016).
219. Sun, J.B.*, et al.* Preparation and anti-tumor efficiency evaluation of doxorubicin-loaded bacterial magnetosomes: magnetic nanoparticles as drug carriers isolated from Magnetospirillum gryphiswaldense. *Biotechnology and bioengineering***101**, 1313-1320 (2008).
220. Alphandery, E.*, et al.* Development of non-pyrogenic magnetosome minerals coated with poly-l-lysine leading to full disappearance of intracranial U87-Luc glioblastoma in 100% of treated mice using magnetic hyperthermia. *Biomaterials***141**, 210-222 (2017).
221. Alphandery, E., Faure, S., Seksek, O., Guyot, F. & Chebbi, I. Chains of magnetosomes extracted from AMB-1 magnetotactic bacteria for application in alternative magnetic field cancer therapy. *ACS nano***5**, 6279-6296 (2011).
222. Mannucci, S.*, et al.* Magnetosomes Extracted from Magnetospirillum gryphiswaldense as Theranostic Agents in an Experimental Model of Glioblastoma. *Contrast Media & Molecular Imaging***2018**, 12 (2018).
223. Lee, N.*, et al.* Magnetosome-like ferrimagnetic iron oxide nanocubes for highly sensitive MRI of single cells and transplanted pancreatic islets. *Proceedings of the National Academy of Sciences of the United States of America***108**, 2662-2667 (2011).
224. Xiang, Z.*, et al.* Tumor detection using magnetosome nanoparticles functionalized with a newly screened EGFR/HER2 targeting peptide. *Biomaterials***115**, 53-64 (2017).
225. Boucher, M.*, et al.* Genetically tailored magnetosomes used as MRI probe for molecular imaging of brain tumor. *Biomaterials***121**, 167-178 (2017).
226. Orlando, T.*, et al.* Characterization of magnetic nanoparticles from Magnetospirillum Gryphiswaldense as potential theranostics tools. *Contrast media & molecular imaging***11**, 139-145 (2016).

CHAPTER II

MOTION COMPENSATED TUMOR IMAGING FOR THERMOMETRY AND DRUG DELIVERY MONITORING USING ULTRASOUND IMAGEABLE ECHOGENIC LIPOSOMES

Graphical Abstract

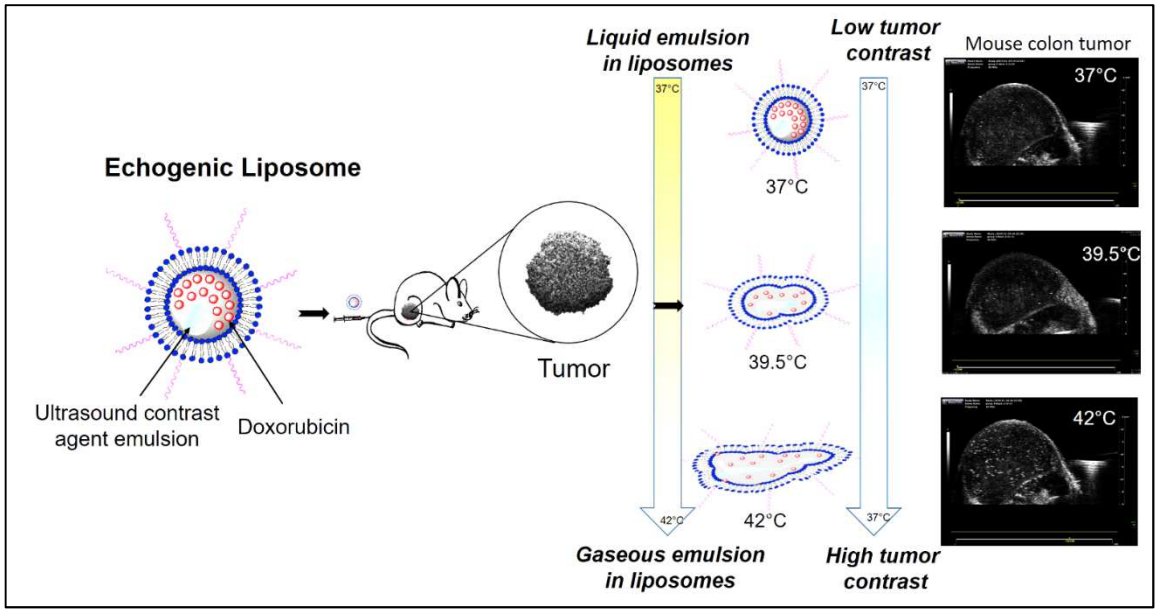

[1] Earlier version of this chapter has already been published as Ektate K, Kapoor A, Maples D, Tuysuzoglu A, VanOsdol J, Ramasami S, Ranjan A. Motion Compensated Ultrasound Imaging Allows Thermometry and Image Guided Drug Delivery Monitoring from Echogenic Liposomes. Theranostics 2016; 6(11):1963-1974. doi:10.7150/thno.15922.

Abstract

Ultrasound imaging is widely used both for cancer diagnosis and to assess therapeutic success, but due to its weak tissue contrast and the short half-life of commercially available contrast agents, it is currently not practical for assessing motion compensated contrast-enhanced tumor imaging, or for determining time-resolved absolute tumor temperature while simultaneously reporting on drug delivery. The objectives of this study were to: 1) develop theranostic echogenic heat sensitive (E-LTSL) and non-thermosensitive liposomes (E-NTSL) to enhance tumoral half-life of contrast agents, and 2) measure motion compensated temperature induced state changes in acoustic impedance and Laplace pressure of liposomes to monitor temperature and doxorubicin (Dox) delivery to tumors. LTSL and NTSL containing Dox were co-loaded with an US contrast agent (perfluoropentane, PFP) using a one-step sonoporation method to create E-LTSL and E-NTSL. To determine temperature induced intensity variation with respect to the state change of E-LTSL and E-NTSL in mouse colon tumors, cine acquisition of 20 frames/second for about 20 min (or until wash out) at temperatures of 42°C, 39.5°C, and 37°C was performed. A rigid rotation and translation was applied to each of the "key frames" to adjust for any gross motion that arose due to motion of the animal or the transducer. To evaluate the correlation between US intensity variation and Dox release at various temperatures, treatment (5 mg Dox/kg) was administered via a tail vein once tumors reached a size of 300–400 mm^3, and mean intensity within regions of interest (ROIs) defined for each sample was computed over the collected frames and normalized in the range of [0,1]. When the motion compensation technique was applied, a > 2-fold drop in standard deviation in mean image intensity of tumor was observed, enabling a more robust estimation of temporal variations in tumor temperatures for 15-20 min. due to state change of E-LTSL and E-NTSL. Consequently, a marked increase in peak intensity at 42°C compared to 37°C that corresponded with enhanced Dox delivery from E-LTSL in tumors was obtained. Our results indicate that echogenic liposomes provide a predictable change in tumor vascular contrast with temperature, and this property could be applicable to nanomonitoring of drug delivery in real time

1. Introduction

A major challenge in image guided drug delivery (IGDD) is developing accurate means to implement real-time drug delivery control with motion compensation. In prior research, locally inducible image guided drug release using heat-activated liposomes (low temperature sensitive liposomes; LTSLs) that are sensitive to mild, non-destructive temperature elevations above normal body temperature (40–42 °C) has been investigated [1-4]. LTSLs can achieve significantly improved drug accumulation and distribution in tumors compared to conventional treatment [5-8]. Additionally, imageable LTSLs containing a combined payload of magnetic resonance (MR) contrast agents (e.g., gadolinium, manganese) and doxorubicin (Dox) combined with MR guided high intensity focused ultrasound (MR-HIFU) can provide a real-time estimation of tumor chemotherapy coverage [4,9-11]. This is achieved by mild heating of imageable LTSLs to release the contrast agent in order to enhance tumor areas in the MR images to allow estimation of the mean amount of anticancer drug (e.g., Doxorubicin or Dox) that has been delivered to the cancerous tissue. Mild hyperthermia (40–45°C) is fundamentally distinct from hyperthermia-based ablative technologies (> 55°C) that are intended to destroy tumor tissue by heating [12]. Thus, to achieve maximal LTSL-mediated drug release, tissue temperatures must be delicately balanced and precisely controlled with feedbacks for real-time monitoring of chemotherapy delivery [13,14].

The most commonly used method for performing absolute MR-based thermometry is based on temperature-dependent chemical shift changes in proton resonance relative to that of a reference resonance [15]. However, use of MRI is expensive, requires large dedicated facilities, and has technical limitations (e.g., interference by target tissue movement), and the agents that are required to create tumor imageability (e.g., gadolinium) may alter the chemical shift, thereby disrupting the fidelity of temperature measurement and drug delivery [16,17]. Thus, there is a critical clinical need to develop an alternative, less-constrained technology using a modality such as ultrasound (US) that is low-cost and portable for accurate IGDD. US imaging is widely used both for cancer diagnosis and to assess therapeutic success, but due to its weak tissue contrast and the short half-life of commercially available microbubble (MB)-based contrast agents, it is

currently not practical for visualizing localized drug release in real time or for determining chemotherapy distribution.

To address the limitations of the short half-life of MBs, recently we developed a theranostic echogenic LTSL (E-LTSL) that co-encapsulates the US contrast agent perfluoropentane (PFP) and Dox in a size-controlled manner [18,19]. PFP is a very hydrophobic, nontoxic, noncarcinogenic fluoroalkane with a boiling point (29 °C) between room and body temperatures [20]. The phase transition temperature for PFP is clinically relevant, as it allows PFP to be injected in the form of liquid droplets dispersed in an aqueous medium that then are converted to echogenic bubbles upon warming to body temperature [21]. Moreover, when stabilized by a lipid shell, the Laplace pressure (i.e., the pressure difference between the inside and the outside of PFP) substantially increases its boiling temperature due to the surface tension at the interface between PFP and bulk liquids [22]. Based on these features, we hypothesized that the predictable boiling point changes of encapsulated PFP with temperature due to Laplace pressure variation can be applied to nanothermometry and nanomonitoring of drug delivery. To achieve this goal, a robust motion compensation technology for tumor imaging is required to translate the contrast intensity variations into quantifiable state changes of nanoparticles.

In this study, we used our long circulating theranostic liposomes for motion compensated vascular contrast determination, and we applied this methodology to evaluate the temperature-dependent liposomal state change in combination with US imaging. Finally, we applied the predictable change in tumor vascular contrast of theranostic echogenic liposomes (thermosensitive [E-LTSL] and non-thermosensitive [E-NTSL]) for nanomonitoring of drug delivery. In vivo data obtained from a mouse tumor model suggest that co-encapsulated PFP in liposomes can be used to determine the temperature-dependent state of nanoparticles, and this property could be applicable to nanomonitoring of IGDD in real time, especially from E-LTSLs.

2. Materials and Methods

2.1 Materials

PFP (99%, Exfluor Research Corporation, TX, and USA) was used as the US contrast agent. Monostearoyl-2-hydroxy-sn-glycero-3-phosphocholine (MSPC), 1,2-dipalmitoylsn-glycero-3-phosphocholine (DPPC), and 1,2-distearoyl-sn-glycero-3-phosphoethanolamine-N-[methoxy (polyethylene glycol)2000] (DSPE-mPEG2000) were obtained from Corden Pharma Corporation (CO, USA). Dox was obtained from LC laboratory (MA, USA). Agarose and psyllim fiber were purchased from BDH (PA, USA) and Konsyl Pharmaceuticals, (MD, USA), respectively. Graphite was purchased from Alpha Aesar (Ward Hill, MA, USA). Acetonitrile (HPLC grade) was obtained from Pharmco-AAPER (CT, USA). Ethylene glycol (99%, spectrophotometric grade), phenylboronic acid (98%), and 2,2-dimethoxypropane (98%) were purchased from Alpha Aesar. The PD-10 column was obtained from GE Healthcare Life Sciences (Buckinghamshire, UK). C26 cells were kindly provided by the National Cancer Institute.

2.2 Synthesis of E-LTSLs and E-NTSLs

LTSLs (lipid composition: DPPC, MSPC, and DSPE-mPEG2000 in the molar ratio of 85.3:9.7:5.0) and NTSLs (DPPC, cholesterol, and DSPE-mPEG2000 in the molar ratio of 58.1:36.8:5.07) were prepared by hydration of a lipid film followed by the extrusion method described previously [23]. Briefly, lipid mixtures were dissolved in chloroform. The solvent was evaporated and the resulting lipid film was hydrated in citrate buffer (pH 4.0) mixed with 1,3-propanediol (1,3-PD (0.65 M, for PFP emulsification) at 55 ^{0}C for 30 min and extruded five times through double stacked 200 nm polycarbonate filters to yield a final lipid concentration of 50 mg lipid/ml (80.8 mM for LTSLs and 70.3 mM NTSLs)[24]. A PD-10 size-exclusion column equilibrated with 5–10 column volumes of 1x phosphate buffered saline (PBS) was used to remove free 1,3-PD from the outside of the liposomes.

Encapsulation of Dox into the E-LTSLs and E-NTSLs was carried out using the pH gradient loading protocol described by Mayer et al. [21]. The outside of the E-LTSLs was adjusted (by column) to about pH 7.4 using PBS, whereas the inside remained acidic at pH 4. Dox was loaded at 2 mg per 100 mg lipid concentration at 37°C for 1 h. PFP-loaded E-LTSLs and E-NTSLs were prepared using a one-step sonoporation method.

Briefly, 2 mL of the liposomal formulations were incubated under continuous sonication (~20 khz) in 3 mL vials along with PFP (boiling point 30°C; 20 µL/100 mg lipid) for 1–2 min. PFP and LTSLs were kept cold prior to being combined, and the sonication bath was kept at 4°C to minimize PFP vaporization. This method was repeated at least in triplicate (n = 3) for evaluation. Free Dox and PFP were removed using a PD-10 column. For all in vitro characterizations, LTSLs were used as a positive control.

2.3 Characterization of E-LTSLs and E-NTSLs

E-LTSLs and E-NTSLs were characterized for size (z-average), polydispersity index and zeta potential using dynamic light scattering (DLS) with a 90 plus PALS Nanobrook device (Brookhaven Instruments, Holtsville, NY, USA). Briefly, 10–20 µl of E-LTSLs or E-NTSLs were added to 2 ml of PBS in a cuvette, and DLS measurements were recorded at room temperature. For each liposomal formulation an average of five measurements were taken, and the mean size and standard deviation were calculated for the E-LTSLs and E-NTSLs samples.

2.4 Dox release from E-LTSLs and E-NTSLs

Stability at body temperature (37°C) was assessed by measuring release of encapsulated Dox from E-LTSLs and E-NTSLs as a function of temperature (25–42°C) in PBS. E-LTSLs (50 mg lipid/ml) and E-NTSLs (50 mg lipid/ml) were diluted 300 fold in PBS, and 3 mL of sample were placed in a quartz cuvette equipped with a stopper and magnetic stirrer. Fluorescence of the released Dox was recorded at an excitation wavelength of 480 nm and fluorescence emission at 590 nm using a Cary Eclipse Fluorescence Spectrometer (Agilent Technologies, Santa Clara, CA, USA) equipped with an inbuilt temperature control system. Fluorescence readings were recorded for every degree ramp in temperature of the sample from 25 to 42 ^{0}C.

Drug release based on fluorescence quantification as a function of change in temperature was determined using the equation below:

$$\%\ Dox\ release = \left[\frac{\mathrm{It} - \mathrm{Io}}{\mathrm{Im} - \mathrm{Io}}\right] \times 100$$

where I_o is the initial fluorescence intensity for E-LTSLs and E-NTSLs in suspension at 25°C, I_t is the intensity of the same sample at a predetermined temperature, and I_m is the fluorescence intensity of completely released Dox from E-LTSLs at 45°C or from E-NTSLs post breaking of the liposomes with 10x triton.

2.5 Transmission electron microscopy (TEM) imaging of E-LTSLs and E-NTSLs

TEM with negative staining was used to image E-LTSLs and E-NTSLs at various temperatures. Briefly, E-LTSLs and E-NTSLs were heated at 37°C, 39.5°C, and 42°C in a water bath for 15 min. The heated liposomes were diluted 500–1000X in PBS, and 10 µl of sample were loaded onto a carbon grid (Lacey and Holey grid). The grid was allowed to dry for 30 seconds followed by a 30 second treatment with 9 µl of 2% phosphotungstic acid. All TEM images were captured at 200 kV using a JOEL JEM-2100 TEM (JEOL, Peabody, MA, USA).

2.6 Monitoring of E-LTSL and E-NTSL intensity in an agarose phantom model

For US imaging, the phantom recipe (3% (w/v) agarose and 0.25% (w/v) graphite) was optimized to withstand hyperthermia temperatures up to ~70°C. Prior to imaging, free PFP was removed from E-LTSLs and E-NTSLs using PD-10 columns, and 1 ml of liposomes (~20–30 mg of total lipid) was added to the phantom wells for imaging. The phantom wells were positioned vertically in an Isotemp water bath (Fisher Scientific, Pittsburgh, PA, USA) with the visualsonics ultrasound transducer MS250 (13–24 MHz) positioned obliquely against the wells. Temperatures of the phantom wells were recorded before initiating imaging and during imaging using thermocouples positioned at the top of each well ~1 cm below the sample surface. Each minute the water temperature was increased by 1°C. Unpurified PBS mixtures containing PFP were used as positive controls. Column-purified PBS mixtures containing PFP alone or 1,3-PD plus PFP were used as additional controls.

To evaluate the correlation between US intensity and Dox release at various temperatures,a cine acquisition of 100 frames at 20 frames per second was acquired for each temperature point simultaneously for E-LTSLs and E-NTSLs. Mean intensity within regions of interest (ROIs) defined for each sample was computed over the collected frames and normalized in the range of [0,1]. Data were fitted with two exponential curves

using the least squares method, one for each part between 31 and 39°C and 39 and 45°C, respectively. The inflection point was determined by the rapid change in intensity of the two fitted curves.

2.7 In vivo US imaging setup and hyperthermia treatment protocol

All animal-related procedures were approved and carried out under the guidelines of the Oklahoma State University Animal Care and Use Committee. For tumor initiation, C26 colon carcinoma cells were established in athymic nude mice as previously described [18,19]. Briefly, confluent C26 cells grown as a monolayer in RPMI medium supplemented with 10% v/v fetal bovine serum and 1% v/v streptomycin/penicillin were harvested, washed, and diluted with sterile cold PBS at 0.5x 10^5 cells/50 µl. Next, 50 µl of cell inoculum were injected subcutaneously in the thigh region of the mouse hind leg with a 25-gauge needle (BD; Franklin Lakes, NJ, USA). Mice were monitored and tumor growth was measured by serial caliper measurements (General Tools Fraction+™, NY, USA). Tumor volumes were calculated using the formula (length X width^2)/2, where length is largest dimension and width is the smallest dimension perpendicular to length.

Tumor imaging was initiated once the tumors reached a volume of 300-400 mm^3. For imaging, mice were anesthetized with 2–5% isoflurane and then secured on a heating stage maintained at 37°C (Stryker, MI, USA). For imaging, only the tumor bearing leg was isolated in specialized holders and immersed in the water bath, which was maintained at the desired temperatures of 37, 39.5, or 42°C. Tumor temperatures were allowed to equilibrate with the water bath for 10–15 min before injection of E-LTSLs/E-NTSLs. The water bath temperature was set 1°C higher relative to the target temperature, as this had already been calibrated to yield mean tumor temperatures of 37, 39.5, and 42°C.

2.8 Image acquisition procedure

For in vivo studies, all US imaging was conducted using a VisualSonics Vevo 2100 ultrasound MS550D transducer (22–55 MHz) (22–33 MHz, Fujifilm, Toronto, ON). For imaging, the transducer was placed in a stationary position oblique to the tumor with special clamps built in-house. Mice were injected with 100µl of E-LTSLs or E-NTSLs (~10 mg total lipid) followed by 50µl of saline flushed through a catheter placed in the

tail vein. To assess image intensity over time, a cine acquisition of 100 frames at 20 f/sec was acquired at different time points up to 15–30 min.

2.9 Motion compensation for image intensity determination

To assess motion correction in the in vivo model and determine the variation of image intensity over time, a cine acquisition of 100 frames at 20 f/sec was acquired at different time points up to 15 min in our mouse model (Fig. 8a). A ROI encompassing the tumor was defined in the first frame and tracked in subsequent images by applying a rigid translation and rotation to the ROI to maximize the similarity between ROIs in each successive frame pair. Multiple ROIs were selected to include the region of tumor as well as other areas with high feature variations. In cases in which the tumor region did not have sufficient features to reliably compute similarity measures, alternative feature-rich ROIs were used. The rigid transformation computed using the alternative ROI was then applied to the tumor ROI. Similarity between ROIs was computed using Normalized Cross-Correlation (NCC). Once motion corrected, ROI sequences were analyzed over time as median intensity over the ROI normalized to the range [0,1]. This averaging method provided implicit regularization for noise and allowed determination of general characteristics of the ROI (peak intensity, rise time).

2.10 Validation of temporal vascular intensity variation of liposomes under motion compensation with temperature for drug delivery monitoring

To validate intensity variation with respect to temperature and the state change of the E-LTSLs and E-NTSLs in the mouse tumor, acquisition of 100 frames at temperatures of 37, 39.5, or 42°C (n=5-6 per temperature point) was performed. The temperature was kept constant for about 20 min (until wash out) at 42°C and then lowered to 39.5°C, followed by another injection of E-LTSLs. For each of these datasets, motion compensation was applied to each of the image frames as described in section 2.9. ROI sequences were analyzed to result in one median “key frame” per time period. Subsequently, a rigid rotation and translation was applied to each of these key frames to adjust for any gross motion that arose due to motion of the animal or the transducer by maximizing NCC between consecutive key frames. The normalized intensity visualized

as a function of time allowed determination of general characteristics of the peak intensity, wash-in AUC—wash-out AUC) for each of the temperature points.

2.11 Nanomonitoring of drug delivery and Dox quantification by high performance liquid chromatography (HPLC)

For nanomonitoring, the tumor was kept at fixed temperatures of 37 and 42°C in a water bath. After the baseline ultrasound images of target tumor was obtained, the mice were injected with Dox-loaded E-LTSLs or E-NTSLs, and US images were collected to confirm intensity variation. One hour following treatment, mice were euthanized, and cardiac perfusion was performed. The tumors and other organs were excised, weighed, snap frozen over liquid nitrogen, and then stored at –80°C until HPLC was performed to estimate the amount of drug in the tumor samples (n=3-5/treatment group).

For HPLC, stock solutions of Dox (0.25–100µg) and internal standard (Daunorubicin; 2.5µg/ml) were prepared in deionized water[1]. For calibration standards, a tumor from a control mouse was spiked with 10µl of Dox (0.25–100µg Dox/ml) and Daunorubicin (2.5µg/ml). Tumors were homogenized in aqueous KH_2PO_4 solution (20mM, pH 3.8) at a concentration of 100 mg/ml with zirconia beads (2 mm diameter, Biospec Products Inc., OK, USA) with Mini-Beadbeater-16 (Biospec) at 3450 oscillations/min for 3 min. For HPLC analysis, 90µl (n = 3, 100 mg/ml) of the tumor homogenate were mixed with 50µl of internal standard solution (2.5µg Daunorubicin /mL) incubated at 37°C for 15 min. Post-incubation, 250µl of acetone and 100µl of ZnSO4 solutions (saturated) were added to the homogenate, and it was re-incubated at 37°C for another 15 min to precipitate the proteins. Subsequently, the samples were centrifuged in a Microfuge 22R (Beckman Coulter, CA, USA) at 18110 x g at 4°C for 10 min. Finally, 200µL of supernatant were transferred to another vial and evaporated using TurboVap® LV (Caliper Life Sciences, MA, USA) at 60°C under a stream of compressed air. Prior to HPLC, the dried residue was completely dissolved in 100µl HPLC mobile phase, and 20µL of this solution were introduced into the Shimadzu HPLC system for analysis.

2.12 Statistical analysis

Treatment groups were compared for differences in mean Dox concentration using analysis of variance (ANOVA) followed by Tukey's multiple comparison post-hoc test. All analyses were performed using GraphPad Prism 5.0 (GraphPad Software Inc.). All p-values were two-sided, and a p-value < 0.05 indicated statistical significance. Values are reported as mean ± SEM unless otherwise indicated.

3. Results

3.1 Characterization of E-LTSLs and E-NTSLs

Active loading of Dox by transmembrane pH gradient yielded an encapsulation efficiency of ~95% and ~65% for E-LTSLs and E-NTSLs, respectively. Following PFP loading by one-step sonoporation, E-LTSLs and E-NTSLs retained about 70–80% of the encapsulated drug. Table 1 shows the hydrodynamic diameter, polydispersity index and zeta potential values of E-LTSLs and E-NTSLs at room temperature (25°C), and these were fairly similar between various groups following PFP loading.

Table 1: Physicochemical characterization of E-LTSL and E-NTSL

Liposome	Diameter ± SD (nm)	Poly dispertsity Index ± SD	Zeta Potential ± SD (mv)
E-LTSL	172.765 ± 3.44	0.189 ± 0.0222	-36.9 ± 2.7474
E-NTSL	193.39 ± 1.93	0.115 ± 0.011	-22.234± 4.2628

3.2 Dox release from E-LTSLs and E-NTSLs in physiological buffer

Percent Dox release from E-LTSLs and LTSLs was minimal (< 5%) at 25–39°C, more gradual at 40°C (~20%), and rapid and complete (> 95%) near the temperature with the maximum release rate (~41–42°C) (Fig. 1). In contrast to E-LTSLs, Dox release from E-NTSLs and NTSLs was < 5% at all temperature points tested, which confirms their non-thermosensitivity.

3.3 TEM analysis of E-LTSLs and E-NTSLs

TEM confirmed the presence of PFP and 1,3-PD emulsion within the liposome aqueous core between 37°C to 42°C for E-LTSLs (2a-c) and E-NTSLs (2d-f). E-LTSLs and E-NTSLs were spherical at 37°C, but the membranes deformed at ~42°C. In general,

membrane deformation of E-LTSLs at 39.5°C and 42°C was more prominent compared to E-NTSLs.

3.4. Intensity variation of E-LTSLs and E-NTSLs in tissue mimicking phantom

For E-LTSLs, as the sample was heated from 25to42°C, US signal intensity progressively increased (4–5 fold from 25 to 39.8°C; Fig.3a-b), and at ~40°C a further 2–3 fold increase occurred. The inflection point for these changes was computed as~39.5°C, which in our model corresponds to the transition temperature of liposomal lysolipids. Likewise, E-NTSL contrast also increased from 25–42°C, but the increase was more linear in nature (3b).

3.5 Kinetics of E-LTSLs and E-NTSLs in mouse tumors in vivo

US images obtained in B mode from time zero to wash out time of liposomes from the tumor (~15–30 min) showed significant contrast enhancement in the tumors for both E-LTSLs (Fig. 4a–d) and E-NTSLs (Fig. 4e–h). In general, maximum contrast enhancement was observed for 15–20 min post-liposome injection. Additionally, development of contrast with E-NTSLs was more gradual with temperature in comparison to E-LTSLs.

3.6 Fidelity of motion compensation in mouse tumors

In the absence of motion compensation in vivo, as time progressed, the contrast variation of E-LTSL and E-NTSL was obscured and minimized relative to baseline images (Fig. 5a–d). When the motion compensation technique was applied for E-LTSLs, a > 2-fold drop in standard deviation for mean image intensity occurred, enabling a more robust estimate of temporal variations due to state change of liposomes (Fig. 5 e-h, 6a). Furthermore, a 6-fold increase in within-ROI signal intensity occurred after injection (once the liposomes reached a steady-state temperature greater than their transition temperature) vs. background (pre-injection) (Fig. 6b). Similar results were observed for E-NTSLs (data not shown).

3.7 Relationship between motion compensated image intensity and temperature in mouse tumors

Corresponding to our phantom results, following motion compensation, we saw a marked increase in peak intensity at 42°C compared to 37°C, which was 2-fold larger than the

increase in peak intensity between 39.5°C and 37°C for both E-LTSLs and E-NTSLs (Fig. 7). These data were consistent across a cohort of six animals. Interestingly, like in vitro tissue mimicking data phantom data, the change in tumor contrast was more prominent (~2-fold greater) for E-LTSLs than for E-NTSLs at 42°C.

3.8. Nanomonitoring of drug delivery in mouse tumors by HPLC

The heated tumor Dox concentrations were 1.6 ± .04, 1.94 ± 0.35, 1.8 ± 0.06 and 3.8± 0.6 μg Dox/g tissues for NTSLs, LTSLs, E-NTSLs, and E-LTSLs, respectively (Fig. 8). E-LTSLs + hyperthermia resulted in a 2-fold greater tissue drug delivery compared to E-NTSLs +hyperthermia and E-LTSLs alone ($p < 0.05$, Tukey's test). Importantly, the level of tumor Dox corresponded to the E-LTSL tumor contrast measure for 15 min at 37, and 42°C, with higher tumor contrast indicating greater drug delivery for E-LTSL samples. Such differences were not noted for E-NTSL due to their non-thermosensitive characteristics.

4. Discussion

MBs can produce up to 15–25 dB in echo intensities of blood flow signals and help better determine tortuous angiogenic vasculature than conventional US imaging [25]. This is a significant advantage, but the degree of contrast enhancement following MB injection is rapid and complete, and systemically MBs are degraded quickly after injection [26]. To circumvent these problems, in this study we encapsulated the US contrast agent PFP in a size-controlled manner within liposomes to create long circulating E-LTSLs and E-NTSLs. The feasibility of incorporating PFP into stealth liposomes in a size-controlled manner has been reported previously using lipid-based surfactants (1,2-dihexadecanoyl-sn-glycero-3-phosphocholine and 1,2-dipalmitoyl-sn-glycero-3-phosphate) to emulsify perfluorohexane (PFC6) for loading into liposomes [27,28]. Negatively stained liposomes synthesized using these surfactants suggested that PFC6 emulsions were effectively loaded. Recently, we adapted a method proposed by Ibsen et al. that involves incorporation of the water-soluble surfactant 1,3-PD into the aqueous core of the liposome to entrap PFP and induce emulsion formation in the liposome [19,24,29]. TEM conducted following PFP encapsulation suggested that nanoemulsified PFP can be successfully encapsulated within the aqueous core at body temperature independent of

liposome composition and without impacting the size (~150–200 nm for both E-LTSLs and E-NTSLs, Table 1). Interestingly, TEM imaging revealed that at higher temperatures (> 40°C), E-LTSLs demonstrate relatively greater membrane relaxation compared to E-NTSLs (Fig. 2c&f). This is likely due to the presence of lysolipids in the E-LTSLs that induce formation of thermodynamically favored micelle-like conformation and lateral lipid domains [30]. Additionally, the presence of lysolipid impacted the Dox release, with > 95% drug release for E-LTSLs and < 5% release from E-NTSLs in physiological buffer (Fig.1). Importantly, the 1,3-PD method of PFP emulsification in the liposome aqueous core provided excellent thermal stability of encapsulated PFP when they transitioned to the bubble state at higher temperature, as evidenced by sustained vascular imaging (~15–20 min) with longer clearance kinetics versus that seen with relevant controls (Fig.4). This result is promising, but it is not clear whether the PFP vapors transition back to the liquid state when the mouse tumors are cooled down. Additionally, whether the tumor accumulated E-LTSLs and E-NTSLs can be used to longitudinally track tumor growth needs more investigation in future studies.

A major challenge of hyperthermia mediated IGDD is the motion of the target (solid tumor), particularly in the abdominal region, due to respiration or patient movement. Movement impairs precise triggered release of drugs, especially from LTSLs under US guidance. In recent years, a variety of techniques to compensate for target motion, including increasing the transducer angle increment and using a dual-mode combination of the tissue and contrast-MB responses to perform alignment of both tissue and vascular structures, have been proposed [31-33]. These are promising findings, but the short half-life of currently available MBs still prevents their use for IGDD guidance. To assess motion correction in an in vivo model and determine the variation of image intensity over time, we applied a rigid transformation to the ROIs using our long circulating theranostic echogenic liposomes. This procedure maximized the similarity between the ROI in each successive frame pair, resulting in a significantly enhanced estimation of temporal variation in tumor vascular intensity (Fig 5&6). Thus, we believe that this property hypothetically can be used to provide a precise spatiotemporal control of drug release from thermosensitive liposomes [34].

Clinically, hyperthermia is achieved by using a variety of applicators (e.g., microwave applicators, radiofrequency applicators, HIFU) [35]. However, these devices and methods have drawbacks, including lack of spatial precision and temperature accuracy (e.g., hot or cool spots) and inability to achieve controlled mild hyperthermic temperatures (40–45°C). Previously, we and others showed that MR-thermometry provides high spatial and temporal resolution for IGDD of tumors [5,36,37], but MR technology is sensitive to tissue motion and to external perturbation of the magnetic field [38]. Like MRI, US imaging can also determine temperature-based changes in the speed of sound or thermal expansion within the mildly heated tissue region by comparing US images frame-by-frame over time, but temperature mapping is still problematic due to tissue motion and effects of non-thermal and unintended thermal effects on the US signal [39]. In the current, we took an alternative approach to directly estimate the state of the nanoparticles and thus monitor hyperthermia-responsive drug delivery. We mapped the relative intensity variations to the temperature-dependent changes in the state of E-LTSLs and E-NTSLs. To do this, we relied on changes in acoustic impedance between tissues, fluids, and their surrounding microenvironments at various temperatures and transformed these changes into a surrogate of relative tissue temperature. Our data show that the motion-corrected US intensity of E-LTSLs changes with temperature (Fig. 3a-b). When PFP vaporization within E-LTSLs is complete, contrast intensity stabilizes to a fixed level (~37–39°C) and then increases at the transition temperature of liposomes (~39.5°C) as the interface between liposome and surrounding medium is replaced by multiple interfaces between nanobubbles and surrounding fluids. Interestingly, the change in vaporization and US intensity was more prominent for E-LTSLs than for E-NTSLs (Fig. 7a-b). We speculate that the relative echo obtained for liposomes is a function of PFP vaporization, membrane state at higher temperature, and the concentration and agglomeration status of the liposomes in blood vessels. E-LTSLs have relatively higher membrane relaxation, and this fundamental property may provide stronger echo signals during US imaging at relatively greater vascular concentration compared to E-NTSLs at temperatures > 40°C. An important utility of such a phenomenon could be in nanomonitoring of drug delivery from E-LTSL. As shown in Fig. 8, in the mild hyperthermia ranged (~40-42°C), estimations of tumor contrast could reliably predict drug delivery. This discreet

prediction and control of drug delivery will likely be negated at temperatures> 45°C due to perfusion shutdown, and thus our state-changing echogenic liposomes can serve as an excellent surrogate marker of mild hyperthermia in tumors (especially in the absence of MR-thermometry).

Our study has several addressable limitations. First, hyperthermia treatment of tumors was performed using the traditional water bath methodology. This method of hyperthermia achieves spatially homogeneous heating of selected tissue and controlled tumor vascular enhancement, but is not feasible to use clinically for deep seated tumors [7]. Also, for deep seated tumors this homogeneity may not exist with other types of hyperthermia applicators (e.g., HIFU), especially if the treatment cell area (focal spot) is smaller than the tumor volume. This has been addressed to some extent through the recent development of phased array transducers with appropriate driving electronics that enable the creation of a desired focal pattern by making fast temporal displacements of multiple foci, thereby significantly enhancing the treatment volume [36]. In addition, Bing et al. successfully created 3D-printed sector-vortex lenses with annular focal regions that enabled customization of the heating volume in rodent models[40]. Studies are currently underway to investigate the contrast variations using sector-vortex lenses with various types of animal tumor models to demonstrate this idea in our laboratory. The second limitation of this study was reliance on vascular contrast of E-LTSLs and E-NTSLs. Given the relatively small size of the liposomes, they may passively accumulate in the tumor by the enhanced permeation and retention effect and influence the contrast assessment in real time. Our liposomes demonstrate the highest rate of vaporization at higher temperature (> 40°C), and a passive accumulation is not expected to dramatically alter the imaging feedback at body temperature; in fact, it would help provide a stronger signal that may have diagnostic value. Despite this, if tests of the current formulations do not meet the proposed criteria, we will adjust the PFP level in the liposomes prior to translation into human studies to reduce background artifacts. Third, the temperature monitoring by PFP phase-shift in liposomes may not be as precise as the PRFS method currently in clinical trials for MRI thermometry. This could impact targeted IGDD, as temperatures > 45°C have been shown to shut down tumor vascular perfusion [41]. The theranostic liposomes proposed in this study is not intended to replace the MR-

thermometry technology, which has merits for clinical use. We believe that the phase-changing liposomes may have utility for hyperthermia devices where PRFS cannot be applied easily (e.g., Radiofrequency applicators, microwave, ultrasound guided HIFU) or for nanomonitoring of drug delivery in tumors with US imaging feedback that is currently not possible to achieve with MBs with short-half lives.

In summary, this work provides important evidence that robust estimation of the state of theranostic liposomes and vascular contrast can be obtained from motion compensated US images in both tissue mimicking phantom and mouse models of colon cancers using temperature induced variations of Laplace pressure. Such elevations in relative image contrast correspond to drug delivery. This theranostic technology has the potential to guide non-invasive IGDD for tumors that require accurate temporal and spatial monitoring of drug treatments.

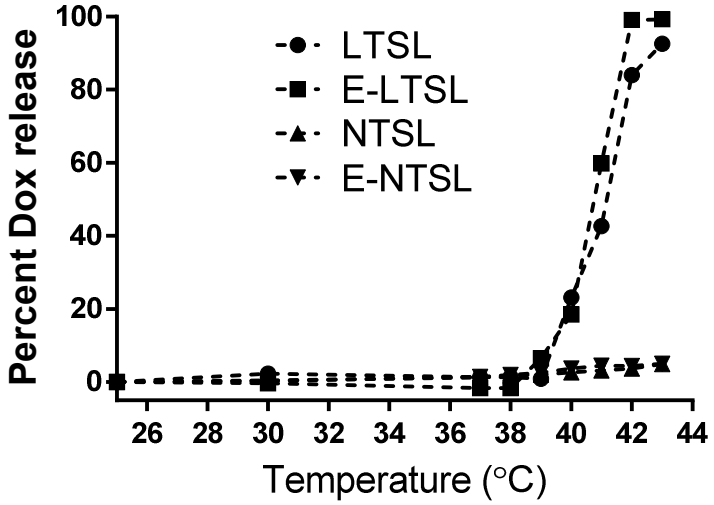

Figure. 1. Release of Dox with temperature as the sample (LTSL, E-LTSL, E-NTSL, and NTSL) is heated from 20-43°C at 1°C. Percent release was calculated by assuming 100% release with Triton-X, and 0% release at 25°C.

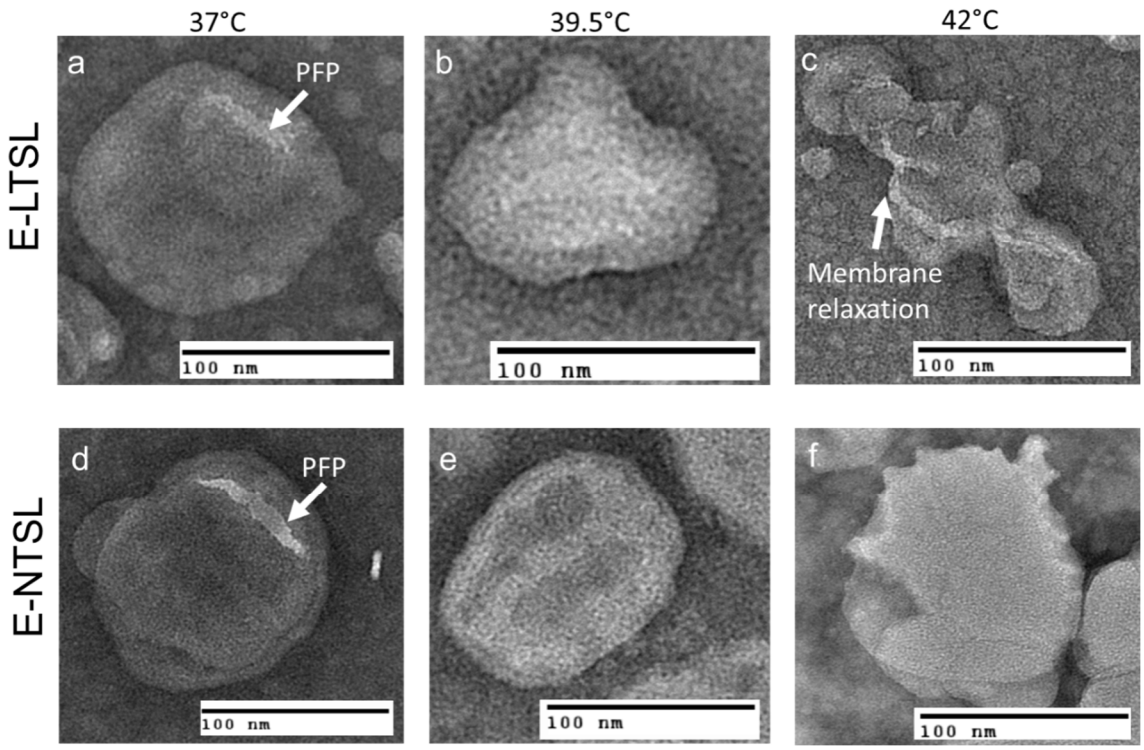

Figure. 2. a & d: TEM images of Echogenic thermosensitive (E-LTSL) and non-thermosensitive (E-NTSL) liposomes showing the spherical liposomes containing PFP-PD emulsion; (a-c) Gradual and significant relaxation of the E-LTSL membranes due to hyperthermia from 37 to 42^0C; (d-f) E-NTSL from 37-42^0C showing moderate structural changes at 42^0C

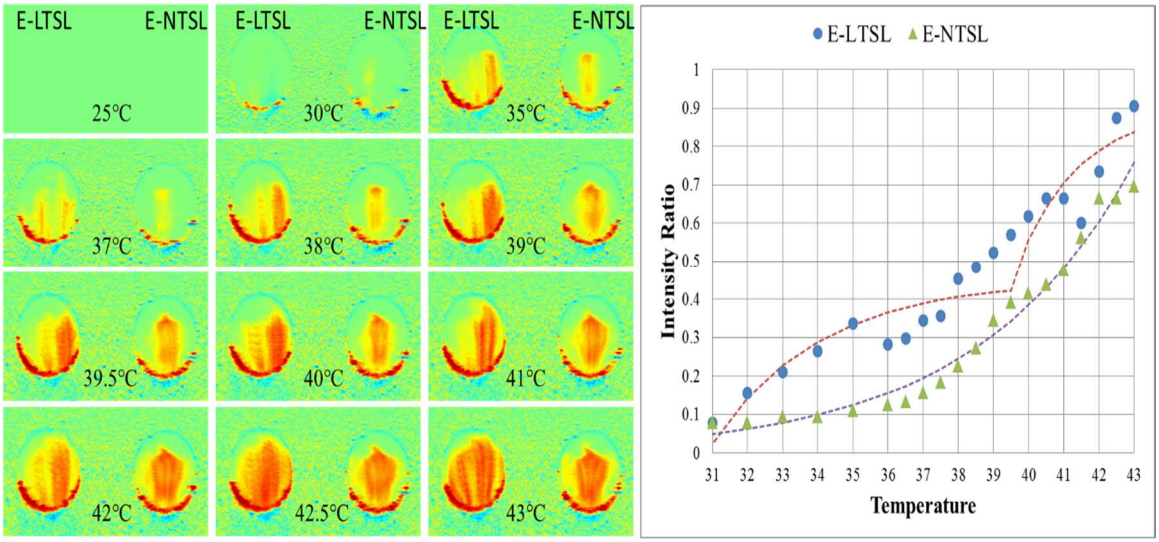

Figure. 3. a) Intensity of observed ultrasound image with respect to temperature in the range of 31-44°C, b) Fitted curves of the ultrasound image intensity of the liposome as a function of temperature by using an evolutionary solver to fit exponential models between collected release curve data points.

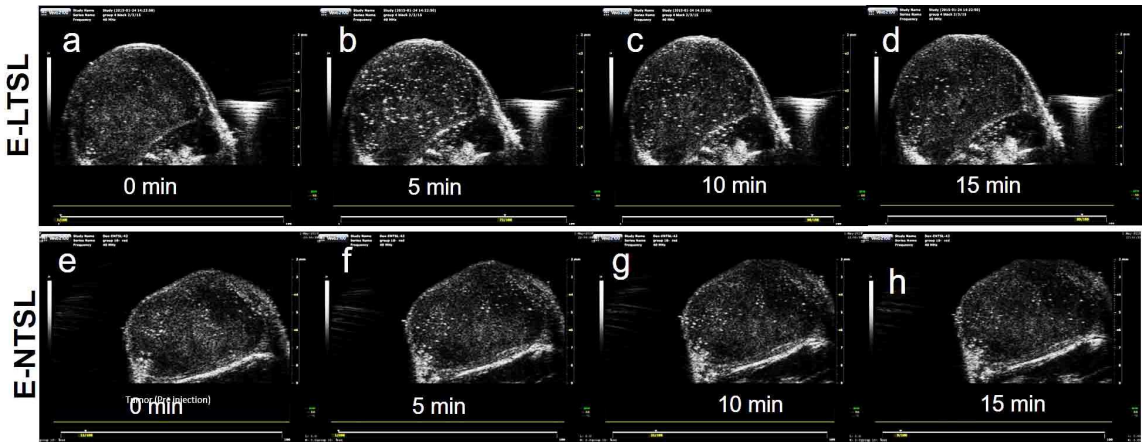

Figure. 4. Enhanced tumor contrast (B-mode) following intravenous injection of echogenic liposomes in a mouse model of colon cancer. A sustained increase in tumor contrast for E-LTSL and E-NTSL was noted compared to baseline tumor images at 10-15min. (a)Tumor image prior to E-LTSL injection; (b-d) Enhanced tumor contrast 5, 10, 15 min post E-LTSL injection respectively; (e) Tumor image prior to E-NTSL injection; (f-h) Enhanced tumor contrast at 5, 10, 15 min post E-NTSL injection respectively.

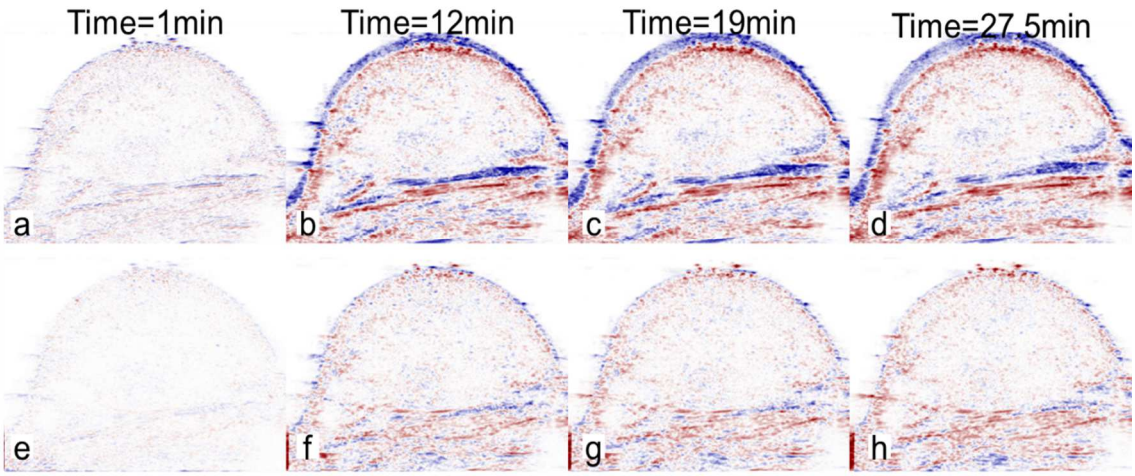

Figure. 5. Difference between ultrasound image at a given time and the reference image at time t=0s. Values are blue if difference is positive; values are red if difference is negative. Intensity values are proportional to difference.

(a-d) Tumors without motion compensation. As time progresses, difference due to motion obscures difference due to nanoparticles (E-LTSL or E-NTSL).

(e-h) Tumors with motion compensation. Gross motion is compensated allowing intensity difference due to nanoparticles to be computed.

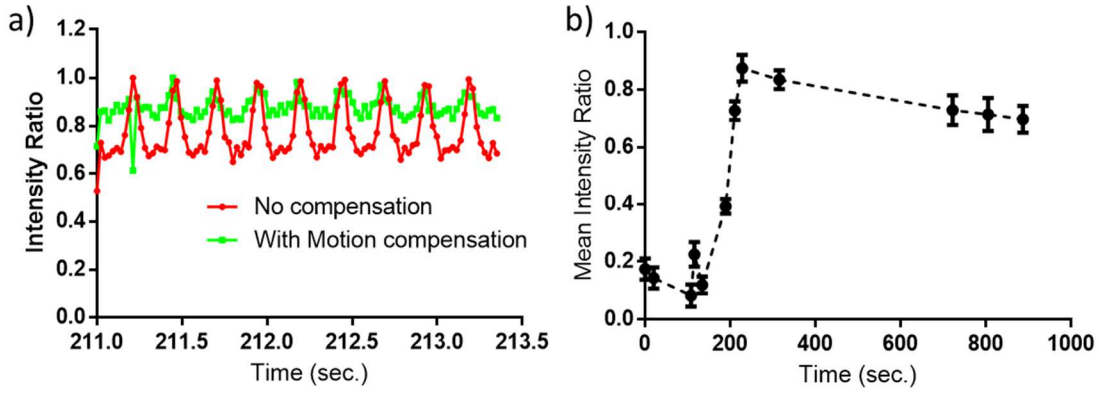

Figure. 6. (a) A magnified view of average intensity inside the ROI over 100 frames (2.35s). Motion compensation reduces the standard deviation by a factor of over 2; (b) Mean intensity inside the ROI after motion compensation of observed ultrasound image as a function of time. The error bars indicate the standard deviation in the average intensity over 100 frames (2.35s) at that time point

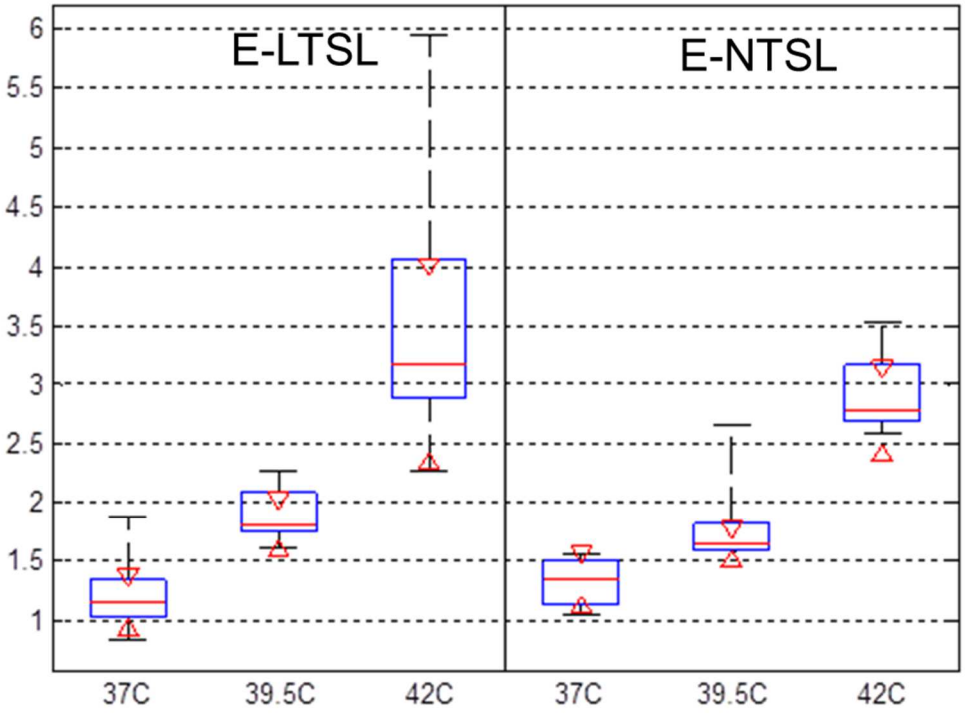

Figure. 7. Relationship between tumor vascular contrast and temperature from 37- 42°C. With increase of temperature, a corresponding increase in tumor intensity was noted (maximal signal at 42°C)

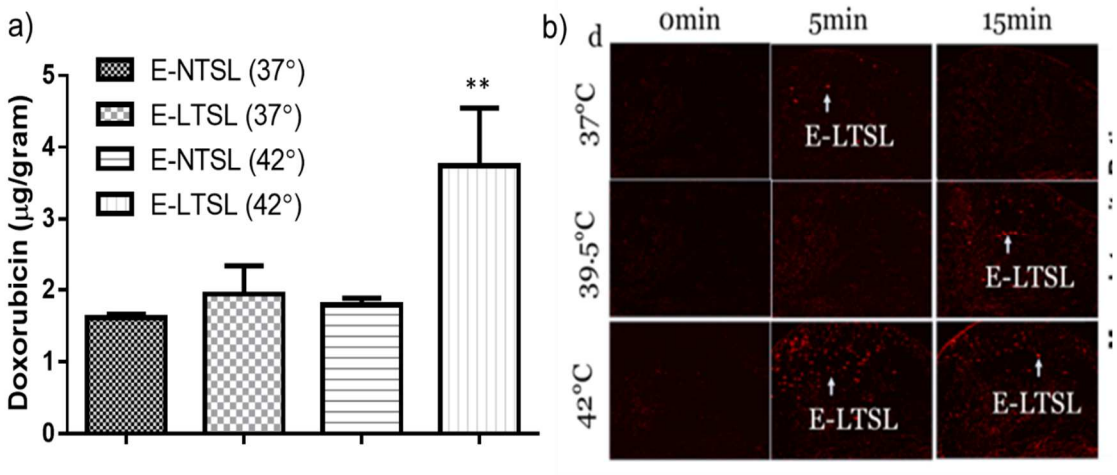

Figure. 8. a) Doxorubicin concentration determined in tumors post Dox E-LTSL and Dox E-NTSL injection. b) Motion compensated B-mode tumor contrast at 37 and 42°C contrast from 0-15min.

References

1. Ranjan, A.*, et al.* Image-guided drug delivery with magnetic resonance guided high intensity focused ultrasound and temperature sensitive liposomes in a rabbit Vx2 tumor model. *Journal of Controlled Release***158**, 487-494 (2012).
2. de Smet, M., Heijman, E., Langereis, S., Hijnen, N.M. & Grull, H. Magnetic resonance imaging of high intensity focused ultrasound mediated drug delivery from temperature-sensitive liposomes: an in vivo proof-of-concept study. *Journal of controlled release : official journal of the Controlled Release Society***150**, 102-110 (2010).
3. Needham, D., Anyarambhatla, G., Kong, G. & Dewhirst, M.W. A new temperature-sensitive liposome for use with mild hyperthermia: characterization and testing in a human tumor xenograft model. *Cancer research***60**, 1197-1201 (2000).
4. Negussie, A.H.*, et al.* Formulation and characterisation of magnetic resonance imageable thermally sensitive liposomes for use with magnetic resonance-guided high intensity focused ultrasound. *Int J Hyperthermia***27**, 140-155 (2010).
5. Ranjan, A.*, et al.* Image-guided drug delivery with magnetic resonance guided high intensity focused ultrasound and temperature sensitive liposomes in a rabbit Vx2 tumor model. *Journal of controlled release : official journal of the Controlled Release Society***158**, 487-494 (2012).
6. de Smet, M.*, et al.* Magnetic resonance guided high-intensity focused ultrasound mediated hyperthermia improves the intratumoral distribution of temperature-sensitive liposomal Doxorubicin. *Investigative radiology***48**, 395-405 (2013).
7. Kong, G.*, et al.* Efficacy of liposomes and hyperthermia in a human tumor xenograft model: importance of triggered drug release. *Cancer research***60**, 6950-6957 (2000).
8. Tashjian, J.A., Dewhirst, M.W., Needham, D. & Viglianti, B.L. Rationale for and measurement of liposomal drug delivery with hyperthermia using non-invasive imaging techniques. *International Journal of Hyperthermia***24**, 79-90 (2008).
9. Viglianti, B.L.*, et al.* Chemodosimetry of in vivo tumor liposomal drug concentration using MRI. *Magnetic resonance in medicine : official journal of the Society of Magnetic Resonance in Medicine / Society of Magnetic Resonance in Medicine***56**, 1011-1018 (2006).
10. Viglianti, B.L.*, et al.* In vivo monitoring of tissue pharmacokinetics of liposome/drug using MRI: illustration of targeted delivery. *Magnetic resonance in medicine : official journal of the Society of Magnetic Resonance in Medicine / Society of Magnetic Resonance in Medicine***51**, 1153-1162 (2004).
11. Davis, R.M.*, et al.* A method to convert MRI images of temperature change into images of absolute temperature in solid tumours. *Int J Hyperther***29**, 569-581 (2013).
12. Grull, H. & Langereis, S. Hyperthermia-triggered drug delivery from temperature-sensitive liposomes using MRI-guided high intensity focused ultrasound. *Journal of controlled release : official journal of the Controlled Release Society***161**, 317-327 (2012).

13. Kircher, M.F. & Willmann, J.K. Molecular body imaging: MR imaging, CT, and US. Part II. Applications. *Radiology***264**, 349-368 (2012).
14. Kircher, M.F. & Willmann, J.K. Molecular body imaging: MR imaging, CT, and US. part I. principles. *Radiology***263**, 633-643 (2012).
15. Fernando, R., Downs, J., Maples, D. & Ranjan, A. MRI-Guided Monitoring of Thermal Dose and Targeted Drug Delivery for Cancer Therapy. *Pharmaceutical research* 30(11):2709-2717 (2013).
16. Deckers, R.*, et al.* Absolute MR thermometry using nanocarriers. *Contrast Media Mol I***9**, 283-290 (2014).
17. Hijnen, N.M.*, et al.* The magnetic susceptibility effect of gadolinium-based contrast agents on PRFS-based MR thermometry during thermal interventions. *Journal of therapeutic ultrasound***1**, 8 (2013).
18. Maples, D.*, et al.* Synthesis and characterisation of ultrasound imageable heat-sensitive liposomes for HIFU therapy. *Int J Hyperthermia***31**, 674-685 (2015).
19. Maples, D.N., Ryan.; Ranjan, A. . Novel ultrasound imageable low temperature sensitive liposomes for use with ultrasound-guided high intensity focused ultrasound. *Society for Thermal Medicine Annual Meeting***31**, 153 (2014).
20. Rapoport, N.*, et al.* Ultrasound-mediated tumor imaging and nanotherapy using drug loaded, block copolymer stabilized perfluorocarbon nanoemulsions. *Journal of controlled release : official journal of the Controlled Release Society***153**, 4-15 (2011).
21. Kandadai, M.A.*, et al.* Comparison of surfactants used to prepare aqueous perfluoropentane emulsions for pharmaceutical applications. *Langmuir : the ACS journal of surfaces and colloids***26**, 4655-4660 (2010).
22. Rapoport, N. Phase-shift, stimuli-responsive perfluorocarbon nanodroplets for drug delivery to cancer. *Wiley interdisciplinary reviews. Nanomedicine and nanobiotechnology***4**, 492-510 (2012).
23. Senavirathna, L.K.*, et al.* Tumor Spheroids as an In Vitro Model for Determining the Therapeutic Response to Proton Beam Radiotherapy and Thermally Sensitive Nanocarriers. *Theranostics***3**, 687-691 (2013).
24. Ibsen, S.*, et al.* A novel nested liposome drug delivery vehicle capable of ultrasound triggered release of its payload. *Journal of controlled release : official journal of the Controlled Release Society***155**, 358-366 (2011).
25. Brodersen, J. & Siersma, V.D. Long-term psychosocial consequences of false-positive screening mammography. *Annals of family medicine***11**, 106-115 (2013).
26. Larsen, L.P. Role of contrast enhanced ultrasonography in the assessment of hepatic metastases: A review. *World journal of hepatology***2**, 8-15 (2010).
27. Rapoport, N., Gao, Z.G. & Kennedy, A. Multifunctional nanoparticles for combining ultrasonic tumor imaging and targeted chemotherapy. *J Natl Cancer I***99**, 1095-1106 (2007).
28. Javadi, M., Pitt, W.G., Belnap, D.M., Tsosie, N.H. & Hartley, J.M. Encapsulating Nanoemulsions Inside eLiposomes for Ultrasonic Drug Delivery. *Langmuir : the ACS journal of surfaces and colloids***28**, 14720-14729 (2012).
29. Chen, C.C. & Borden, M.A. The role of poly(ethylene glycol) brush architecture in complement activation on targeted microbubble surfaces. *Biomaterials***32**, 6579-6587 (2011).

30. Ickenstein, L.M., Arfvidsson, M.C., Needham, D., Mayer, L.D. & Edwards, K. Disc formation in cholesterol-free liposomes during phase transition. *Biochimica et biophysica acta***1614**, 135-138 (2003).
31. Denarie, B.*, et al.* Coherent plane wave compounding for very high frame rate ultrasonography of rapidly moving targets. *IEEE transactions on medical imaging***32**, 1265-1276 (2013).
32. van den Oord, S.C.*, et al.* Quantitative contrast-enhanced ultrasound of intraplaque neovascularization in patients with carotid atherosclerosis. *Ultraschall in der Medizin***36**, 154-161 (2015).
33. Bouhlel, N., Coron, A., Barrois, G., Lucidarme, O. & Bridal, S.L. Dual-mode registration of dynamic contrast-enhanced ultrasound combining tissue and contrast sequences. *Ultrasonics***54**, 1289-1299 (2014).
34. Pysz, M.A., Guracar, I., Foygel, K., Tian, L. & Willmann, J.K. Quantitative assessment of tumor angiogenesis using real-time motion-compensated contrast-enhanced ultrasound imaging. *Angiogenesis***15**, 433-442 (2012).
35. Hinshaw, J.L., Lubner, M.G., Ziemlewicz, T.J., Lee, F.T., Jr. & Brace, C.L. Percutaneous tumor ablation tools: microwave, radiofrequency, or cryoablation-what should you use and why? *Radiographics : a review publication of the Radiological Society of North America, Inc***34**, 1344-1362 (2014).
36. Partanen, A.*, et al.* Mild hyperthermia with magnetic resonance-guided high-intensity focused ultrasound for applications in drug delivery. *International journal of hyperthermia : the official journal of European Society for Hyperthermic Oncology, North American Hyperthermia Group***28**, 320-336 (2012).
37. Staruch, R.M., Ganguly, M., Tannock, I.F., Hynynen, K. & Chopra, R. Enhanced drug delivery in rabbit VX2 tumours using thermosensitive liposomes and MRI-controlled focused ultrasound hyperthermia. *International journal of hyperthermia : the official journal of European Society for Hyperthermic Oncology, North American Hyperthermia Group***28**, 776-787 (2012).
38. Salomir, R.*, et al.* Reference-free PRFS MR-thermometry using near-harmonic 2-D reconstruction of the background phase. *IEEE transactions on medical imaging***31**, 287-301 (2012).
39. Lai, C.Y.*, et al.* Noninvasive thermometry assisted by a dual-function ultrasound transducer for mild hyperthermia. *IEEE transactions on ultrasonics, ferroelectrics, and frequency control***57**, 2671-2684 (2010).
40. Bing, C.*, et al.* Localised hyperthermia in rodent models using an MRI-compatible high-intensity focused ultrasound system. *Int J Hyperthermia*, 1-10 (2015).
41. Bicher, H.I.*, et al.* Effects of hyperthermia on normal and tumor microenvironment. *Radiology***137**, 523-530 (1980).

CHAPTER III

CHEMO-IMMUNOTHERAPY WITH FOCUSED ULTRASOUND AND SALMONELLA-LADEN THEMPERATURE SENSITIVE LIPOSOMES (THERMOBOTS) IN MURINE COLON TUMOR MODEL

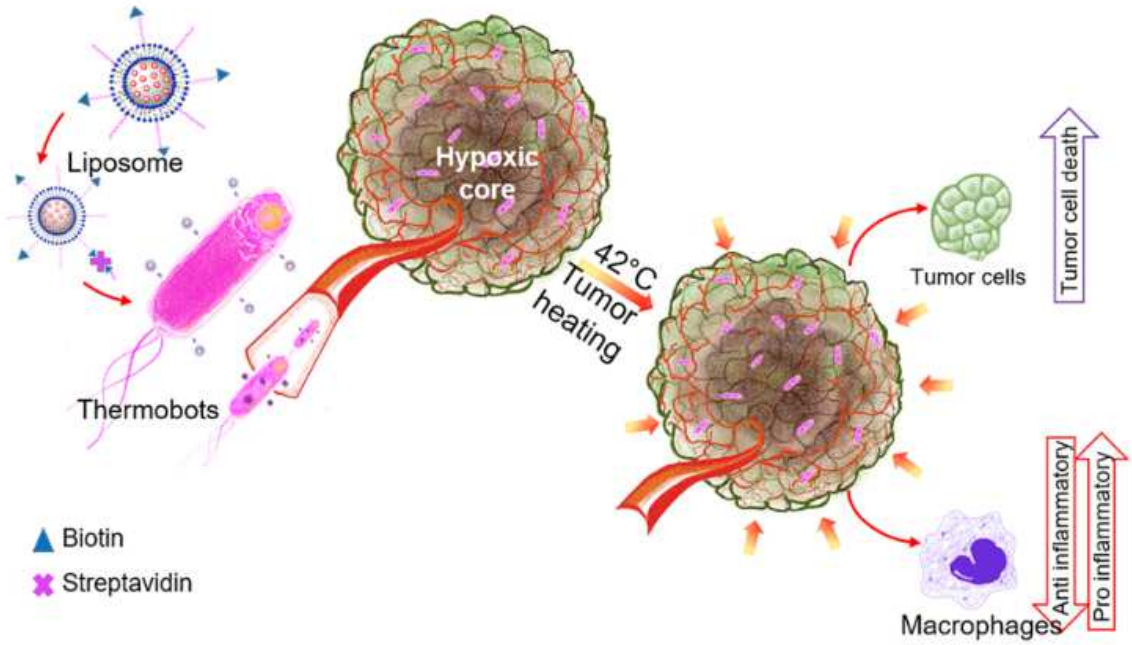

Schematic of thermobot and heat-combined chemo-immunotherapy approach against colon cancer

---

[1] Earlier version of this chapter has already been published as Ektate, K.; Munteanu, M.C.; Ashar, H.; Malayer, J.; Ranjan, A. Chemo-immunotherapy of colon cancer with focused ultrasound and Salmonella-laden temperature sensitive liposomes (thermobots). *Sci. Rep.* **2018**, *8*, 13062.

Abstract

Using attenuated *Salmonella* that efficiently homes in solid tumors, here we developed thermobots that can actively transport membrane attached low-temperature sensitive liposomes (LTSL) to colon cancer cells for triggered doxorubicin release and simultaneous polarization of macrophages to M1 phenotype in combination with high intensity focused ultrasound (HIFU) heating (40-42°C). Biocompatibility studies showed that the synthesized thermobots were highly efficient in LTSL loading without any impact on its viability. Thermobots demonstrated efficient intracellular trafficking, high nuclear localization of doxorubicin, and induced pro-inflammatory cytokine expression in colon cancer cells in vitro. TB and Image-guided non-invasive HIFU heating applied for a total of ~30 min to murine colon tumors enhanced therapeutic efficacy and polarization of macrophages to M1 phenotype in vivo. Data suggest that the innovative dual-mode thermobots/HIFU modality may improve therapeutic targeting of colon cancer.

Introduction

Colorectal cancer (CRC) is the second leading cause of cancer-related deaths with an incidence rate of 40 % in the United States and an average 5-year survival rate of <15% in metastatic disease [1]. Chemotherapy of metastatic CRC has modest efficacy and is typically associated with significant toxicities. Some recent clinical trials suggest that patients with refractive CRC tumors can benefit from the enhancement of the tumor-immune system interactions [2,34,5]. The objective of this study was to combine novel thermosensitive liposome-laden *Salmonella* (Thermobots; TBs) with high intensity focused ultrasound (HIFU) heating (~40-42ºC) to determine whether this approach influences tumor immunological changes to enhance chemotherapy outcomes.

Attenuated bacterial microorganisms such as *Clostridium*, *Listeria*, *Salmonella*, *Shigella* and *Escherichia coli* are known to self-propel and home within a solid tumor as tumoricidal agents [6-12]. In particular, *Salmonella typhimuriu*m (YS1646) demonstrates high chemotaxis towards the serine, ribose, and aspartate produced within the benign and metastatic tumor core by the quiescent and hypoxic cells[7,13,14]. Like bacteria, conventional liposomes can also accumulate in tumor due to the leaky vasculature[15-17].

Both liposome and Salmonella provide some levels of tumor clearance, however, each modality by itself is insufficient in the killing of tumor cells[18]. To overcome this barrier, we developed TBs by loading Salmonella with low-temperature sensitive liposomes (LTSL). LTSLs contains the lyso-pc lipid that undergoes a structural and chemical phase change in response to HIFU heating (~42ºC) to achieve triggered drug delivery in tumors [19-26]. HIFU heating also augments the release of heat shock protein antigens to stimulate anti-tumor immunity [23,27,28]. We posit that the immune effects in the tumor microenvironment will be aided further by the simultaneous interactions of the Salmonella membrane lipopolysaccharide (LPS) and doxorubicin (Dox) that are known pro-inflammatory agents [29]. Towards this goal, here we provide insights on the feasibility ofTB design principles and chemoimmunomodulatory effects with HIFU heating in murine melanoma.

2. Results

2.1 ***Salmonella efficiently loads and maintains the therapeutic efficacy of LTSLs.*** Prior research has shown that stealth liposomes passively adsorb on the bacteria membrane by electrostatic or Van der Waals type attraction [30]. However, the detachment of the liposomes from the bacterial membrane in a circulatory environment can be a concern. To address this, we synthesized TBs by attaching LTSL onto Salmonella membrane using Biotin-Streptavidin chemistry [14,31]. Epifluorescence microscopy showed the presence of fluorescent Dox (red) overlapped with the rod-shaped*Salmonella* membranes (Fig 1a). SEM confirmed that this likely came from the LTSL as indicated by the presence of punctate dots on the bacterial membrane (Fig. 1b). In general, an average of 15-20 liposomal dots (n=25) were notedon the bacterial membrane. In contrast, *Salmonella* alone appeared smooth. Next, we quantified the Dox loading potential of TBs by flow cytometry and fluorescence spectroscopy.A gradual shift in the mean fluorescence intensity of TBs in the Dox filter was noted relative to Salmonella alone (Fig. 1c). Also, compared to TBs that were passively incubated with LTSLs (TB1; MFI: 8.16±.014), the shift was significantly higher for Biotin-Streptavidin attached TBs (TB2; MFI: 21±0.14; Fig. 1d; see Table 1 for lipid compositions). These observations matched with fluorescence spectroscopy measurement that showed ~7.5 times more Dox/bacteria

for TB2 (540± 80 ng/ml) compared to TB1 (70± 10 ng/ml) (Fig 1e). Notably, the enhanced loading of Dox was not associated with significant changes in the bacterial viability between *Salmonella* and TBs as determined by SYTOX staining (Fig 1f).

We next characterized the intracellular trafficking and cytotoxicity of TBs. C26 colon cancer cells were incubated with Dox, LTSL, TB1, and TB2 in the presence and absence of heating (~42°C). Confocal microscopy showed significant nuclear localization of Dox in the heated cells. Specifically, 4 h post infection, the uptake and nuclear localization of Dox from TBs were significantly higher with 42°C compared to body temperature (Fig 1i). The increased TB2 uptake and Dox release with heat correlated with enhanced therapeutic efficacy (~80% C26 killing) compared to TB alone (~50%). Importantly, while the efficacy of TB1 and TB2 was similar at body temperature (~35-40% killing), TB2 demonstrated relatively higher potency upon adding heat (~80% killing) compared to TB1 (60%), presumably due to enhanced stability of membrane attachment and Dox transport inside the colon cell. Based on these data, TB2 (abbreviated as TB) was selected for further in vitro and in vivo evaluation.

2.2. TB and heat treatment enhances pro-inflammatory gene expression in vitro. LPSendotoxin present in the outer leaflet of *Salmonella* interacts with immune cells to promote the secretion of proinflammatory cytokines, nitric oxide, and eicosanoids [32]. Whether the LPS immune effects synergizes with TB/heat therapy is not known. Thus, the conditioned media from C26 cells that were treated with Dox, LTSL, Salmonella, and TB2 in the presence and absence of heat was added to RAW264.7 macrophages, and the pro-inflammatory (TNF-α) and anti-inflammatory (IL10) cytokine expression was assessed. Heat plus TB treatment significantly enhanced TNF-α in the macrophages compared to all treatment groups at 37°C (Fig. 2a). This increase in pro-inflammatory cytokine was also accompanied by a decrease in IL10 expression in the heated groups compared to controls (Fig. 2b). These results suggest that adding heat to TB or Salmonella treatment increases pro-inflammatory properties of colon cancer cells.

2.3 *TBs and HIFU therapy enhances therapeutic efficacy in vivo.* The efficacy of TB/HIFU was evaluated by tumor growth and histological measurements. Briefly, when

the C26 tumors reached >400mm^3 volume, the mice were treated with TBs and Salmonella (Fig. 3a). 24h post injection, a single non-cytotoxic HIFU treatment (~42°) for ~30 min was administered, and tumor volumes were measured for 5days post treatment. A pronounced increase in tumor volume (400-500 mm$^{3)}$ was observed for HIFU similar to untreated control mice (fig. 3b). In the bacteria treated mice, the tumor colonization rates were similar for Salmonella and TBs (Fig.3c). *Salmonella*-alone treatments induced significant tumor volume reduction; however, the effects were not impacted by the HIFU treatment. In contrast, the addition of HIFU heating to TB treatment resulted in greater suppression of tumor growth rates compared to Salmonella or TB alone, likely due to triggered Dox release in colon cells. Next the treated tumors were investigated by H&E staining. Mild HIFU heating didn't induce focal necrosis, however a slight increase in the apoptotic bodies was noted. This increase in tumor apoptosis with HIFU was not accompanied with a significant increase in the overall lymphocyte populations between various treatments groups (Fig. 3d)

2.4. *TB and HIFU treatment alters tumor immune environment towards M1 phenotype.* The mechanisms underlying the in vivo immunomodulatory effects of TB/HIFU combination was analyzed in the harvested tumor by flow cytometry. TB/HIFU combination caused the highest increase in the expression of M1 macrophages when expressed as per gram of tumor compared to all other treatments. HIFU heating also enhanced the M1 phenotype in Salmonella alone group; however, this was accompanied with a proportional increase in the M2 phenotype. In contrast, TB/HIFU M1 induction didn't result in a compensatory increase in M2 phenotype (Fig. 4a-b). The immune microenvironment was also characterized for changes in the influx of either granulocytic (Ly6G+) or monocytic (Ly6C+) myeloid-derived suppressor cells (MDSCs) and T-cells. The MDSCs, and the general cytotoxic/killer (CD3+, CD8+) T cells and helper (CD3+, CD4+) cells and interferon gamma (IFN-γ) expressing CD4+/CD8+ cells/g tumor expression didn't show significant changes at the time of tumor harvest (Fig. 4c-i).

3. Discussion

In this study, the feasibility of combining bacteriolytic chemotherapy with TB in combination with HIFU heating was assessed. We hypothesized that TBwill

simultaneously induce tumoricidal effects, while also aiding in the antitumoral immunity with HIFU heating. To enhance in vivo stability, TBs were created by attaching LTSLs onto *Salmonella* membrane actively using Biotin-Streptavidin chemistry [14,31]. Biotin-Streptavidin isamongst the strongest known non-covalent protein-ligand reaction (Ka=2.5 x 1013M-1) [33,34]. This method of cross-linking resulted in a ~7.5 fold greater membrane binding of LTSL compared to passive incubation without impacting bacterial viability or cellular uptake (Fig. 1c-i). Also, in contrast to some prior reports where *Salmonella* achieved drug deposition mostly in the perinuclear region, TBs with heat achieved efficient drug delivery in both the cytoplasm and the nucleus of C26 cells [35]. Most likely, the heat treatment of cells enhanced membrane fluidity and protein rearrangement in the cells aided the Dox transport kinetics molecules [36]. An additional unexplored but key finding was the initiation of pro-inflammatory phenotype in macrophages following exposure to TB/Heat treated 10% conditioned media. 10% condition medium was chosen in vitro to mimic *in-vivo* condition of colon tumors where the peritumoral macrophages are likely exposed to such level of tumor-derived cytokines [37]. A high expression of TNF-α, and decreased expression of IL10 was noted in the macrophages. Macrophages and dendritic cells are the main producers of TNF-α and their activation typically shifts the macrophage phenotype from pro-tumoral M2 to M1 [37,38]. To explore this premise, we assessed M1 and M2 macrophage population in the treated tumors. Both TB and TB/HIFU treatment enhanced M1 phenotype compared to all other treatment groups (Fig.4), thereby resulting in a relatively enhanced regression of tumor cell in vitro and in vivo compared to controls.

Our study has some limitations. First, while heat treatment decreased IL10 expression in vitro, contrastingly an enhanced IL-10 serum protein level expression was observed in vivo (Fig. 2, 5). IL-10 is commonly regarded as an immunosuppressive cytokine that favors tumor escape from immune surveillance [39]. However, there are also some reports that suggest that IL-10 inhibits tumor-induced angiogenesis and enhance the production of tumor-toxic molecules [e.g., nitric oxide (NO)], especially in lymphoma tumors[39]. While a detailed interplay of cytokines and immune vascularity was not fully characterized, we believe that the pro-inflammatory TNFα mediated macrophage activation mitigated the IL10 immune suppressive effects to some extent. Studies to

delineate the role of IL10 on tumor modulatory pathways especially in the context of Doxorubicin, HIFU and Salmonella combinatorial therapy are currently in works.

Another limitation was lack of significant changes in the T cell and MDSC population in the tumors (Fig 4c-i). In particular, the clonal expansion of T-cells is key to resistance against recurrence. Although the exact reasons are unclear, late stage growing necrosing tumors with reduced presence of patent vasculature (>400 mm3) can decrease the infiltration of T-cells form lymph node. To address this, future studies can explore these mechanisms further especially by analyzing the T-cell dynamics in draining lymph node, and MDSCs in spleen tissue.

4. Conclusion

We report for the first time novel thermobots for chemoimmunotherapy with HIFU heating. TBs enrich M1 macrophage phenotype and achieve triggered release in tumors to enhance therapeutic effects. This technology has the potential for further investigation for application in dual-modality therapy settings.

5. Materials and methods

5.1 Materials

The lipids monostearoyl-2-hydroxy-sn-glycero-3-phosphocholine (MSPC), 1, 2-dipalmitoyl sn-glycero-3-phosphocholine (DPPC), and 1,2-distearoyl-sn-glycero-3-phosphoethanolamine-N-[methoxy (Polyethylene glycol)2000] (DSPE-mPEG2000) were obtained from Corden Pharma Corporation (Boulder, CO, USA). DSPE-PEG (2000)-Biotin was purchased from NANOCS (NY, USA), and Streptavidin (97062-810) was bought from VWR (PA, USA). EZ-link NHS-LC-Biotin and trypsin-EDTA, MatTek 35 mm glass bottom dish with 10 mm glass diameter (NC0445924), SYTOX™ Blue dead cell stain (S348557), TRIzol reagent (15596018), and DNase I (EN0525) was obtained from Thermo Scientific (MA, USA). iScript™ Reverse Transcription Supermix for RT-qPCR (1708840) was purchased from Bio-Rad (CA, USA). Doxorubicin (Dox) was acquired from LC Laboratory (MA, USA). The PD-10 column was obtained from GE Healthcare Life Sciences, (Buckinghamshire, United Kingdom).

Ethylenediaminetetraacetic acid (EDTA) and 4-(2-Hydroxyethyl) piperazine-1-ethane sulfonic acid, and N-(2-Hydroxyethyl) piperazine-N′-(2-ethanesulfonic acid) (HEPES) were acquired from Sigma (St. Louis, MO). Luria broth (LB) agar and broth were purchased from BD (NJ, USA). Fetal bovine serum was procured from Atlanta Biologicals (GA, USA), and Penicillin/ Streptomycin was acquired from Invitrogen (CA, USA). Fluorochrome-conjugated anti-mouse monoclonal antibodies were purchased from BioLegend (CA, USA: APC-CD11b (101212), PE-CD86 (105008), PE-Ly6C (128008), PE-CD4 (100512), APC Cy7-IFNg (505850), Pacific blue-F4/80 (123124), Alexa fluor 700-CD206 (141734), and BD biosciences: FITC-Ly6G (1A8) (551460). UltraComp eBeadswere purchased from Fisher Scientific (Hampton, NH). SYBR green reagent (qPCR Master Mix Plus for SYBR green) was purchased from Eurogentec (Liège, Belgium). ELISA kits for TNF-α(MTA00B), IL1-β (MLB00C) and IL-10 M1000B were purchased from R&D (MN,USA). C26 cells were kindly provided by the National Cancer Institute, and RAW 264.7 cells were obtained from ATCC. *Salmonella typhimurium* (YS1646) was purchased from ATCC (Manassas, VA, USA).

5.2 LTSL synthesis and characterization

LTSLs (lipid composition: DPPC, MSPC, and DSPE-mPEG2000; molar ratio of 85.3:9.7:5.0) were prepared by hydration of lipid film followed by the extrusion [40]. For cross-linking to *Salmonella* membrane, DSPE-PEG2000-biotinlipid was incorporated in the LTSL membrane (lipid composition: DPPC, MSPC, DSPE-mPEG2000, and DSPE-PEG2000-Biotin; the molar ratio of 85.3:9.7:4.0:1). Briefly, lipids were dissolved in chloroform, and the solvent was evaporated. The resulting lipid film was hydrated in citrate buffer (pH 4.0) at 55 ^{0}C for 30 minutes and extruded five times through double stacked 200nm polycarbonate filters. Encapsulation of Dox into the liposomes was carried out using a pH gradient loading protocol as described by Mayer et al. [41] LTSLs were characterized for size (z-average), polydispersity index and zeta potential using dynamic light scattering (DLS) with a 90 plus PALS Nanobrook device (Brookhaven Instruments, Holtsville, NY, USA). Briefly, 10-20 µl of LTSLs were added to 2 ml of PBS in a cuvette, and DLS measurements were recorded at room temperature. An average of five measurements was taken, and the mean size and standard deviation were

calculated for the LTSLs. For recording the zeta potential, 10 µl of the liposomes were suspended in 1500 µl of double distilled water, and an average of 5 measurements was taken to record the mean zeta potential.

5.3 Synthesis of LTSL attached *Salmonella* (Thermobot or TB)

Table 1. Cross-linking schemes for Thermobot (TB)

Thermobot (TB)	**Lipid Composition**	**Diameter± SD (nm) (LTSL)**	**Poly dispersity Index± SD (LTSL)**	**Zeta Potential± SD (mv) (LTSL)**	**Biotin-Streptavidin reaction**
TB1	DPPC, MSPC, and DSPE-mPEG2000	170.41 ±3.1	0.125 ±0.02	-27.41 ±4.3	No
TB2	DPPC, MSPC, DSPE-mPEG2000, and DSPE-PEG2000-Biotin	177.67 ±3.3	0.104 ±0.01	-34.34 ±13.3	Yes

A library of LTSL attached *Salmonella* with active and passive cross-linking schemes as given in Table 1 were synthesized [42]. For cross-linking, 3 x 10^8 CFU of *Salmonella* was suspended in 0.5 ml PBS with 100µg of EZ link NHS-Biotin (dissolved in 5µl DMSO) for 45 min at room temperature under mild shaking.Free EZ link NHS-Biotin was removed by centrifuging at 3000 x g for 10 min and washing 2 times with PBS. Cross-linkingwith LTSL'swas achieved by incubating 3 x 10^8 CFU of Salmonella with 100µg of Streptavidin solubilized in deionized water and 100µl of 22mM Dox loaded LTSL for 1 h at room temperature. As additional controls, Salmonella was passively co-incubated with 100µl of 22mM Dox loaded LTSL for 1h. Unattached liposomes were separated out

by centrifuging the bacterial suspension at 3000 x g for 10 minutes. The bacterial pellet was washed 2x with PBS and resuspended in 500µl of PBS for further analysis.

5.4 Quantification of Dox in TBs with flow cytometry and spectroscopy

TBs (n=3; 3 x 10^8 CFU) were examined in a FACS Aria flow sorter (BD Biosciences, Franklin Lakes, NJ, USA) at an excitation wavelength of 488 nm and a 590/30-nm emission filter using BD FACS Diva 8.0.1 software. Data were computed and compared from the dot *plots* and histogram plot by counting 10,000 single cell events.

For Dox quantification by fluorescence spectroscopy, TBs (3 x 10^8 CFU) suspended in 0.5 ml of PBS was heated in a water bath maintained at 45°C for 30 minutes. The bacteria were centrifuged at 3000 x g for 10 min., the supernatant containing the released Doxwas collected and the fluorescence was measured at a wavelength of 480/590 nm with Spectramax (CA, USA) microplate reader. Concentrations of the Dox in supernatants were determined from the linear calibration curve using least squares regression method based on the nominal concentration.

5.5 Dox imaging in TB by fluorescence and SEM imaging

Based on flow and Dox loading, TB2 was selected from 5.4. 200ul of diluted TB was added to cover the glass surface of MatTek dish (10 mm glass diameter) for imaging with 60x oil immersion objective. All imaging was acquired using Olympus ZDC2 IX81 fluorescence microscope equipped with a color CCD camera, cooled monochrome CCD camera, motorized scanning stage, and Metamorph mosaic stitching software. Dox fluorescence was collected and measured at a wavelength of 480/590 nm using a 20 ms exposure time with a custom made a filter (excitation 480/40 nm, emission 600/60 nm, and dichroic 505lp) at 60x APO.

For SEM, TB2 and control *Salmonella* wasfixed for 2h in 2.0% glutaraldehyde in 0.2M cacodylate at room temperature, rinsed 3x with PBS, and then fixed for 1 hour in 1% OsO4 in 0.2M (in water). Fixed samples were then washed 3x with PBS and 20µl of fixed TB3 and *Salmonella* was placed onto a poly-L-lysine coated 12mm glass slide and incubated for 30 minutes. The slides were washed with ultrapure deionized water.

Samples were dehydrated with increasing content of ethanol for 15 minutes. at each concentration (30%, 50%, 70%, 90%, 95% and 100%). A critical point dryer (BAL-TEC CPD030), was used to remove ethanol from the dehydrated samples. Samples were immediately mounted on stubs with carbon tape and a wafer coated with gold/palladium prior to imaging (Cressington Carbon Coater; Balzers Union MED 010 Au/Pt coater). High-resolution images were captured with FEI Quanta 600 field emission gun ESEM with Evex EDS and HKL EBSD at an accelerating voltage of 20 kV, and a working distance of <10mm and the number of nanoparticles attached on the surface of 25 bacteria was counted manually to determine the average number of nanoparticles attached on bacteria.

5. 6 Assessment of TB viability by Flow cytometry

5 X10^7 CFU of *Salmonella* and TB's was diluted in PBS to achieve a final volume of 1 ml for viability analysis with SYTOX blue dead cell stain. 1µl of SYTOX blue was added to each sample to achieve a final dye concentration of 1µM followed by 5 min. incubationin dark at room temperature [43]. *Salmonella* with no treatment and no SYTOX blue was used as a control for setting up the flow voltage and gate parameters. Samples were analyzed without washing or fixing using a 440/40 nm bandpass filter with BD FACS Diva 8.0.1 software. Datawere computed and compared from the dot *plots* and histogram plot by counting 10,000 single cell events.

5.7 Assessment of cellular uptake of TB

2.5 x 10^4 C26 cells were seeded in glass bottom Petri dishes overnight and were incubated at a multiplicity of infection of 50 with *Salmonella*, TB1 and TB2 at 37°C or 42 °C for 1, 4 and 12 h. LTSL (containing 0.02µg of Dox) incubated under similar conditions as TB served as a control.Prior to imaging, cells were rinsed with PBS 2x, fixed by adding 1ml of 4% paraformaldehyde to the plates for 15-20 minutes at room temperature. The nucleus was counterstained with DAPI (3uM) for 10 minutes at room temperature and rinsed 2x with PBS. Imaging was performed using Olympus IX81 confocal microscope with the Doxorubicin filter (ex/em of 480/590) and the DAPI filter (ex/em of 365/440) at 40x by randomly selecting multipleregions in the petri dish.

5.8 Evaluation of TB cytotoxicity

Cytotoxicity was assessed for TB at 50 MOI (multiplicity of infection) at 37 and 42^0C. C26 cells ($1x10^5$ cells/well) cultured in RPMI 1640 media supplemented with 10% Fetal Bovine Serum (FBS) and 1% Penicillin/Streptomycin at 5% CO_2 and 37^0C were seeded into 96 well flat bottom plate for 24 h. Cells were washed 2x with PBS to remove antibiotic. TBs and *Salmonella* (50 MOI) suspended in no antibiotic and serum-free medium containing 10μM of Dox was added to the culture well and incubated for 4h at 37 °C and 42°C. Extracellular TB were removed by treating with RPMI containing 50μg/ml of gentamicin for 1h at 37°C. Next, the culture media was discarded, well were washed with PBS and re-suspendedin 100 μL of cell culture media, and incubated at 37°C for ~20h. An *in-vitro* homogeneous, colorimetric method for determining the number of viable cells using the MTT (3-(4, 5-dimethylthiazol-2-yl)-2, 5-diphenyltetrazolium bromide) was used to determine any cytotoxic effects of the released Dox. Briefly, 10μl of 12mM MTT was pipetted into each well, and the plates were incubated for 4 hours at 37 °C in a humidified 5% CO_2 atmosphere. The absorbance was recorded at 540 nm with Spectramax (CA, USA) microplate reader.

5.9 Immune analysis in vitro

5.9.1C26 cell conditioned mediumcollection

5 x 10^5 C26 cells /well were treated with 50 MOI of *Salmonella*, TBs and LTSL (containing 50 ng Dox) for 4 h at 37 or 42 °C in RPMI medium (no antibiotic, no serum). Extracellular bacteria were removed by treating with gentamicin (50μg/ml) for 1h, and cells were cultured for 6h in serum free media. Next, tumor cell conditioned media was collected, centrifuged at 1000 rpm for 5 minutes to remove cell debris and the supernatant was stored at -80°C.

5.9.2 Treatment of RAW 264.7 macrophages with colon cancer conditioned medium

0.5 x 10^6 RAW 264.7 cells suspended in 2mL media were seeded in 24 well culture plates overnight. Confluent cells were treated for 24 h with 10% C26 conditioned media

from 5.9.1 at 37°C in 5% CO2 incubator. For RNA extraction, media was discarded and cells were collected in 1 ml TRIzol reagent and stored at -80°C until RNA extraction was performed.

5.9.3 RNA isolation and DNase treatment from RAW 246.7 cells and tumors for gene expression analysis

Total RNA from the RAW 264.7 cells was extracted using TRIZOL according to the manufacturer's instructions. RNA concentration was measured using NanoDrop ND-100 and 5µg of total RNA was treated with DNase I according to manufacturer's protocol. Post DNase I treatment, the RNA was purified with the phenol-chloroform methodology.

5.9.4 Reverse Transcription Polymerase Chain Reaction (RT-PCR).

cDNA synthesis was performed using 1µg DNase I treated RNA per reaction using iScript Reverse Transcription Supermix for RT-qPCR. Real-Time RT-PCR reaction was performed with cDNA diluted 5 x.

5.9.5 Quantitative Real-Time Reverse Transcription Polymerase Chain Reaction (qRT-PCR)

Relative gene expression for IL1β, TNFα (M1 cytokines), and IL10 (M2 specific cytokines)was evaluated by qRT-PCR using SYBR green reagent using Applied Biosystem 7500 fast Real-Time PCR instrument and indicated specific primers sequences (Table 3). qRT-PCR data were analyzed by the $2^{(-\Delta\Delta CT)}$ method using GAPDH as a reference gene.

Table 2. qRT-PCR primers sequences

qPCR primers	Species	Sequences
mGapdh-forward	*Mus musculus*	CATCACTGCCACCCAGAAGACTG
mGapdh-reverse	*Mus musculus*	ATGCCAGTGAGCTTCCCGTTCAG
mTnf-alpha-forward	*Mus musculus*	CACCACCATCAAGGACTCAA
mTnf-alpha-reverse	*Mus musculus*	AGGCAACCTGACCACTCTCC

mIl1-beta-forward	*Mus musculus*	TGGACCTTCCAGGATGAGGACA
mIl1-beta-reverse	*Mus musculus*	GTTCATCTCGGAGCCTGTAGTG
mIl10-forward	*Mus musculus*	CGGGAAGACAATAACTGCACCC
mIl10-reverse	*Mus musculus*	CGGTTAGCAGTATGTTGTCCAGC

5.10 Evaluation of CD86 and CD206 on RAW 264.7 cells by flow cytometry

0.5 x 10^6 RAW 264.7 cells treated with 10% C26 cell conditioned media for 24h were imaged at 20x magnification with Olympus ZDC2 IX81 microscope to observe the cellular morphology of macrophages. For CD86 and CD206 marker evaluation, cells were trypsinized and fixed in 4% paraformaldehyde for 10-15 minute at room temperature. Next, cells were washed and re-suspended in 1 ml PBS containing 2% fetal bovine serum. 5 x 10^4 cells were incubated for 30 min with the primary anti CD86-PE antibody and primary anti CD206-Alexa Fluor 700 antibody. Isotype corresponding to each primary antibody was included as a control. Three washes with 1x PBS containing 2% FBS were performed, and cells were analyzed by flow cytometry with FACScalibur (BD Biosciences). Data were analyzed with FlowJo software v.10.2 (Tree Star Inc, OR, USA).

5.11 In vivo study model of colon cancer

All animal-related procedures were approved and carried out under the regulations and guidelines of the Oklahoma State University Animal Care and Use Committee. Female 10-week Balb/c mice (Charles River, Wilmington, MA) were inoculated with 0.5 x 10^5 cells/50µl in the thigh region using a 25-gauge needle (BD, Franklin Lakes, NJ, USA). Mice were monitored and tumor growth was measured by serial caliper measurements (General Tools Fraction+™, New York, NY, USA). Tumor volumes were calculated using the formula (length X $width^2$)/2, where length is the largest dimension and width is the smallest dimension perpendicular to the length. When the tumors reached a volume of 400-500 mm^3 mice, were randomized into 6 groups (n=6-7/group). Treatment groups were designed as follows: Control+/– HIFU, *Salmonella*+/– HIFU, TB+/– HIFU. For in vivo treatment, 10^6 *Salmonella* or TB were administered by intravenous injection, and

HIFU was administered 24h later. All mice were sacrificed 5 days after the injection and the tumor, liver and spleen and blood were collected for further processing.

5.12 HIFU hyperthermia treatment set-up and methodology

For HIFU treatment, mice were anesthetized with 2–5% isoflurane and restrained in custom built mouse holders attached to a 3D positioning stage. An integrated ultrasound-HIFU Alpinion platform with 1.0 MHz central transducer frequency, 45 mm radius, and 64 mm aperture diameter with a central opening 40 mm in diameter was used for tumor identification and treatment. The mouse was oriented so that its dorsal side was facing the transducer and the caudal half was lowered into a 37 ºC water bath. The path from the transducer to the tumor was aligned along the z-axis. The center of the tumor was aligned with the HIFU focus at a fixed focal depth for efficient coverage, and VIFU-2000 software was used to define the target boundary and slice distance in X, Y, and Z directions for automatic rastering of the transducer as demonstrated previously [44]. HIFU treatment parameters used were as follows: 35% duty cycle, 5Hz PRF, and 6W Power to achieve a mean target temperature of 40–42.5 ºC at the focus. A 3 x 3 raster pattern was followed for hyperthermia treatment of tumors with HIFU. The distance between any two central focus points on a tumor was 2 mm to ensure that the entire volume was heated to ~42 ºC. Each point (1 x 1 x 10 mm) within the raster pattern was heated 60 s. The total treatment duration was ~30 min. to cover the entire tumor.

5.13 Post-treatment tissue analysis

Upon completion of treatment, mice were euthanized. Tumor and tissue samples from liver, spleen blood were collected for flow cytometry, qPCR and ELISA. Tumor and serum samples for qPCR and ELISA were snap-frozen over liquid nitrogen, and stored at −80 °C until analysis.

5.14 Flow cytometric analysis

Tumor tissues were minced and digested in 200 U/ml collagenase IV buffer at 37^0C for 1.5 hours. The digested tissue was strained using a 70µm cell strainer (Corning Inc., Corning, NY) to obtain single cell suspensions. Cells were stained using antibody mixes, for different immune cell populations, prepared in 1X PBS with 2% FBS staining buffer, incubated for 1 hour at 40C in dark. For IFNγ detection, staining buffer contained 0.1%

saponin was used for permeabilization. The labeled cells were then fixed in 4% paraformaldehyde and analyzed using FACS Aria flow sorter (BD Biosciences, NJ) using the following panel - M1 macrophages (CD11b+ F4/80+ CD86+), M2 macrophages (CD11b+ F4/80+ CD206+), myeloid-derived suppressor cells (MDSCs)- granulocytic (CD11b+ Ly6G+ Ly6C-) and monocytic (CD11b+ Ly6G- Ly6C+), and T cells (CD3+ CD4+ CD8+ IFNγ). UltraComp eBeads were used for compensation controls as per the manufacturer's instructions. Fluorescence-minus-one (FMO) samples were used as negative controls. Data was analyzed using FlowJo software v.10.2 (Tree Star Inc, OR, USA). Data is expressed expressed as cell number per g of tumor using the formula N=NSxNT/NAxW, where NS is cells of interest, NA - number of cells counted in flow cytometer (singlet tumor cells), and NT as tumor cells = 20000, W – weight of tumor.

5.15 Determination of serum cytokine levels by ELISA

IL1β, TNFα and IL10 protein levels were measured in the serum by enzyme linked immunosorbent assay (R&D Inc., MN, USA – Quantikine ELISA), according to the manufacturer's instructions. For serum separation, the whole blood was collected and allowed to clot at room temperature for 30 minutes. The clot was removed by centrifugation at 6000xg for 20 minutes, at 4°C. The serum was transferred into a new polypropylene tube and stored at -80°C until used for ELISA cytokine analysis.

5.16 Bacteria quantification

Aseptically collected tumors were individually placed in a pre-weighed sterile tube containing 500µl of cold sterile PBS and placed on ice. Briefly, all tumor samples were homogenized and serially diluted with PBS and plated on LB agar plates. The colonies were enumerated and expressed as CFU per gram of tumor.

5.17 Statistical Analysis

The relative gene expression from real time quantitative PCR analysis was conducted with comparative C_T method ($2^{-\Delta\Delta CT}$) using GAPDH as a reference gene. Mean values for conditioned media treatment were compared to control with one way ANOVA and Tukey's multiple comparisonspost-hoc test.

Values were reported as a mean ± standard error of the mean (SEM) and the number of independent replicates is indicated in the figure legends. Treatment groups were compared for differences in mean using analysis of variance (ANOVA) followed by Tukey's multiple comparisons posthoc test. All analyses were performed using GraphPad Prism 7.0 (GraphPad Software Inc.). All p-values were two-sided, and $p < 0.05$ was taken to indicate statistical significance.

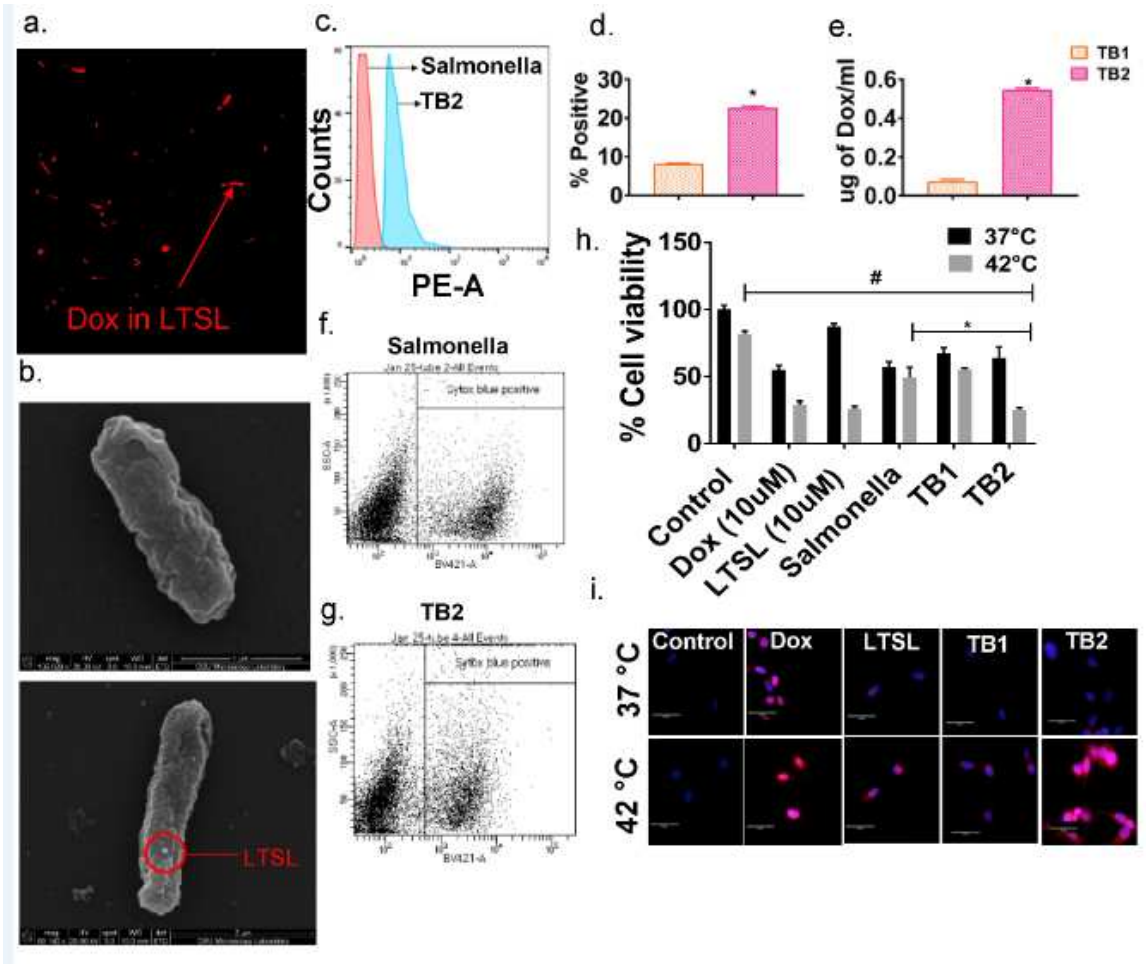

Fig. 1: In-vitro characterization of thermobots. a) Fluorescence microscopy showed LTSL presence on the Salmonella as indicated by red fluorescence of Dox. Salmonella (not shown) was used as control and didn't demonstrate any fluorescence. All images were captured with the 60x oil immersion objective lens; b) SEM image of Salmonella showed punctate liposomal dots on the membrane; c) Histogram plots indicated a gradual increase in the MFI for bacterial population positive for dox (depicted in blue) compared to the control (depicted as red peak); d) Dox quantification by spectroscopy and flow cytometry demonstrated 2-4fold greater Dox loading with streptavidin-biotin crosslinking for TB2 compared to TB1 ($p<0.0001$); e-f) Viability of TB post crosslinking determined with SYTOX blue show no major shift in the dead cell population)fluorescence for TB's from controls in the FACS density plot; h) Cellular viability of C26 cells post treatment with dox, LTSL and TBs suggested enhanced bacterial killing at 42°C compared to 37 °C. Streptavidin-biotin cross linking improved intracellular Dox delivery from TB2

compared to TB1. Data normalized to control samples at 37°C. Values represent mean± SE (n=6); i) C26 cells were efficiently infected by Salmonella, and achieved efficient intracellular Dox delivery at 4 h post infection with heat. Confocal images were captured at 40x magnification. Dox was shown in red and nuclei in blue

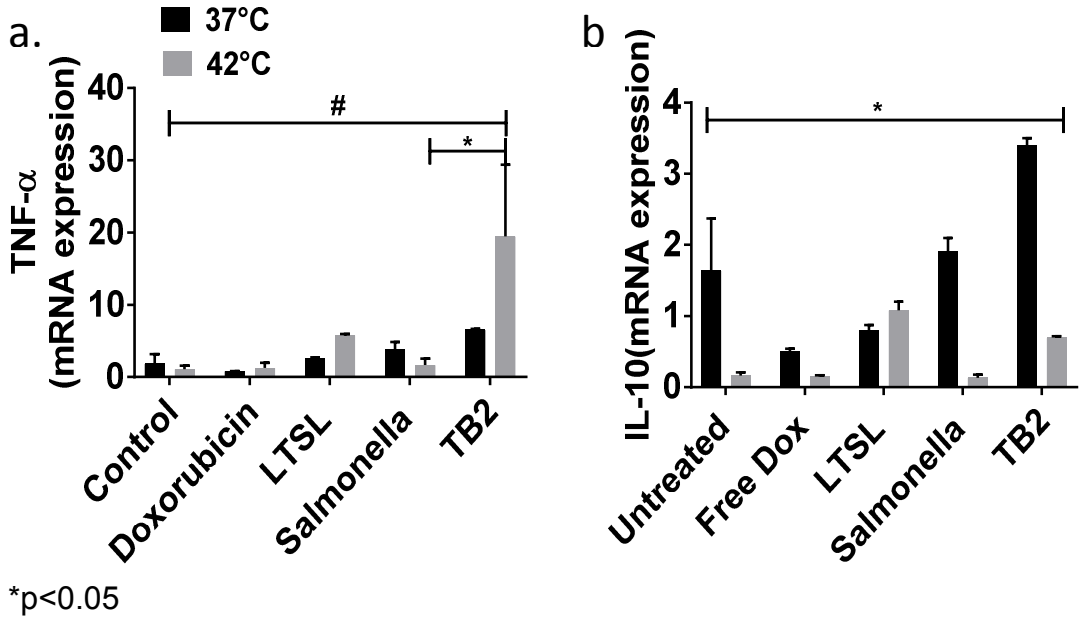

Figure 2: Impact of TB/heat treated C26 condition media on RAW264.5 macrophage cytokine gene by qRT-PCR. a) TB2/42°C achieved significantly higher TNF-α gene expression compared to controls, dox and LTSL treatment at 37°C and 42°C; b) Significant drop in IL1-β expression at 42°C compared to body temperature was noted for all treatments. Values represent means ± SE (n = 3) for each treatment, #,*$p < 0.05$

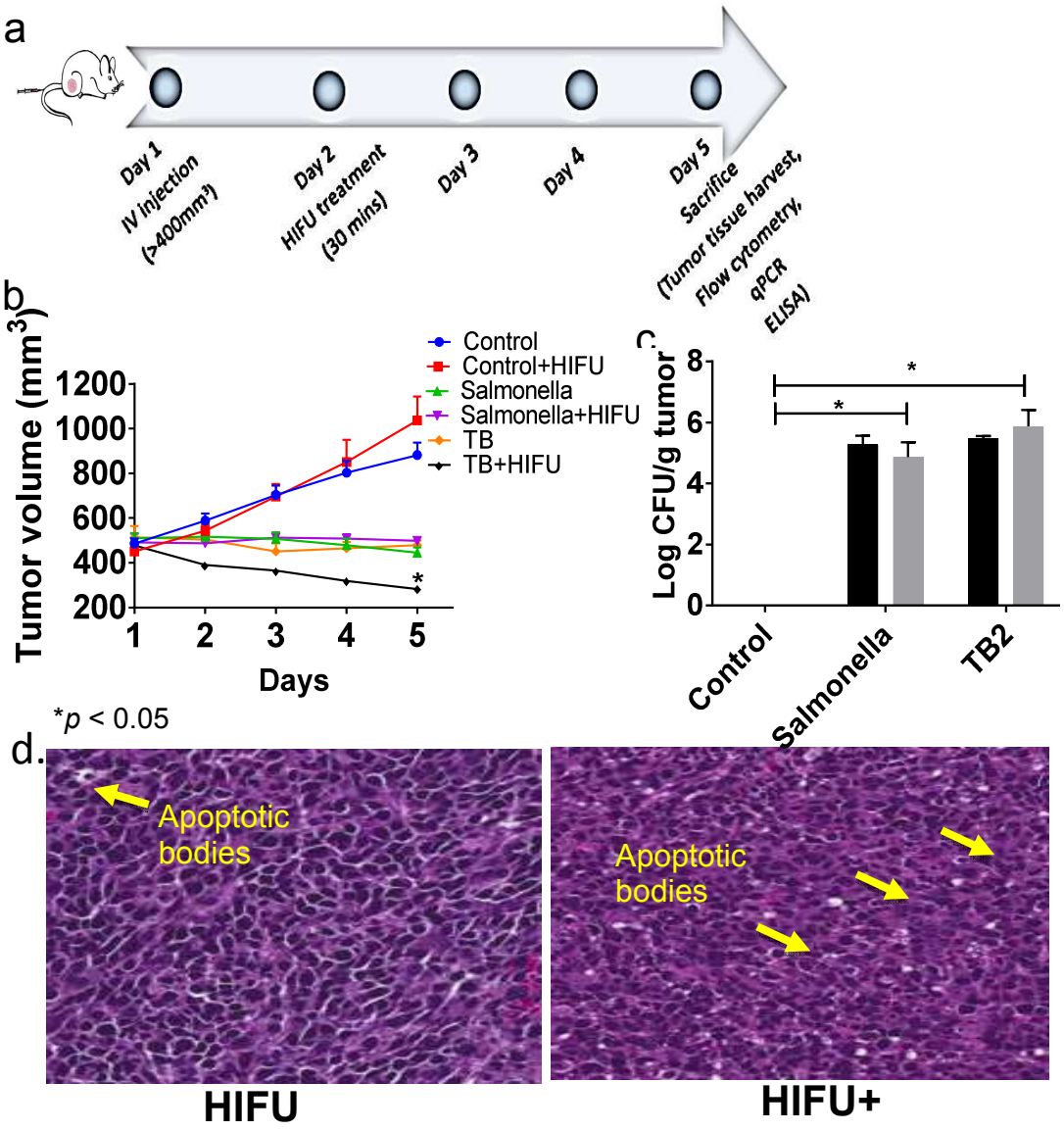

Figure 3: In vivo efficacy in C26 colon tumor model following HIFU/TB treatment. a) Female Balb/c mice (N=6/group) were inoculated with $0.5*10^6$ C26 cells subcutaneously in the upper thigh region. When the tumors reached a volume of $>400mm^3$ mice, were injected with a single dose of saline/Salmonella/TB followed by HIFU treatment for 30 mins 24h post injection. Mice were sacrificed on day 5 and the organs were processed; b) Tumor volume over the 5-day treatment duration suggested significant tumor regression in the treated groups. TB/HIFU demonstrated highest

efficacy compared to other groups; c) Colony forming unit (CFU) per gram of tumor enumerated by plating tumor homogenates on LB agar suggested efficient tumor colonization with TB with and without HIFU; d) H&E sections of mice tumors suggested an increase in the apoptotic bodies for HIFU+ tumors in comparison untreated tumors. Values represent means ± SE for each treatment; *$p < 0.05$ from control (ANOVA followed by Tukey's)

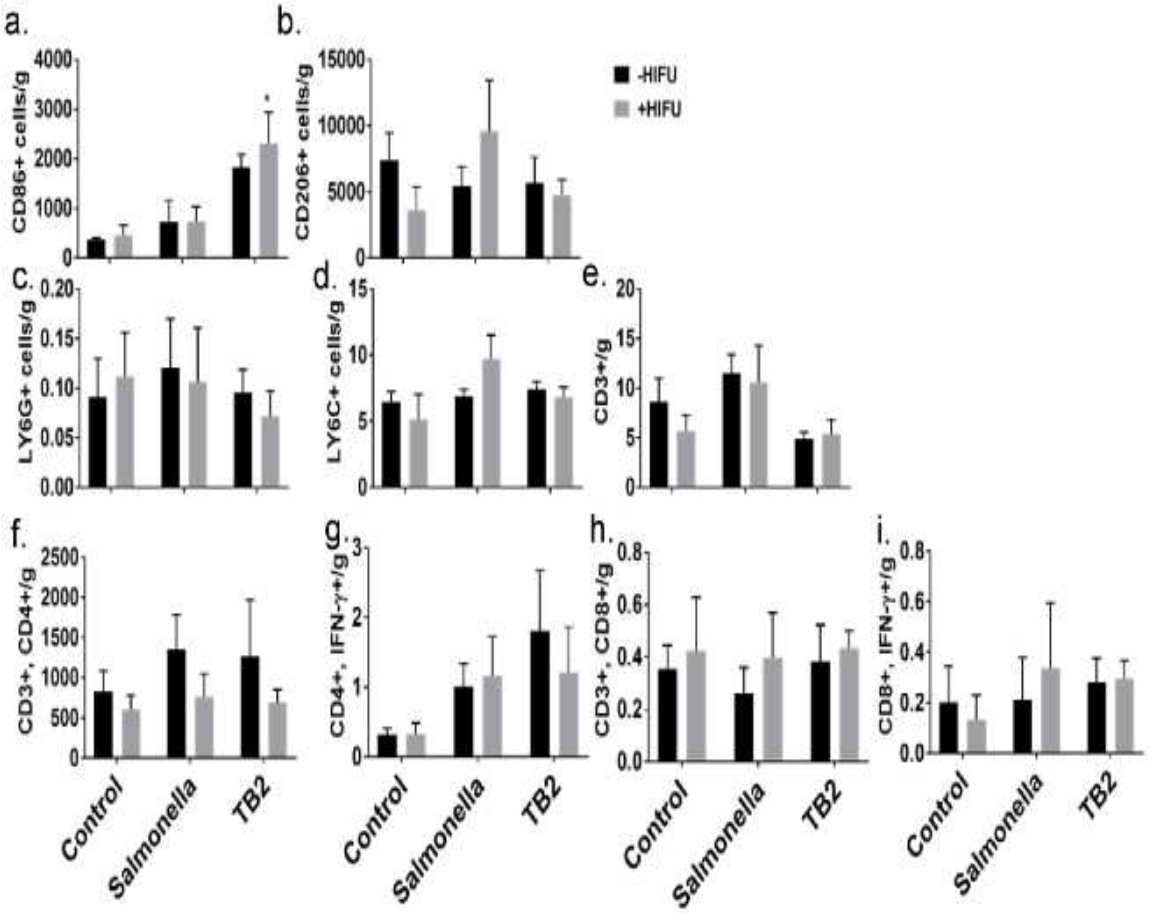

Figure 4: Evaluation of infiltration of immune cells in colon tumors by flow cytometry. Tumor cells were labelled ex vivo with following panels: macrophages (CD11b+, CD86+/CD206+), MDSC's (CD11b+, Ly6C+/Ly6G+) and T cells (CD3+, CD4+/CD8+, IFN-γ+). A significant enhancement in M1 macrophage for TB/HIFU was noted. Values represent means ± SEM (n = 6) for each treatment *$p < 0.001$

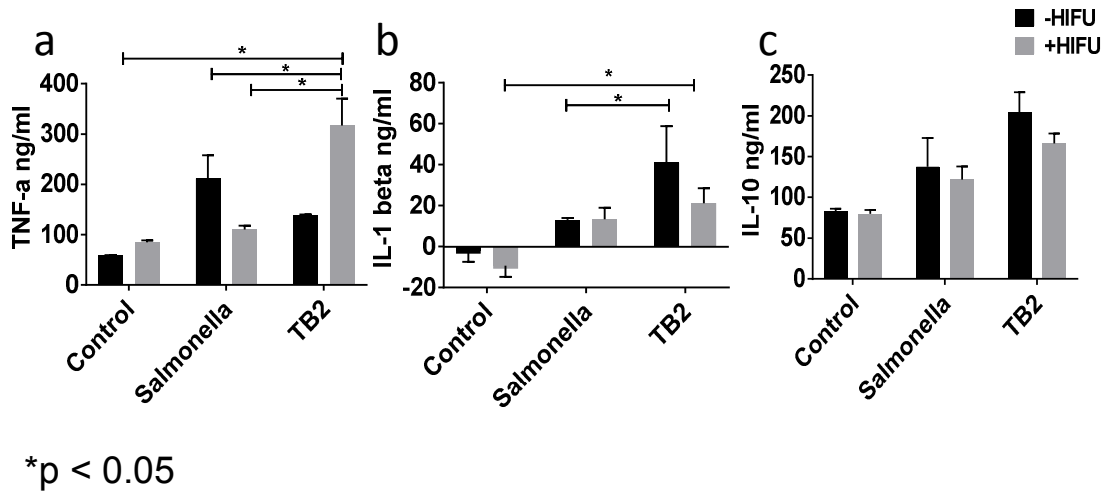

Fig 5: Enhanced levels of pro-inflammatory cytokines in serum in response to TB treatment. ELISA was performed to detect the serum cytokine levels of TNF-α, IL1-β and IL-10; a) TB2 + HIFU achieved highest TNF-α serum cytokine level, significantly different from control, *Salmonella* and TB treatment at body temperature and HIFU heating; b) IL-1β serum cytokine levels suggested 2-3 fold increase in response to TB treatment compared to controls; c) IL-10 increased for TB±HIFU in comparison to controls. Values represent means ± SEM (n =4) for each treatment *p < 0.05

References

1. Siegel, R.L., Miller, K.D. & Jemal, A. Cancer statistics, 2017. *CA: A Cancer Journal for Clinicians***67**, 7-30 (2017).
2. Pages, F.*, et al.* Immune infiltration in human tumors: a prognostic factor that should not be ignored. *Oncogene***29**, 1093-1102 (2010).
3. Van Eynde, B.D.*, et al.* Presence on a human melanoma of multiple antigens recognized by autologous CTL. *International journal of cancer***44**, 634-640 (1989).
4. Banerjea, A., Bustin, S.A. & Dorudi, S. The immunogenicity of colorectal cancers with high-degree microsatellite instability. *World Journal of Surgical Oncology***3**, 26-26 (2005).
5. de Vries, N.L., Swets, M., Vahrmeijer, A.L., Hokland, M. & Kuppen, P.J.K. The Immunogenicity of Colorectal Cancer in Relation to Tumor Development and Treatment. *International Journal of Molecular Sciences***17**, 1030 (2016).
6. Wei, M.Q., Mengesha, A., Good, D. & Anné, J. Bacterial targeted tumour therapy-dawn of a new era. *Cancer Letters***259**, 16-27 (2008).
7. Ganai, S., Arenas, R.B., Sauer, J.P., Bentley, B. & Forbes, N.S. In tumors Salmonella migrate away from vasculature toward the transition zone and induce apoptosis. *Cancer gene therapy***18**, 457-466 (2011).
8. Dang, L.H., Bettegowda, C., Huso, D.L., Kinzler, K.W. & Vogelstein, B. Combination bacteriolytic therapy for the treatment of experimental tumors. *Proceedings of the National Academy of Sciences of the United States of America***98**, 15155-15160 (2001).
9. Sasaki, T.*, et al.* Genetically engineered Bifidobacterium longum for tumor-targeting enzyme-prodrug therapy of autochthonous mammary tumors in rats. *Cancer Science***97**, 649-657 (2006).
10. Rosenberg, S.A., Spiess, P.J. & Kleiner, D.E. Antitumor Effects in Mice of the Intravenous Injection of Attenuated Salmonella Typhimurium. *Journal of immunotherapy (Hagerstown, Md. : 1997)***25**, 218-225 (2002).
11. Hayashi, K.*, et al.* Cancer metastasis directly eradicated by targeted therpay with a modified *Salmonella typhimurium*. *Journal of cellular biochemistry***106**, 992-998 (2009).
12. Jia, L.-J.*, et al.* Enhanced therapeutic effect by combination of tumor-targeting salmonella and endostatin in murine melanoma model. *Cancer Biology & Therapy***4**, 840-845 (2014).
13. Kasinskas, R.W. & Forbes, N.S. Salmonella typhimurium lacking ribose chemoreceptors localize in tumor quiescence and induce apoptosis. *Cancer Res***67**, 3201-3209 (2007).
14. Akin, D., et al. Bacteria-mediated delivery of nanoparticles and cargo into cells. *Nature Nanotechnology***2,** 441 (2007).
15. Northfelt, D.W., et al. Pegylated-liposomal doxorubicin versus doxorubicin, bleomycin, and vincristine in the treatment of AIDS-related Kaposi's sarcoma: results of a randomized phase III clinical trial. *Journal of Clinical Oncology***16**, 2445-2451 (1998).

16. Audouy, S.L., de Leij, L.M.H., Hoekstra, D. & Molema, G. In Vivo Characteristics of Cationic Liposomes as Delivery Vectors for Gene Therapy. *Pharm Res***19**, 1599-1605 (2002).
17. Krishnamurthy, S., Ke, X. & Yang, Y.Y. Delivery of therapeutics using nanocarriers for targeting cancer cells and cancer stem cells. *Nanomedicine (London, England)***10**, 143-160 (2015).
18. Toso, J.F.*, et al.* Phase I Study of the Intravenous Administration of Attenuated Salmonella typhimurium to Patients With Metastatic Melanoma. *Journal of clinical oncology : official journal of the American Society of Clinical Oncology***20**, 142-152 (2002).
19. Ranjan, A.*, et al.* Image-guided drug delivery with magnetic resonance guided high intensity focused ultrasound and temperature sensitive liposomes in a rabbit Vx2 tumor model. *Journal of controlled release : official journal of the Controlled Release Society***158**, 487-494 (2012).
20. Ektate, K.*, et al.* Motion Compensated Ultrasound Imaging Allows Thermometry and Image Guided Drug Delivery Monitoring from Echogenic Liposomes. *Theranostics***6**, 1963 (2016).
21. Kong, G.*, et al.* Efficacy of liposomes and hyperthermia in a human tumor xenograft model: importance of triggered drug release. *Cancer research***60**, 6950-6957 (2000).
22. Negussie, A.H.*, et al.* Formulation and characterisation of magnetic resonance imageable thermally sensitive liposomes for use with magnetic resonance-guided high intensity focused ultrasound. *International journal of hyperthermia : the official journal of European Society for Hyperthermic Oncology, North American Hyperthermia Group***27**, 140-155 (2010).
23. Partanen, A.*, et al.* Mild hyperthermia with magnetic resonance-guided high-intensity focused ultrasound for applications in drug delivery. *International journal of hyperthermia : the official journal of European Society for Hyperthermic Oncology, North American Hyperthermia Group***28**, 320-336 (2012).
24. Bing, C.*, et al.* Localised hyperthermia in rodent models using an MRI-compatible high-intensity focused ultrasound system. *International journal of hyperthermia : the official journal of European Society for Hyperthermic Oncology, North American Hyperthermia Group***31**, 813-822 (2015).
25. Maples, D.*, et al.* Synthesis and characterisation of ultrasound imageable heat-sensitive liposomes for HIFU therapy. *International journal of hyperthermia : the official journal of European Society for Hyperthermic Oncology, North American Hyperthermia Group***31**, 674-685 (2015).
26. Ranjan, A.*, et al.* Image-guided drug delivery with magnetic resonance guided high intensity focused ultrasound and temperature sensitive liposomes in a rabbit Vx2 tumor model. *Journal of Controlled Release***158**, 487-494 (2012).
27. Ito, A.*, et al.* Tumor regression by combined immunotherapy and hyperthermia using magnetic nanoparticles in an experimental subcutaneous murine melanoma. *Cancer Science***94**, 308-313 (2003).

28. Skitzki, J.J., Repasky, E.A. & Evans, S.S. Hyperthermia as an immunotherapy strategy for cancer. *Current opinion in investigational drugs (London, England : 2000)***10**, 550-558 (2009).
29. Calderwood, S.K., Theriault, J.R. & Gong, J. How is the immune response affected by hyperthermia and heat shock proteins? *International journal of hyperthermia : the official journal of European Society for Hyperthermic Oncology, North American Hyperthermia Group***21**, 713-716 (2005).
30. Huang, Y.-F., Wang, Y.-F. & Yan, X.-P. Amine-Functionalized Magnetic Nanoparticles for Rapid Capture and Removal of Bacterial Pathogens. *Environmental Science & Technology***44**, 7908-7913 (2010).
31. Nguyen, V.D*., et al.* Active tumor-therapeutic liposomal bacteriobot combining a drug (paclitaxel)-encapsulated liposome with targeting bacteria (Salmonella Typhimurium). *Sensors and Actuators B: Chemical***224**, 217-224 (2016).
32. Abbas, A.K., Lichtman, A.H.H. & Pillai, S. *Basic Immunology E-Book: Functions and Disorders of the Immune System*, (Elsevier Health Sciences, 2012).
33. Chilkoti, A. & Stayton, P.S. Molecular Origins of the Slow Streptavidin-Biotin Dissociation Kinetics. *Journal of the American Chemical Society***117**, 10622-10628 (1995).
34. Hermanson, G.T. Chapter 11 - (Strept)avidin–Biotin Systems. in *Bioconjugate Techniques (Third edition)* 465-505 (Academic Press, Boston, 2013).
35. Panariti, A., Miserocchi, G. & Rivolta, I. The effect of nanoparticle uptake on cellular behavior: disrupting or enabling functions? *Nanotechnology, Science and Applications***5**, 87-100 (2012).
36. Lepock, J.R. Involvement of membranes in cellular responses to hyperthermia. *Radiation research***92**, 433-438 (1982).
37. Wang, N., Liang, H. & Zen, K. Molecular mechanisms that influence the macrophage m1-m2 polarization balance. *Frontiers in immunology***5**, 614 (2014).
38. Balkwill, F. Tumour necrosis factor and cancer. *Nat Rev Cancer***9**, 361-371 (2009).
39. Cervenak, L*., et al.* Abolished angiogenicity and tumorigenicity of Burkitt lymphoma by interleukin-10. *Blood***96**, 2568-2573 (2000).
40. Senavirathna, L.K*., et al.* Tumor Spheroids as an in vitro model for determining the therapeutic response to proton beam radiotherapy and thermally sensitive nanocarriers. *Theranostics***3**, 687 (2013).
41. Mayer, L.D., Cullis, P.R. & Bally, M.B. The Use of Transmembrane pH Gradient-Driven Drug Encapsulation in the Pharmacodynamic Evaluation of Liposomal Doxorubicin. *Journal of Liposome Research***4**, 529-553 (1994).
42. Ivask, A*., et al.* Genome-wide bacterial toxicity screening uncovers the mechanisms of toxicity of a cationic polystyrene nanomaterial. *Environ Sci Technol***46**, 2398-2405 (2012).
43. Lebaron, P., Catala, P. & Parthuisot, N. Effectiveness of SYTOX Green Stain for Bacterial Viability Assessment. *Applied and Environmental Microbiology***64**, 2697-2700 (1998).
44. VanOsdol, J*., et al.* Sequential HIFU heating and nanobubble encapsulation provide efficient drug penetration from stealth and temperature sensitive liposomes in colon cancer. *Journal of Controlled Release***247**, 55-63 (2017).

CHAPTER IV

MAGNETIC BACTERIA BOUND THERMOSENSITIVE LIPOSOMES FOR CELLULAR DELIVERY OF DOXORUBICIN IN MURINE COLON TUMOR MODEL WITH HALBACH ARRAY

Abstract

Low-Temperature sensitive liposomes (LTSLs) release doxorubicin in tumor blood vessels with hyperthermia (~40-45^{0}C), but its therapeutic efficacies can be limited by a short half-life (<1h) and poor extravasation in the tumor tissues. Objectives of this study were to 1) Synthesize *Magnetospirillum magneticum* (AMB-1) conjugated LTSL (AMB-LTSL) 2) determine doxorubicin delivery and cell killing in-vitro with AMB-LTSL and 3) Utilize Halbach array to localize AMB-LTSL in mice colon tumors. AMB-LTSL generated by biotin-streptavidin affinity reaction was assessed for binding efficiencies, cellular uptake, and viability by flow cytometry, confocal microscopy, and cytotoxicity assays. Localization of AMB-LTSL in murine colon tumors following intravenous injection with Halbach array was assessed by histopathology, fluorescence imaging, and bacterial colony culture. Results indicated that biotin-streptavidin affinity reaction achieved > 90% binding of LTSLs on AMB membrane. < 5% doxorubicin was released from the LTSL at body temperature (37°), while > 95% was released at ~42ºC.

AMB-LTSLs were viable and enabled efficient intracellular doxorubicin delivery compared to LTSL alone. In addition, the Halbach focusing for 1h enhanced AMB-1 localization in the murine colon tumor. Our initial data suggest that AMB-LTSL can aid doxorubicin therapy of colon cancer with magnetic guidance.

Introduction

Low-Temperature sensitive liposomes (LTSLs) are currently in clinical trials for the treatment of hepatocellular carcinoma and liver tumors in combination with Radio frequency ablation (RFA) and focused ultrasound [1-3]. LTSLs mediated intravascular content release has been found to enhance targeted doxorubicin therapy of solid tumors[4]. Although superior to conventional liposomes, LTSL currently have a short half-life, and demonstrate poor extravasation in tumors[5,6]. Since solid tumors (e.g. colorectal, pancreatic and breast cancer) in advanced stages lack vascular network and functional lymphatics in the tumor core, the intravascular nature of LTSL delivery can impact homogeneous therapy in such cases[7,8]. Thus, modulation of the extracellular matrix of solid tumors with newer approaches is an unmet need [9,10]. One approach to address this can be by the development of dual-mode bacterial carriers that target hypoxic tumor cores[11,12]. We propose that the magnetic bacteria *Magnetospirillum magneticum* (AMB-1) attached LTSLs can achieve delivery of LTSLs to tumor core with a magnetic focusing device (e.g. Halbach array).

AMB-1 is flagellated gram-negative, magnetic, aquatic bacteria that can colonize murine tumors[13,14]. AMB-1 also contains magnetite (Fe_3O_4) particles that allow them to align along the geomagnetic field of the earth [15], [16]. It is currently believed that AMB-1 prefer low oxygen (hypoxic) conditions for optimal growth and reproduction[17], and in the presence of the local magnetic field can propel with an average swimming speed of 49μm/s (25-50 body cell lengths/s) [18]. The AMB-1 membrane is rich in amines and can be covalently linked to therapeutics[19]. Thus, if LTSL can be attached to the AMB-1 membrane and are guided using an external magnetic navigation system such as Halbach array, it is possible to achieve intratumoral drug release.

Halbach array is a special arrangement of permanent magnets that augments the magnetic field on one side of the array while canceling the field to near zero on the other side [20]. It was invented in the 1980s by Physicist Klaus Halbach at the Lawrence Berkeley National Laboratory[21]. Halbach array creates a strong pull and push force within the magnetic field [8,22] . Halbach array pulls the magnetic nanoparticles within the tumors against the blood flow whereas the push properties direct particles to a precise location [23,24]. Although prior research that used permanent magnets or electromagnets for magnetic localization of nanoparticle, drug and/or gene delivery to tumors/diseased location were somewhat successful, they were limited by the sharp fall in the magnetic field at the depth of tumors/lesion, limiting localizations and therapeutic outcomes [25,26]. For example, current 0.2-.8T magnetic devices achieve a maximum focusing depth of 5-12 cm in animal and human models with 100-500nm particles[2728]. However, the targeting of magnetic particles to deep-seated/ larger solid tumors in the tumor core requires a much stronger magnetic field at the depth of the tumor. We hypothesize that the strong magnetic field at depth created by Halbach array will help enhance localization of magnetic particles, maximizing delivery of therapeutics at the targeted regions[22]. If successful, AMB-1 will also address the current limitations of microbe based navigational limitation through a guided approach in the systemic circulation [29,30]. AMB-1 does not induce a systemic immune response, and thus high dosage administration of the bacteria can be performed in patients without adverse effects [11]. Furthermore, AMB-1 can be imaged with MRI for the correlation between drug delivery and treatment outcomes. Thus, our proposed objectives of creating AMB-1-LTSL with Halbach focusing stems should increase the overall therapeutic index. Here, we covalently attached AMB-1 membrane amines with LTSL[19], assessed feasibility of AMB-LTSL navigation propulsion with external Halbach guidance, drug delivery, and imageable features in vitro and in murine xenograft tumor models. Data suggest that AMB-LTSL synergistically enhance colon cancer cell death and targeted drug release from LTSL with mild hyperthermia.

Materials and methods

2.1 Materials

Monostearoyl-2-hydroxy-sn-glycero-3-phosphocholine (MSPC), 1,2-dipalmitoylsn-glycero-3-phosphocholine (DPPC), and 1,2-distearoyl-sn-glycero-3-

phosphoethanolamine-N-[methoxy (Polyethylene glycol)2000] (DSPE-mPEG2000) were obtained from Corden Pharma Corporation (Boulder, CO, USA). DSPE-PEG (2000)-Biotin (NANOCS), Streptavidin (VWR), EZ-link NHS-LC-Biotin (Thermo Scientific), Chloroform, Citrate buffer 300mM, and Dox was obtained from LC Laboratory (Woburn, MA, USA). Modified magnetic growth media **(**MSGM) and MSGM agar plates with 0.7% agar with hypoxia jar were obtained from Oxoid. The PD-10 column was obtained from GE Healthcare Life Sciences, (Buckinghamshire, United Kingdom, UK). C26 cells were kindly provided by the National Cancer Institute, and Halbach array was built by Dr. Piao.

2.2 Bacterial culture

AMB-1 was cultured in modified *Magnetospirillum* growth medium (MSGM) at 30°C in sealed tubes with <5 % headspace till a brown pellet was observed at the bottom of the tube (5-6 days)[31].

2.3 LTSL synthesis

LTSLs with lipid ratio combinations (lipid composition: DPPC, MSPC, DSPE-PEG2000 and DSPE-PEG2000-Biotin molar ratio of 85.3:9.7:4:1 were prepared by hydration of lipid film followed by the extrusion method[32]. Briefly, lipid mixtures dissolved in chloroform was evaporated and the resulting lipid film was hydrated in citrate buffer (pH 4.0) at 55^0C for 30 min and extruded five times through double stacked 200nm polycarbonate filters to yield a final lipid concentration of 50mg lipid/ml. Encapsulation of doxorubicin (Dox) into the LTSLs was carried out using a pH-gradient loading protocol as described by Mayer et al. [33]. To do so, the pH LTSL solution was adjusted (by column) to 7.4 using PBS, whereas the aqueous core remained acidic at pH 4. Dox was loaded at 2 mg per 100 mg lipid concentration at 37 °C for 1h. Free Dox was removed using a PD-10 size-exclusion column equilibrated with 5–10 column volumes of 1x phosphate buffer saline (PBS).

2.4 Characterization of LTSL

LTSLs were characterized for size (z-average) using dynamic light scattering (DLS) with 90 plus PALS Nanobrook (Brookhaven Instruments, Holtsville, NY). Briefly, 10-20µl of LTSL were added to 2 ml of PBS in a cuvette and DLS measurements were recorded at room temperature. For each liposomal formulation, an average of 5 measurements was taken and the mean size and standard deviation were calculated for the biotin-LTSL.

2.5 Synthesis of AMB-LTSL

AMB-LTSL was prepared with biotin and streptavidin chemistry. Briefly, the surface of the AMB-1 was modified with biotin and subsequently linked to LTSL's with terminal biotin functional group with streptavidin intermediate molecule. 0.5 ml of AMB-1 at an OD_{470} of 2 was co-incubated with 100µg of EZ-Link NHS Biotin (ThermoFisher Scientific) for 45 minutes at room temperature with mild shaking. Unreacted EZ-Link Biotin was removed by centrifuging at 4000x g for 20 minutes and washed 2x times with PBS. One pot-click reaction for crosslinking LTSL to AMB was carried out by incubating AMB-1 with terminal biotin with 100µg of Streptavidin and 100µl of 22mM Doxorubicin loaded LTSL for 1h at room temperature. Unattached liposomes were separated out by centrifugation at 4000x g for 20 min. The AMB-LTSL pellet was washed 2x times to remove residual unattached liposomes and suspended in RPMI1640 (No FBS and Penicillin-Streptomycin) or further experiments. To record the size, 10-20µl of the AMB-LTSL sample was added to 2 ml of PBS in a cuvette and DLS measurements were recorded at room temperature. An average of 5 measurements was taken, and the mean size and standard deviation were calculated.

2.6 In vitro assessment of Magnetic Behavior of AMB-LTSL complexes

AMB-LTSLs were placed in an array of magnets made-up of 5 permanent magnets placed in a circle with the focus of the magnetic field in the center. 1.5 ml Eppendorf tubes with the complexes were placed in the hollow of the magnet array for 30 min, and the magnetotaxis in the tubes was characterized.

2.7 Quantification of LTSL on AMB-LTSL by flow cytometry and spectroscopy

AMB-1 and AMB-LTSL (n=3; 3 x 10^8 CFU) were examined in a FACS Aria flow sorter (BD Biosciences, Franklin Lakes, NJ, USA) [34] at an excitation wavelength of 488 nm and a 590/30-nm emission filter using BD FACS Diva 8.0.1 software. Data was computed and compared from the dot plots and histogram plot by counting 10,000 single cell events. For determining the amount of Dox positive LTSL on the AMBs, 0.5 ml of AMB-LTSL and AMB (same OD_{470} as AMB-LTSL) suspended in PBS were heated in a water-bath maintained at 45°C for 30 minutes. The bacteria were pelleted at 2000xg for 10 minutes, and the supernatant with the released dox was collected for fluorescence measurements. AMB-1 was used as a control for the drug estimation studies of AMB-LTSL.

2.8 Assessment of viability of AMB-LTSL

The viability of the AMB-1 pre and post-crosslinking of LTSL was determined by staining the cells with SYTOX blue. 1ul of SYTOX blue (1uM) was added to 5x10^7 bacterial cells/ml, incubated for 5 min in dark for viability assessments. Samples were protected from light, and the staining procedure was not allowed to proceed for longer than 30 min. Samples were analyzed with flow cytometry without fixing using a BV421 (440/40 nm) band pass laser.

2.9 Evaluation of cellular toxicity of AMB-LTSL at mild hyperthermia

C26 colon cancer cells cultured in RPMI 1640 media supplemented with 10% Fetal Bovine Serum (FBS) and 1% Penicillin/Streptomycin were harvested using trypsin-EDTA (Gibco). For cytotoxicity assessment, C26 cells seeded at the cellular density of 1x 10^5 cells/well in 96 well flat bottom plate were incubated overnight to allow adhesion to the plate. Non-adherent cells were removed by washing with media (No FBS and Penicillin-Streptomycin). 5µM concentrations of Dox, Dox-LTSL, AMB-1 (OD_{470}= 4) and AMB-LTSL (5µM Dox) was added at 37 and 42 °C. For hyperthermia treatment, samples were incubated for 4h in a CO_2 incubator at 42°C. Post-treatment, the wells were treated with RPMI containing 50µg/ml of Gentamicin for 1h to kill extracellular bacteria

and additional incubation for ~20h at 37°Cwas performed. For the non-hyperthermia (37°C) group, cells were treated for 1h followed by treatment with RPMI containing 50µg/ml gentamicin for 1h. Following gentamicin treatment, cells were washed and incubated for an additional 22h before performing MTT.

For MTT, 10µl of 12mM MTT reagent was added to the treated cells for 3h and incubated at 37°C. MTT reagent was also added to empty wells with media as blank control. Next, all but 25µl of media was removed from the well, and 50µl of DMSO was added to assess formazan products spectrophotometrically at 540nm. Cells viability was calculated by normalizing absorbance values obtained from untreated C26 cells.

2.10 In vivo assessment of AMB-LTSL targeting in murine colon cancer

All animal-related procedures were approved and carried out under the regulations and guidelines of the Oklahoma State University Animal Care and Use Committee (VM 16-4). C26 cells were cultured at 80–90% confluence in RPMI supplemented with 10% v/v fetal bovine serum (FBS) and 1% v/v streptomycin/penicillin. Female Balb/c mice (~10wk old, Charles River, Wilmington, MA) were inoculated with 0.5 x 10^6 C26 cells suspended in 50µl PBS of cells in the thigh region of the mouse hind leg using a 25-gauge needle (BD, Franklin Lakes, NJ, USA). Mice were monitored for tumor growth by serial caliper measurements (General Tools Fraction+™, New York, NY, USA). Tumor volumes were calculated using the formula (length x $width^2$)/2, where length is the largest dimension and width is the smallest dimension perpendicular to the length.

Mice with tumor volume of 400-500 mm^3 were assigned to the following treatment groups: control, AMB-1 (± Halbach array), AMB-LTSL (± Halbach array). 1.5 x 10^9 AMB-1 and AMB-LTSL (23.5µM of Dox) were administered by intravenous injection, and the tumor bearing mice were placed in the Halbach array system for 1h under gas anesthesia (Figure 4a.). Mice were sacrificed 2h post-injection of AMB and AMB-LTSL, and the tumor, liver, spleen and blood were collected for endpoint assessments.

2.11 Evaluation of Colony forming units (CFU) of AMBs in colon tumors

Tumors (n=3) were homogenized with zirconia beads using Mini-Beadbeater-16 (Biospec Products Inc., OK, USA) at 3450 oscillations/min (four cycles of 30 seconds) in

a 7mL polypropylene screw-cap micro-vials (1mm diameter, Biospec Products Inc., OK, USA). 500ul of tumor homogenate suspended in 4.5 ml of warmed Magnetospirillum growth medium (MSGM) with 0.7% agar was serially diluted, and 10µl of diluted suspension (n=5) was plated on the MSGM plates. The plates were incubated in a hypoxia oxoid jar or in zip-locked bags at 30°C periodically flushed with N_2 gas for 3-7 days to allow bacterial replication.

2.13 Prussian blue staining of AMB-LTSL treated tumor sections

Tumor sections (8µm) were de-paraffinized and hydrated in distilled water with 2 changes of xylene each for 10 minutes. Rehydration was performed 2x each for 5min with 100% ethanol, and 2min each with 95% and 70% ethanol. Next, the sections were rinsed with water and dipped in hydrochloric acid and potassium ferrocyanide (prepared immediately before use) mixed in equal parts for 20 min. Finally, the slide containing the tissue sections were washed 3x with distilled water and counter-stained with DAPI nuclear staining, dried and cover-slipped with a resinous mounting medium for imaging using an Aperio scan scope at 20x.

2.14 Fluorescence imaging to detect doxorubicin in tissue sections

Whole tumor tissue sample (n=2) collected from AMB-LTSL± Halbach injected mice were analyzed for Dox distribution. Two 8µm formalin fixed and paraffin embedded tumor sections were mounted per slide using DAPI containing medium (Vector Laboratories). Imaging was performed at an exposure time of 10 ms (ex/em of 365/440) to visualize cell nuclei, and Dox was imaged at an exposure 100 ms (ex/em of 480/590). Image acquisition and display parameters were constant for treatment groups for qualitative comparison. Whole-section digital images were acquired using a 10X objective on an Olympus ZDC2IX81 fluorescence microscope equipped with a color CCD camera, cooled monochrome CCD camera, and motorized scanning stage.

2.15 Tumor MRI imaging of AMB-LTSL

The optical density of AMB-1 suspended in 3% gelatin in 1.5 ml Eppendorf tubes was measured at 600nm. Next, the tubes were aligned in a plastic box, and the box was subsequently filled with 0.7% agar. The boxes were kept at 4°C to solidify gelatin for

maintenance of homogenous distribution of bacteria. For in vivo studies, mice injected with AMB-1 and exposed to Halbach arrays were sacrificed and frozen at -20°C until MRI imaging. MRI imaging was performed on a 7-Tesla MRI scanner (Bruker BioSpin, Ettlingen, Germany) using the T1gradient echo sequence (*t*e= 1300 ms and *t*r = 9 ms), and T2 sequence (*t*e= 2500 ms and *t*r = 33 ms). Single slice images were acquired in all planes (axial, sagittal and coronal). The slice position for the cine also utilized the same sequence. For cine and volume imaging, a field of view (*FOV)* of 3.5 × 3.5 cm was chosen and 256 phase encode and read steps were used to resolve the spatial distribution of excited spins.

2.16 Statistical Analysis

Treatment groups were compared for differences in means for cell viability assay, bacterial viability determination using analysis of variance (ANOVA) followed by Tukey's multiple comparison test. Dox quantification amongst groups and Colony forming unit (CFU) ± Halbach treatments were compared with unpaired t-test. All analyses were performed using GraphPad Prism 5.0 (GraphPad Software Inc.). All p-values were two-sided, and $p < 0.05$ was taken to indicate statistical significance. Values were reported as the mean ± standard error of the mean (SEM).

3. Result

3.1 Characterization of LTSL

The hydrodynamic diameter and polydispersity index of biotin containing LTSL at room temperature (~25^{0}C) value is shown in Table 1. LTSLs were between 170-190nm with a polydispersity index of ~0.2, and showed a zeta potential of -38.7±2.8 (Table 1).

Table 1. Size, polydispersity index, and zeta potential of biotin functionalized LTSL

Liposome	**Diameter ± SD**	**Poly dispersity Index ± SD**	**Zeta Potential ± SD**
LTSL (1% Bitoin)	172.765 ± 3.44	0.189 ± 0.0222	-38.7 ± 2.7474

3.2 Synthesis and characterization of AMB-LTSL complex

LTSL attachment to AMB-1 didn't result in a significant loss in bacterial viability (Fig.1b). The EZ-Link-NHS biotin[35] conjugated schematic of LTSL-biotin functional groups with streptavidin molecule containing 4 binding sites per molecule is shown in Figure 1a). These AMB-LTSL showed efficient magnetotaxis in the center of sphericalHalbach array within 10-30 min (Figure 3a).

Dox emission from AMB-LTSL was evident at 480-590 nm in confocal imaging (Figure 2g.). DLS showed that the size of AMB-1 (448.40 nm) doubled upon complexation of LTSL to AMBs (766.65nm) (Figure2a). The peak side scatter fluorescence moved towards the right under flow cytometry (Figure 2b, c). The autofluorescence of AMB-1 was adjusted to reduce false positives to a minimum and used as a reference gate to test AMB-LTSL. >90% of AMB-LTSL was positive for the Dox signal (Figure 3e). In contrast to this, AMB-1 co-incubated with LTSL attached < 25% of LTSLs (Figure 3e.). The binding was also evident in spectroscopic measurements with a 3 fold higher levels of Dox/ml for AMB-LTSL detected in comparison to the AMB-1 and LTSL passive co-incubation (Figure 3f).

3.3. Evaluation of AMB-LTSL viability by flow cytometry

SYTOX™ Blue is a high-affinity nucleic acid stain that penetrates cells with compromised plasma membranes. Sytox staining for AMB-1 and cross-linked with FACS did not indicate significant changes in the. In general, a 2-4% reduction in viability of crosslinked AMB-LTSL was noted over time (Figure 3b.).

3.4. Efficacy of AMB-LTSL against colon cancer cell with mild hyperthermia

LTSL-Dox and AMB-1 reduced the viability of C26 colon cells by ~20% and ~47% compared to untreated control at 37°C (Figure 3h). Adding heat (42°C) to AMB-LTSL reduced the C26 viability by ~ 70% compared to AMB-1 likely due to Dox release from LTSLs[36].

3.5 Halbach array enhanced AMB-1 and AMB-LTSL localization in colon tumors

Mice injected with AMB-1 and AMB-LTSL were placed on the Halbach array platform for 1 h with the tumor in close proximity to the magnets (Figure 4a). Tumors assessed for AMB-1 population suggested a 5-log increase in CFU with Halbach focusing relative to controls (n=3). Also, the spleen and liver tissues showed a ~50 and ~5 log CFU reduction in the AMB-1 colonies for Halbach focused groups compared to non-focused mice (Figure 4 f, g.). MRI imaging performed to correlate with the CFU in the organ did not demonstrate contrast enhancement for Halbach focused AMB-1s related to untreated controls (Figure 6 b). The population of AMB-1 was evident in the tumor sections in the presence and absence of Halbach array (Figure 4c, d).AMB-1 associated iron oxide was mainly detected along the connective tissue septa or in perivascular locations of tumors [37]. The Prussian blue staining indicated a higher population of tissue macrophages around AMB-1 injected mice relative to AMB-LTSL; reasons of which will need to be investigated in future studies. In general, histological analysis suggests that the Halbach focusing did not impact the migration of AMB-LTSL relative to unfocused bacteria at the time-point tested (Figure 4 b, c, d). This was also evident in fluorescence imaging where a significant enhancement in the dox fluorescence for magnet focused vs. unfocused AMB-LTSL mice was not observed (Figure5).

4. Discussion

Homogeneous drug delivery to tumors with nanoparticle is an area of active research investigation[13,38]. But, the reliance of nanoparticles on systemic circulation and the absence of a self-propelling system that can drive therapeutic to tumors can severely limit these processes[39,40]. Intravascular delivery of drug from LTSL are slightly better, but as a vascular drug delivery systems, their reach in deeper regions of the tumor is still limited[41]. In this study, the ability of AMB-LTSL for magnetically guided delivery of doxorubicin in the tumor was investigated. AMB-LTSL cross-linking was performed with biotin-streptavidin non-covalent chemistry that has a high association constant ($Ka=2.5 \times 10^{13} M^{-1}$)[42]. This chemistry was easy to perform and demonstrated reproducible and high LTSL coupling efficiencies (~90%; Figure 2e) [34]. LTSL attachment to AMB-1 was not associated with loss of magnetic properties and viability; feature crucial for

targeted therapies (Figure3). These data are in line with prior research by Taherkhani et al [43]. When heat was added to AMB-LTSL therapy, a significant reduction in the viability of colon cancer cells (C26) relative to untreated control was noted in vitro (Figure 2h.). We believe that hyperthermia induced dox release from LTSL and sensitized colon cancer cells to doxorubicin therapy[36,44]. Interestingly, AMB-1 alone also induced cytotoxicity at body temperatures. Most likely, the AMB-1 byproducts triggered such effects[12].

Previously, conventional magnets/electromagnets have been utilized for peri-tumoral delivery of the magnetic bacteria[45]. As the conventional magnets or electromagnets magnetic field decays with an increase in depth, achieving the homogeneous distribution of the therapeutic agents in the tumor remains a challenge[46,47]. To overcome such barriers, we innovated by developing the Halbach array. AMB-1 CFU counts revealed a higher population in the focused tumors than the unfocused tumors (Figure4e). Additionally, a ~50 and ~5 log reduction in AMB-1 number in the spleen and liver compared to controls was observed when AMB-1 were magnetically attracted to the tumors with Halbach array (Figure 4f, g). However, the increase in AMB-1 population upon Halbach focusing didn't accompany an enhanced dox fluorescence, iron-staining or MRI-contrast in focused vs unfocused tumors (Figure4, 5, 6). Future studies with a larger cohort of mice subjects and dosing regimens are needed to further uncover the localization mechanisms. In conclusion, our initial data suggest that AMB-LTSL demonstrates magnetic sensitivity and enhanced therapeutic effects in vitro.

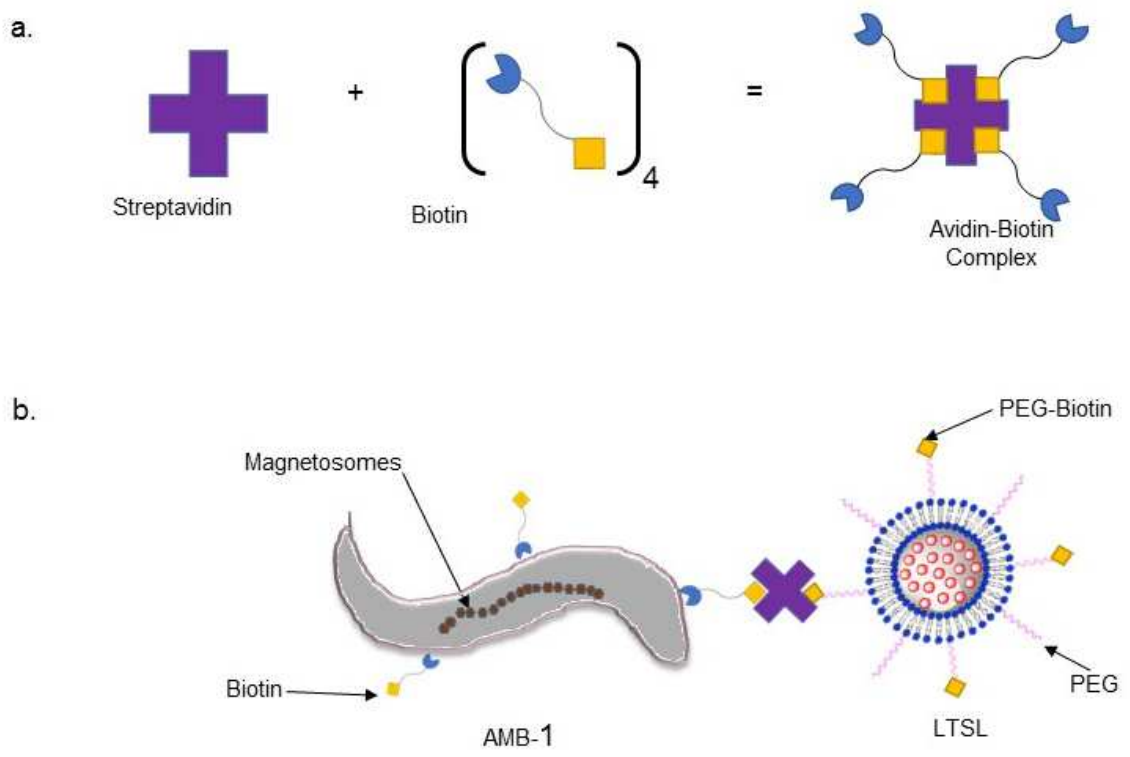

Figure 1: a) Schematic o**f** binding sites of streptavidin and biotin and complex formation; (b) Schematic for the attachment of AMB-1 to LTSL with streptavidin-biotin crosslinking chemistry.

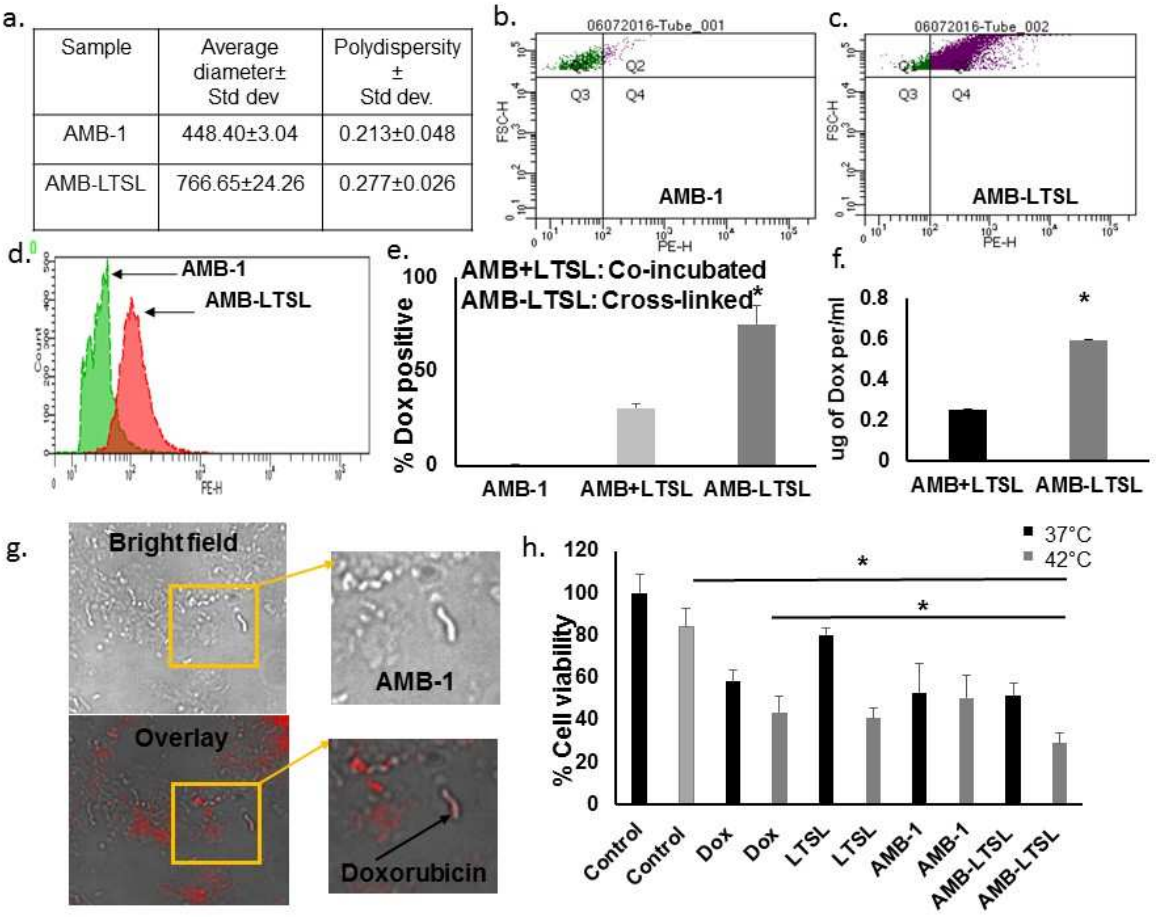

Figure 2: In vitro characterization of AMB-LTSL. a) Dynamic light scattering showed a 2-fold increase in AMB-LTSL size relative to AMB-1; (b-c) FACS density plots and (d) Histogram obtained from AMB-LTSL showed enhanced doxorubicin fluorescence compared to AMB-1, indicating presence of fluorescent LTSLs on AMB membrane; (e) >90% of AMB-1 showed the presence of Dox fluorescence with streptavidin-biotin compared to those that were co-incubated passively with AMB-1; (f) Spectrophotometry showed a 3-3.5 fold enhanced Dox loading with streptavidin-biotin crosslinking compared to AMBs-co-incubated with LTSLs; (g) Fluorescence microscopy of AMB-LTSL showed red fluorescence indicative of LTSL attachment on the AMB-1. In contrast, unlabeled AMB-1control didn't demonstrate dox fluorescence; (h) Dox, LTSL, AMB-1, and AMB-LTSL enhanced C26 killing at 42°C compared to 37 °C. Data normalized to control samples at 37°C. Values represent mean± SE (n=5)

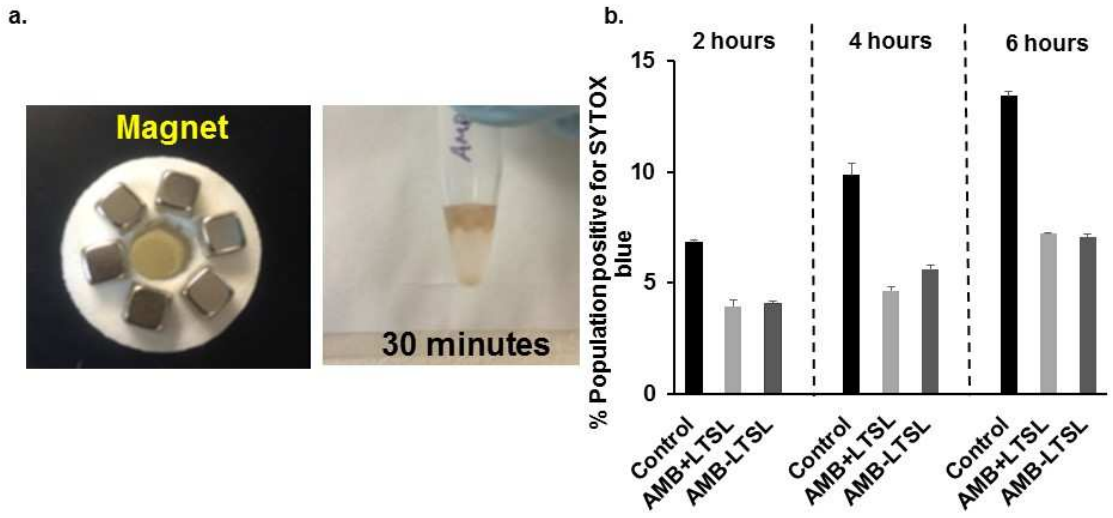

Figure 3: Localization of AMBs with Halbach array and viability of AMB-LTSL: (a) An array-based magnetic arrangement with a hollow center was used to test the localization of AMB-LTSL in 15mL tubes. AMB-LTSLs accumulated in the topmost layer of the falcon tubes with strong magnetic fields; (b) The viability of AMB-LTSL was not impacted with LTSL attachment compared to AMB-1 alone at 2,4,and 6h by sytox staining.

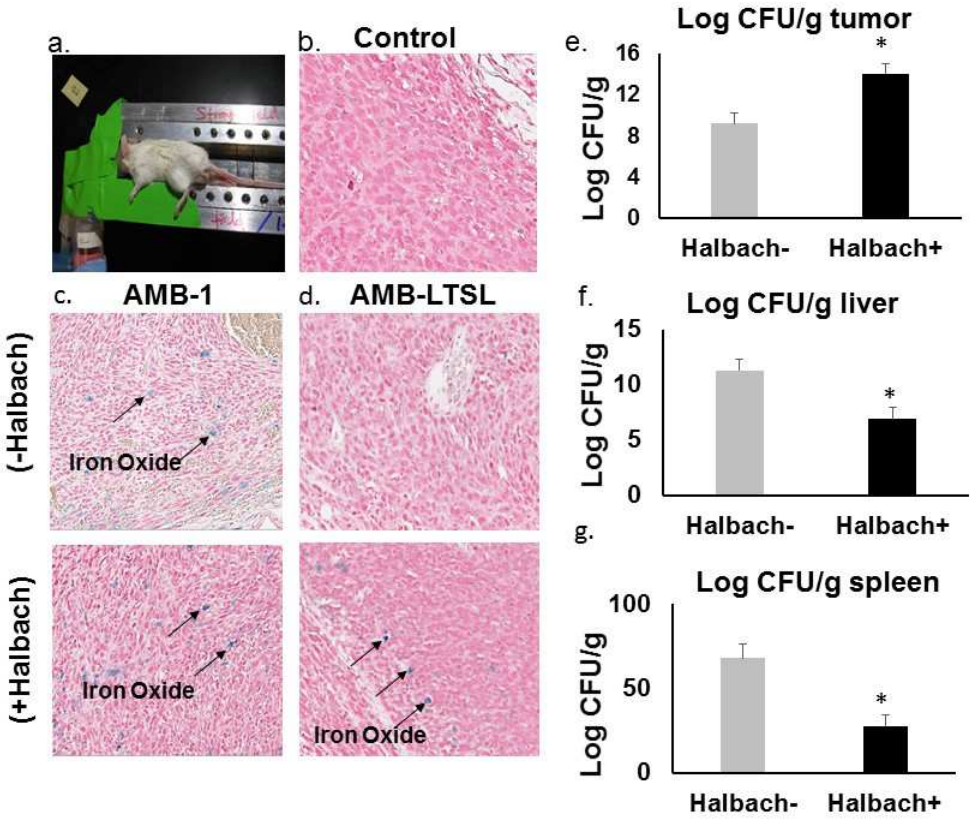

Figure 4: AMB-LTSL targeting of colon tumor with Halbach array. a) Female Balb/c mice with tumor volumes of >400mm^3 mice and injected intravenous (IV) with AMB-1 or AMB-LTSL were placed in the Halbach platform for 1 h; the (b, c, d) Tumor histology 2h post-treatment showed the presence of iron (blue color) in the AMB-1 and AMB-LTSL treated tumors in the presence and absence of Halbach focusing; (e-g) AMB-1 Colony forming unit (CFU) per gram of tumor for AMB-1 was higher in Halbach than un-focused tumors. Conversely, liver and spleen tissues showed reduced AMB populations compared to unfocused mice groups (n=3), Values represent means ± SE for each treatment *$p < 0.05$ from control (t-test).

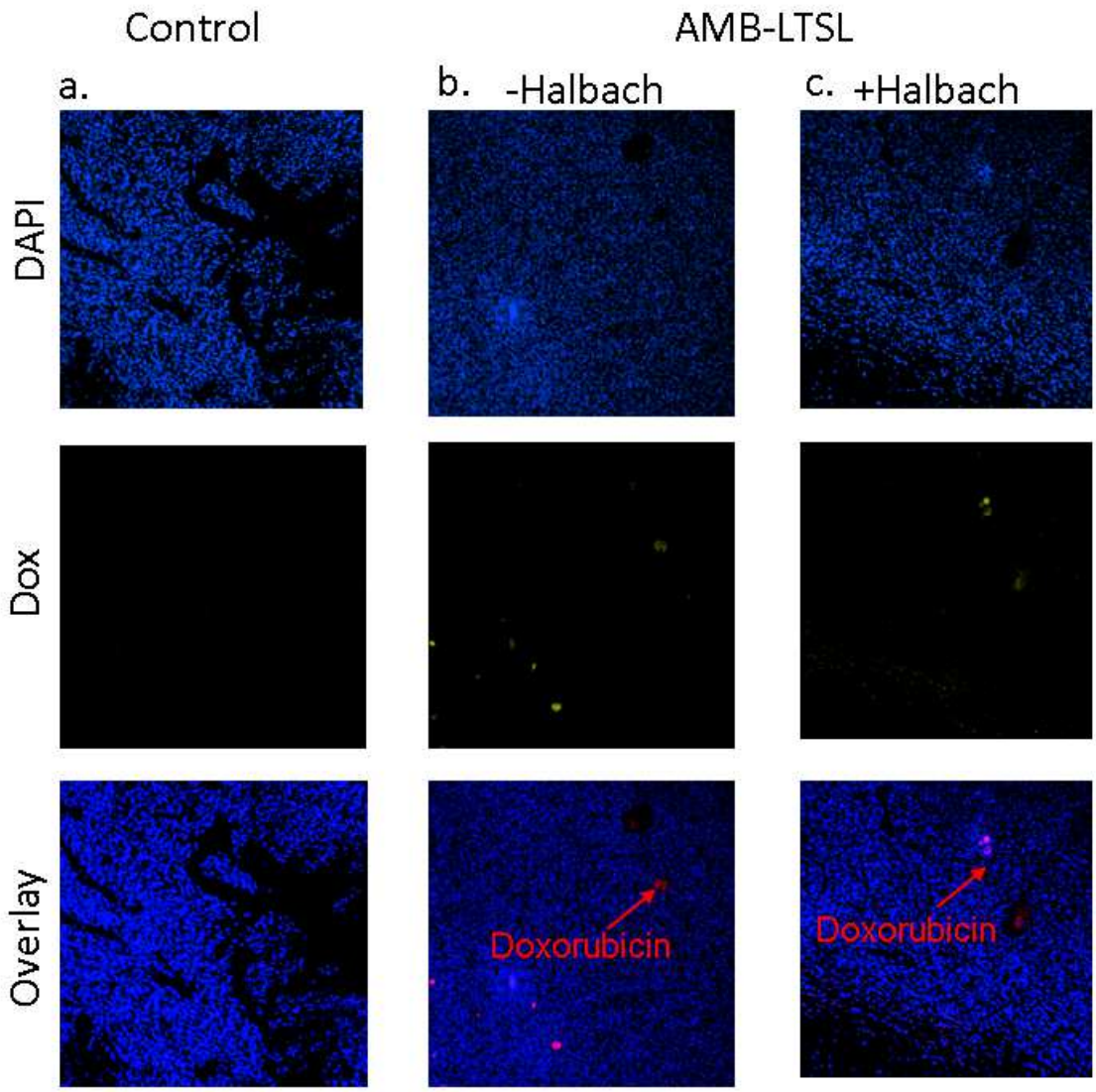

Figure 5: Fluorescence imaging of tumor sections. Whole-section fluorescence images scans acquired for untreated control and AMB-LTSL± Halbach focusing using a 10X objective didn't show a significant difference in the doxorubicin fluorescence between various groups.

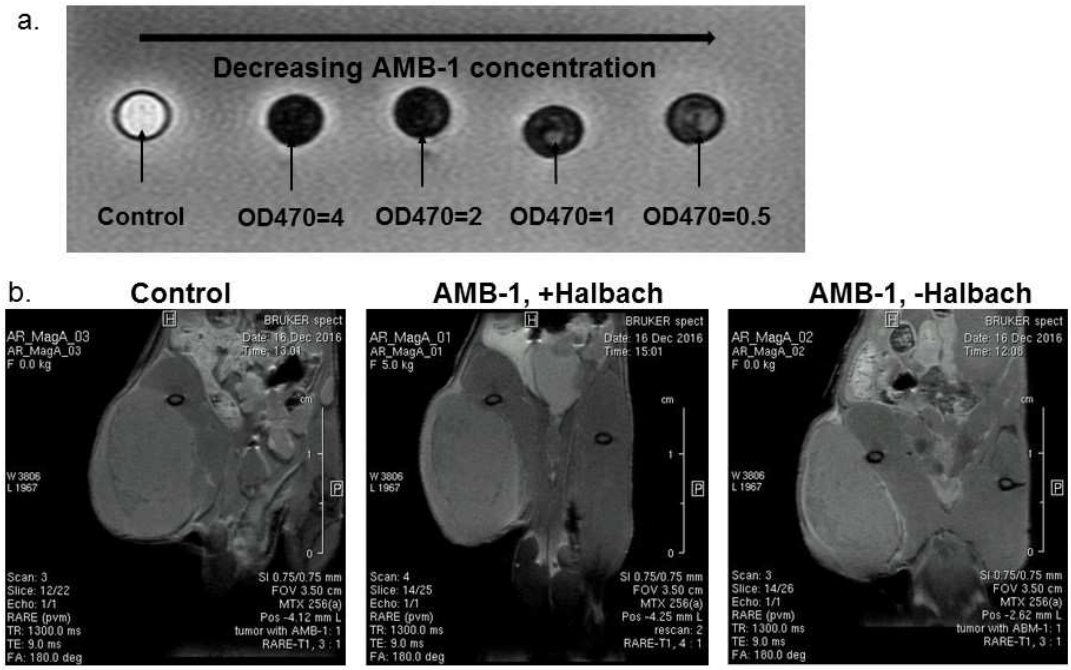

Figure 6: MRI contrast of AMB-1 demonstrated a CFU dependent contrast enhancement in vitro; (b) T1-weighted MR images of tumors following IV delivery of AMB-1 ± Halbach focusing didn't demonstrate an appreciable enhancement of AMB contrast in tumors.

References

1. Mura, S., Nicolas, J. & Couvreur, P. Stimuli-responsive nanocarriers for drug delivery. *Nature materials***12**, 991-1003 (2013).
2. Egusquiaguirre, S.P., Igartua, M., Hernandez, R.M. & Pedraz, J.L. Nanoparticle delivery systems for cancer therapy: advances in clinical and preclinical research. *Clinical & translational oncology : official publication of the Federation of Spanish Oncology Societies and of the National Cancer Institute of Mexico***14**, 83-93 (2012).
3. Wood, B.*, et al.* Phase I study of thermally sensitive liposomes containing doxorubicin (ThermoDox) given during radiofrequency ablation (RFA) in patients with unresectable hepatic malignancies. in *American Society of Clinical Oncology Gastrointestinal Cancers Symposium* (2007).
4. Kneidl, B., Peller, M., Winter, G., Lindner, L.H. & Hossann, M. Thermosensitive liposomal drug delivery systems: state of the art review. *International Journal of Nanomedicine***9**, 4387-4398 (2014).
5. Yingchoncharoen, P., Kalinowski, D.S. & Richardson, D.R. Lipid-Based Drug Delivery Systems in Cancer Therapy: What Is Available and What Is Yet to Come. *Pharmacological reviews***68**, 701-787 (2016).
6. Minchinton, A.I. & Tannock, I.F. Drug penetration in solid tumours. *Nat Rev Cancer***6**, 583-592 (2006).
7. Heldin, C.-H., Rubin, K., Pietras, K. & Ostman, A. High interstitial fluid pressure [mdash] an obstacle in cancer therapy. *Nat Rev Cancer***4**, 806-813 (2004).
8. Siemann, D.W. The unique characteristics of tumor vasculature and preclinical evidence for its selective disruption by Tumor-Vascular Disrupting Agents. *Cancer treatment reviews***37**, 63-74 (2011).
9. Netti, P.A., Berk, D.A., Swartz, M.A., Grodzinsky, A.J. & Jain, R.K. Role of Extracellular Matrix Assembly in Interstitial Transport in Solid Tumors. *Cancer research***60**, 2497 (2000).
10. Jain, R.K. Delivery of Molecular and Cellular Medicine to Solid Tumors. *Microcirculation***4**, 1-23 (1997).
11. Felfoul, O.*, et al.* Magneto-aerotactic bacteria deliver drug-containing nanoliposomes to tumour hypoxic regions. *Nat Nano***11**, 941-947 (2016).
12. Taherkhani, S., Mohammadi, M., Daoud, J., Martel, S. & Tabrizian, M. Covalent binding of nanoliposomes to the surface of magnetotactic bacteria for the synthesis of self-propelled therapeutic agents. *ACS nano***8**, 5049-5060 (2014).
13. Benoit, M.R.*, et al.* Visualizing Implanted Tumors in Mice with Magnetic Resonance Imaging Using Magnetotactic Bacteria. *Clinical Cancer Research***15**, 5170 (2009).
14. Martel, S., Mohammadi, M., Felfoul, O., Lu, Z. & Pouponneau, P. Flagellated Magnetotactic Bacteria as Controlled MRI-trackable Propulsion and Steering Systems for Medical Nanorobots Operating in the Human Microvasculature. *The International journal of robotics research***28**, 571-582 (2009).
15. Bazylinski, D.A. & Frankel, R.B. Magnetosome formation in prokaryotes. *Nat Rev Micro***2**, 217-230 (2004).

16. Smith, M.J.*, et al.* Quantifying the Magnetic Advantage in Magnetotaxis. *Biophysical Journal***91**, 1098-1107 (2006).
17. Lower, B.H. & Bazylinski, D.A. The bacterial magnetosome: a unique prokaryotic organelle. *Journal of molecular microbiology and biotechnology***23**, 63-80 (2013).
18. Seong, S. & Park, T.H. Swimming characteristics of magnetic bacterium, Magnetospirillum sp. AMB-1, and implications as toxicity measurement. *Biotechnol Bioeng***76**, 11-16 (2001).
19. Schulz, G.E. The structure of bacterial outer membrane proteins. *Biochimica et biophysica acta***1565**, 308-317 (2002).
20. Lester C Barnsley, D.C., Joshua Owen and Eleanor Stride. Halbach arrays consisting of cubic elements optimised for high field gradients in magnetic drug targeting applications. *Physics in Medicine & Biolog***60**(2015).
21. Post, R.F. Maglev: A New Approach. in *Scientific American* 82-87 (Scientific American, Inc., 2000).
22. Sarwar, A., Nemirovski, A. & Shapiro, B. Optimal Halbach permanent magnet designs for maximally pulling and pushing nanoparticles. *Journal of Magnetism and Magnetic Materials***324**, 742-754 (2012).
23. Häfeli, U.O., Gilmour, K., Zhou, A., Lee, S. & Hayden, M.E. Modeling of magnetic bandages for drug targeting: Button vs. Halbach arrays. *Journal of Magnetism and Magnetic Materials***311**, 323-329 (2007).
24. Creighton, F.M., Ritter, R.C. & Werp, P. Focused magnetic navigation using optimized magnets for medical therapies. in *2005 IEEE International Magnetics Conference (INTERMAG)* 1253-1254 (2005).
25. Holligan, D.L., Gillies, G.T. & Dailey, J.P. Magnetic guidance of ferrofluidic nanoparticles in anin vitromodel of intraocular retinal repair. *Nanotechnology***14**, 661-666 (2003).
26. Alexiou, C.*, et al.* A High Field Gradient Magnet for Magnetic Drug Targeting. *IEEE Transactions on Applied Superconductivity***16**, 1527-1530 (2006).
27. Goodwin, S., Peterson, C., Hoh, C. & Bittner, C. Targeting and retention of magnetic targeted carriers (MTCs) enhancing intra-arterial chemotherapy. *Journal of Magnetism and Magnetic Materials***194**, 132-139 (1999).
28. Lubbe, A.S.*, et al.* Clinical experiences with magnetic drug targeting: a phase I study with 4'-epidoxorubicin in 14 patients with advanced solid tumors. *Cancer research***56**, 4686-4693 (1996).
29. Ryan, R.M.*, et al.* Bacterial delivery of a novel cytolysin to hypoxic areas of solid tumors. *Gene Ther***16**, 329-339 (2009).
30. Dang, L.H., Bettegowda, C., Huso, D.L., Kinzler, K.W. & Vogelstein, B. Combination bacteriolytic therapy for the treatment of experimental tumors. *Proceedings of the National Academy of Sciences of the United States of America***98**, 15155-15160 (2001).
31. Komeili, A., Vali, H., Beveridge, T.J. & Newman, D.K. Magnetosome vesicles are present before magnetite formation, and MamA is required for their activation. *Proceedings of the National Academy of Sciences of the United States of America***101**, 3839-3844 (2004).

32. Senavirathna, L.K.*, et al.* Tumor Spheroids as an In Vitro Model for Determining the Therapeutic Response to Proton Beam Radiotherapy and Thermally Sensitive Nanocarriers. *Theranostics***3**, 687-691 (2013).
33. Lawrence D. Mayer, M.B.B., and Pieter R. Cullis Strategies for Optimizing Liposomal Doxorubicin *Journal of Liposome Research* 463-480 (1990).
34. Ektate, K., Munteanu, M.C., Ashar, H., Malayer, J. & Ranjan, A. Chemo-immunotherapy of colon cancer with focused ultrasound and Salmonella-laden temperature sensitive liposomes (thermobots). *Scientific Reports***8**, 13062 (2018).
35. Gautam, S., Gniadek, T., Kim, T. & Spiegel, D.A. Exterior design: Strategies for redecorating the bacterial surface with small molecules. *Trends in biotechnology***31**, 258-267 (2013).
36. Ektate, K.*, et al.* Motion Compensated Ultrasound Imaging Allows Thermometry and Image Guided Drug Delivery Monitoring from Echogenic Liposomes. *Theranostics***6**, 1963 (2016).
37. Mannucci, S.*, et al.* Magnetic Nanoparticles from Magnetospirillum gryphiswaldense Increase the Efficacy of Thermotherapy in a Model of Colon Carcinoma. *PLOS ONE***9**, e108959 (2014).
38. Yan, L.*, et al.* Magnetotactic bacteria, magnetosomes and their application. *Microbiological Research***167**, 507-519 (2012).
39. Hong, M., Zhu, S., Jiang, Y., Tang, G. & Pei, Y. Efficient tumor targeting of hydroxycamptothecin loaded PEGylated niosomes modified with transferrin. *Journal of controlled release : official journal of the Controlled Release Society***133**, 96-102 (2009).
40. Blanco, E., Shen, H. & Ferrari, M. Principles of nanoparticle design for overcoming biological barriers to drug delivery. *Nature biotechnology***33**, 941-951 (2015).
41. Wilson, W.R. & Hay, M.P. Targeting hypoxia in cancer therapy. *Nat Rev Cancer***11**, 393-410 (2011).
42. Chilkoti, A. & Stayton, P.S. Molecular Origins of the Slow Streptavidin-Biotin Dissociation Kinetics. *Journal of the American Chemical Society***117**, 10622-10628 (1995).
43. Taherkhani, S., Mohammadi, M., Daoud, J., Martel, S. & Tabrizian, M. Covalent Binding of Nanoliposomes to the Surface of Magnetotactic Bacteria for the Synthesis of Self-Propelled Therapeutic Agents. *ACS Nano***8**, 5049-5060 (2014).
44. VanOsdol, J.*, et al.* Sequential HIFU heating and nanobubble encapsulation provide efficient drug penetration from stealth and temperature sensitive liposomes in colon cancer. *Journal of Controlled Release***247**, 55-63 (2017).
45. Felfoul, O.*, et al.* Magneto-aerotactic bacteria deliver drug-containing nanoliposomes to tumour hypoxic regions. *Nature Nanotechnology***11**, 941 (2016).
46. Felfoul, O., Mathieu, J.B. & Martel, S. A comparative study between MC-1 Cells and magnetic microparticles used for enhanced target delivery of therapeutic agents in the microvasculature. in *2008 2nd IEEE RAS & EMBS International Conference on Biomedical Robotics and Biomechatronics* 606-611 (2008).

47. Rotariu, O.S. Modelling magnetic carrier particle targeting in the tumor microvasculature for cancer treatment. *Journal of Magnetism and Magnetic Materials* 639–646 (2005).

CHAPTER V

DISSERTATION SUMMARY AND CONCLUSIONS

Colon cancer is typically treated with surgery, radiation, and chemotherapy, however, the 5-year survival rates is yet to improve drastically (<15%)[1]. Newer approaches (e.g. immunotherapy) are starting to emerge, but attaining favorable outcomes in advanced stage metastatic disease remains challenging[2]. To overcome these barriers, in this doctoral work, we specifically focused on enhancing chemotherapy outcomes by developing novel colon tumor-targeted low temperature sensitive liposomes (LTSLs)[3]. We modified the LTSLs to create image-guided and bacteria-mediated formulations such that they allowed real-time drug delivery and biodistribution estimations in colon tumors. Additionally, the interplay between chemo and immune-responses of colon tumors were assessed. In order to achieve the research objectives, we tailored LTSLs to achieve heat-sensitive doxorubicin release, co-loaded with an ultrasound contrast agent, and attached to a bacterial membrane for targeted tumor delivery. The key findings of the doctoral research are described herein

Study 1: Chapter II

The goal of this study was to develop ultrasound (US) imageable echogenic low-temperature sensitive liposomes (E-LTSL) for contrast-enhanced reporting of tumor temperatures and doxorubicin delivery in mouse colon tumors. To do so, we first developed novel approaches to attain US images by compensating for tumor motion in real-time. For contrast imaging, E-LTSL was loaded with perfluoropentane (PFP) for active US imaging. We found that loading PFP into E-LTSL dramatically altered the phase-transition temperature from 29^0C to ~40^0C. We leveraged this property of E-LTSL to gain an understanding of tumor temperatures. We found that the vascular contrast of E-LTSL as a function of temperature was strongly co-related, and this enabled a more robust estimation of temporal variations in colon tumor temperatures for 15-20 min. Consequently, a marked increase in peak intensity at 42°C compared to 37°C that corresponded with transition temperatures of LTSL (~40^0C), and enhanced doxorubicin delivery from E-LTSL in tumors was observed. Thus, our murine colon cancer work from this study suggest that E-LTSL monitoring of drug delivery and temperatures within tumors with US imaging feedback has the potential to significantly improve spatiotemporal reporting of colon cancer therap.

Study 2: Chapter III

The objective of this study was to attach LTSLs to *Salmonella* membrane (thermobot). For thermobot synthesis, *Salmonella typhimuriu*m (YS1646), a bacterialstrain with high chemotaxis towards the serine, ribose, and aspartate of benign and metastatic tumors was selected. We hypothesized that lipopolysaccharide (LPS), a classical activator of M1 macrophagespresent in the *Salmonella typhimurium* (YS1646) membrane will help overcome the doxorubicin resistance and immunosuppressive tumor microenvironment within the tumor microenvironment to directly improve LTSL colon cancer therapy. We optimized thermobot design principles; understand chemo-immunomodulatory mechanisms and therapeutic efficacy with and without colon tumor heating. We found that an average of 15–20 LTSLs attached to the *Salmonella* membrane, and actively attaching LTSLs using Biotin-Streptavidin chemistry significantly enhanced the loading of Dox without impacting bacterial

viability. Thermobot demonstrated efficient intracellular trafficking and cytotoxicity against colon cancer cell in vitro, and the cytotoxic effects were enhanced upon adding heat (~42^0C). The efficacy of thermobot following tumor heating was superior in suppressing tumor growth rates compared to *Salmonella* or thermobot alone. This was likely due to triggered doxorubicin release in colon cells. Additional characterization of the treated tumors suggested an alteration of tumor immune environments with the highest increase in the expression of M1 macrophages when expressed as per gram of tumor for thermobot compared to all other treatments. Additionaly, compared to untreated control, both Salmonella and thermobot infection of colon cells achieved a ~2–3 fold increase in the helper (CD3+, CD4+) cells and interferon gamma (IFN-γ) expressing CD4+/CD8+ cells per gram of tumor plus and minus heating. Thus, we found that thermobot can be a novel agent for chemoimmunotherapy of colon cancer with tumor heating. Mechanistically, we learned that the thermobots work by enriching M1 macrophage phenotype and triggering the doxorubicin release in tumors to enhance therapeutic effects against colon cancer.

Study 3: Chapter IV

The aim of this study was to attach LTSLs on to *Magnetospirillum magneticum* (AMB-1) membrane for magnetic-guided localization of doxorubicin in colon cancer[4]. AMB-1 are flagellated, gram-negative, magnetic, aquatic bacteria containing magnetite (Fe_3O_4) particles. AMB-1 membrane surface also contains amines that can be leveraged for covalently attaching therapeutics on their surface. We hypothesized that if LTSL is attached to AMB-1, we would be able to guide them to the targeted area using an external magnetic navigation system such as Halbach array. Halbach array is a special arrangement of permanent magnets that augments the magnetic field on one side of the array while canceling the field to near zero on the other side. Results showed that LTSL attachment to AMB-1 with streptavidin-biotin chemistry did not cause a significant loss in bacterial viability. Adding heat to AMB-LTSL reduced the C26 colon cancer cell viability by ~ 70% at 42°C compared to AMB-1 alone. To assess AMB-1 targeting of colon tumors, mice were injected with AMB-1 and AMB-LTSL and the tumor bearing regions were placed on the Halbach array platform for 1h. This method of focusing

achieved a 5-log increase in AMB-1 population within the tumor compared to mice that were not placed on Halbach array. The population of AMB-1 was evident in the tumor sections and was mainly detected along the connective tissue septa or in perivascular locations of tumors. MRI imaging performed to correlate the bacterial population and histopathological finding did not demonstrate contrast enhancement. Most likely, the time between animal euthanasia and MRI imaging resulted in a reduction in MRI contrast to an undetectable level. These mechanisms will need to be further probed in the future. In conclusion, we successfully developed AMB-LTSL that demonstrates magnetic sensitivity and enhanced therapeutic effects in vitro; however, additional animal studies are required to bridge the translational gap.

Future Perspectives

This dissertation showed that LTSLs modified with therapeutic, imaging and navigations system can improve therapeutic outcomes in murine colon cancers. Our data is insightful in laying down a strong foundation for future studies focused on immune-modulations and longitudinal characterization of survival effects in preclinical and clinical patients. Specifically, how LTSL/bacterial agents impact the polarization of tumor macrophages, and enhance T-cell memory can provide important translational basis for systemic anti-tumor immunity trials in colon cancer patients. Our multifunctional liposomes can also be extended to immune checkpoints inhibitor regimens for improved outcomes. We found that magnetic targeting of LTSL to tumors is limited by the strength of magnetic field. Thus, stronger magnets that localize magnetic nanoparticles at unlimited distance from the body surface are needed. This will require innovations in the designing of novel Halbach arrays, and characterization of focusing with Alternating Magnetic Field (AMF) heating for improved outcomes.

Reference

1. Valderrama-Treviño, A.I., Barrera-Mera, B., Ceballos-Villalva, J.C. & Montalvo-Javé, E.E. Hepatic Metastasis from Colorectal Cancer. *Euroasian journal of hepato-gastroenterology***7**, 166-175 (2017).
2. Kalyan, A., Kircher, S., Shah, H., Mulcahy, M. & Benson, A. Updates on immunotherapy for colorectal cancer. *Journal of gastrointestinal oncology***9**, 160-169 (2018).
3. Bae, Y.H. & Park, K. Targeted drug delivery to tumors: myths, reality and possibility. *Journal of controlled release : official journal of the Controlled Release Society***153**, 198-205 (2011).
4. Alphandéry, E. Applications of magnetosomes synthesized by magnetotactic bacteria in medicine. *Frontiers in bioengineering and biotechnology***2**, 5-5 (2014).

APPENDIX A

Abbreviations

AMB-1	*Magnetospirillim magneticum*
AMB-LTSL	*Magnetospirillim magneticum* covalently bonded to low temperature sensitive liposomes
AMF	Alternating Magnetic Field
APC	antigen presenting cells
BCG	Bacillus Calmette-Guerin
CD	Cluster of differentiation
CFU	Colony forming units
CRC	Colorectal cancer
CTLA-4	Cytotoxic T-Lymphocyte Associated protein 4
Dox	Doxorubicin
DPPC	1,2-dipalmitoyl-sn-glycero-3-phosphocholine
DSPE-PEG-2000	1, 2-distearoyl-sn-glycero-3-phosphoethanolamine-N- [amino (polyethylene glycol)-2000]
ELISA	Enzyme linked immunosorbent assay
E-LTSL	Echogenic low temperature sensitive liposomes
E-NTSL	Echogenic non temperature sensitive liposomes
EPR	Enhanced permeability and retention effect
GM-CSF	Granulocyte-macrophage colony stimulating factor

HIFU	High Intensity Focused Ultrasound
HPLC	High performance liquid chromatography
Hsf	Heat shock factors
HSP	Heat shock proteins
IFN-γ	Interferon-γ
LPS	Lipopolysaccharide
LTSL	Low temperature sensitive liposomes
MDSC	Myeloid-derived suppressor cells
MHC	Major histocompatibility complex
MICA	MHC class I polypeptide-related sequence A
MRI	Magnetic resonance imaging
MSPC	Myristoylstearoyl phosphatidylcholine
NK cells	Natural Killer cells
NMIBC	Non-muscle invasive bladder cancer
NTSL	Non temperature sensitive liposomes
PAMP	pathogen-associated molecular patterns
PD-1	Programmed Death -1
PEG	Polyethylene glycol
PFP	Perfluoropentane
qRT-PCR	Quantitative Real-Time Polymerase Chain Reaction
RES	Reticuloendothelial system
RT-PCR	Reverse Transcription Polymerase Chain
SEM	Scanning electron microscopy

TB	Thermobot
TB1	*Salmonella typhimurium* co-incubated with low temperature sensitive liposomes
TB2	*Salmonella typhimurium* covalently bonded to low temperature sensitive liposomes
TEM	Transmission electron microscopy
Thermobot	*Salmonella typhimurium* covalently bonded to low temperature sensitive liposomes
TLR	Toll-like Receptors
TNF-α	Tumor necrosis factor alpha
Treg	Regulatory T cells

VITA

Kalyani Prashant Ektate

Candidate for the Degree of

Doctor of Philosophy

Thesis: DEVELOPMENT OF TARGETED LIPOSOMAL FORMULATION APPROACHES FOR ENHANCED COLORECTAL CANCER THERAPY

Major Field: Veterinary biomedical Sciences

Biographical:

Education:

Completed the requirements for the Doctor of Philosophy; Veterinary Biomedical Sciences at Oklahoma State University, Stillwater, Oklahoma in 2019.

Completed the requirements for the Bachelor of Veterinary Medicine and Animal Husbandry (BVSc. &AH) at Nagpur Veterinary College, MAFSU, Nagpur, India in 2012.

Experience:

Small animal veterinarian (2012-2013)

Teaching assistant Gross and Developmental Anatomy, Centre for Veterinary Health Sciences (CVHS), Oklahoma State University (2013-2018)

Professional Memberships:

Society of Thermal Medicine (STM)